POWER LOSSES IN HVDC CONVERTER STATIONS

UNIVERSITY OF
KWAZULU-NATAL

INYUVESI
YAKWAZULU-NATALI

Gbadega Peter Anuoluwapo
(Student Number: 217071302)

IN FULFILMENT OF MASTER OF SCIENCE DEGREE IN ENGINEERING

COLLEGE OF AGRICULTURE, ENGINEERING AND SCIENCE

UNIVERSITY OF KWAZULU-NATAL

November 2018

Supervisor: **Prof. A.K Saha**

CERTIFICATION

As the candidate's Supervisor, I agree to the submission of this dissertation.

_____

Signed: Prof. A.K Saha.

Date: 28th November 2018

DECLARATION 1 - PLAGIARISM

I, Gbadega Peter Anuoluwapo, declare that:

1. The research reported in this dissertation, except where otherwise indicated, is my original research.

2. This dissertation has not been submitted for any degree or examination at any other university.

3. This dissertation does not contain other persons' data, pictures, graphs or other information, unless specifically acknowledged as being sourced from other persons.

4. This dissertation does not contain other persons' writing, unless specifically acknowledged as being sourced from other researchers. Where other written sources have been quoted, then:

a. Their words have been re-written but the general information attributed to them has been referenced

b. Where their exact words have been used, then their writing has been placed in italics and inside quotation marks, and referenced.

5. This dissertation does not contain texts, graphics or tables copied and pasted from the internet, unless specifically acknowledged, and the source being detailed in the thesis and in the Reference section.

Signed: Gbadega Peter. A

Date: 28th November 2018

DECLARATION 2 - PUBLICATIONS

DETAILS OF CONTRIBUTION TO PUBLICATIONS AND CONFERENCE PRESENTATIONS that form part and/or include research presented in this thesis (include publications in preparation, submitted, *in press* and published and give details of the contributions of each author to the experimental work and writing of each publication)

Publication 1

Gbadega Peter. A, AK. Saha, "Power Losses Assessments of LCC-based HVDC Converter Stations Using Datasheet Parameters and IEC 61803 STD", 2018 proceedings of the 26th Domestic Use of Energy international conference (DUE), 3-5 April 2018, Cape Peninsula University of Technology (CPUT), Cape Town Campus, Cape Town, South Africa, pp. 173-181; Electronic ISBN: 978-0-9946-7594-1, Print on Demand(PoD) ISBN: 978-1-5386-6732-3, DOI: 10.23919/DUE.2018.8384394, Publisher: IEEE.

Publication 2

Gbadega Peter. A, AK. Saha, "Comparative study of Harmonics Reduction and Power Factor enhancement of six and 12-pulses HVDC system using passive and shunt APFs Harmonic Filters", 2018 proceedings of the 26th Domestic Use of Energy international conference (DUE), 3-5 April 2018, Cape Peninsula University of Technology (CPUT), Cape Town Campus, Cape Town, South Africa. pp. 182-190; Electronic ISBN: 978-0-9946-7594-1, Print on Demand (PoD) ISBN: 978-1-5386-6732-3, DOI: 10.23919/DUE.2018.8384395, Publisher: IEEE.

Publication 3

Gbadega Peter. A, AK. Saha, "Loss Study of LCC-based HVDC Thyristor Valves and Converter Transformers using IEC 61803 Std. and Component Datasheet Parameters", 2018 proceedings of IEEE PES & IAS Power Africa international conference, 26-29 June 2018 Cape Town. Hosted by Tshwane University of Technology, Pretoria, South Africa, pp. 32-37; Electronic ISBN: 978-1-5386-4163-7, USB ISBN: 978-1-5386-4162-0, Print on Demand (PoD) ISBN: 978-1-5386-4164-4, DOI: 10.1109/PowerAfrica.2018.8521016, Publisher: IEEE

Publication 4

Gbadega Peter. A, AK. Saha, "Loss Assessment of MMC-based VSC-HVDC Converters using IEC 62751-1-2 Std. and Component Datasheet Parameters." 2018 proceedings of IEEE PES & IAS Power Africa international conference, 26-29 June 2018 Cape Town. Hosted by Tshwane University of Technology, Pretoria, South Africa, pp. 38-43; Electronic ISBN: 978-1-5386-4163-7, USB ISBN: 978-1-5386-4162-0, Print on Demand (PoD) ISBN: 978-1-5386-4164-4, DOI: 10.1109/PowerAfrica.2018.8521180, Publisher: IEEE.

Publication 5

Gbadega Peter. A, AK. Saha, "Loss Assessment of Key Equipment on LCC-Based HVDC Converter Stations" 2018 proceedings of IEEE PES & IAS Power Africa international conference, 26-29 June 2018 Cape Town. Hosted by Tshwane University of Technology, Pretoria, South Africa, pp. 44-52; Electronic ISBN: 978-1-5386-4163-7, USB ISBN: 978-1-5386-4162-0, Print on Demand (PoD) ISBN: 978-1-5386-4164-4, DOI: 10.1109/PowerAfrica.2018.8521107, Publisher: IEEE.

ACKNOWLEDGEMENTS

I want to give all the glory to God for the gift of life and the strength granted to me in the course of this research and for making it a possibility.

I would also like to appreciate my supervisor the person of Prof. A.K Saha, for all his contributions and supports. I cannot imagine the success of this program without him. His criticism and scrutiny have thus helped me a lot. You did turn a better person out of me through your generous support and guidance.

I would also like to express my beloved gratitude to my parents Mr. and Mrs. Gbadega for their advice and encouragement throughout my study period. My profound gratitude also goes to my siblings: Mr. Emmanuel, Mr. Samuel, Miss. Deborah, Miss Favour and little Mr. Jomiloju for their relentless support.

I would also appreciate the person of Engr. Awogbemi Omojola for his motivations, encouragement and support throughout my stay here in South Africa, may God raise help for you in all your endeavors.

I would also show my profound gratitude to the person of Engr. Babatunde Olubayo .M, who was encouraging and mentoring me on what is expected of me as a researcher, I really do appreciate his relentless efforts throughout the tenure of this research work.

Finally, I hereby appreciate my lovely friend Amu Mary, who has been there for me in terms of good advice that strengthen me to carry on with the research when I feel like been reluctant to proceed.

ABSTRACT

In transmission systems, particularly when the power is transported over a transmission line of distance 500 km and above, a considerable amount of power is lost during power system operations, which consist of all the components that are used in generation and transmission of power. Therefore, it is imperative to estimate the power losses due to some power equipment on the electrical network during transmission systems. More so, it is of importance to comprehend the pros and cons of both LCC-based and VSC-based transmission systems and subsequently carry out detailed research on power losses of both systems using the calculation methods listed in standards. It is the purpose of this research work to determine and calculate the overall losses of various equipment of high-voltage direct current (HVDC) converter stations under operating and standby modes using standards IEC 61803, IEEE 1158, IEC 62751-1-2 and the component datasheet parameters (Phase Control Thyristor Type DCR3030V42 and Dynex IGBT module DIM1200ASM45-TS000). The loss calculations in this research work are precisely applicable to all parts of the converter station and cover standby, partial-load, and full-load losses using the standardized calculation methods stipulated in the aforementioned standards. Furthermore, Switching losses, as well as conduction losses are included in the calculation using a simplified analytical model, based on the standards IEC 62751-1-2 and power semiconductor (Dynex) datasheet information. Therefore, an analytical method was adopted to estimate the power losses of VSC-based HVDC system of two-level, three-level and modular multilevel VSC configurations. Finally, the various HVDC technologies (circuit simulations) models were implemented in the Matlab-Simulink environment. The Matlab models were used to estimate the power losses of these technologies converter losses for various operating conditions. The simulation technique has been devised to provide an independent crosscheck on the results obtained using idealized mathematical representations (analytical technique). Subsequent to these circuit implementations, some results were obtained and consequently validated with other commercial power loss simulation tools or electronic software, such as Semisel and Melcosim. The use of different contrasting techniques to provide equivalent characteristics losses calculations provide a good method of validating the feasibility of the HVDC technology loss study, giving confidence in the results for the converter losses that have been obtained. This research work is based on an existing method of loss evaluation, but strictly followed the IEEE loss calculation methods stipulated in standards. The major contribution of this research work was the new approach adopted in the power loss evaluation of various HVDC technologies such as the LCC-based and VSC-based topologies of the converter stations using the idealized mathematical representations stipulated in standards IEC 61803, IEEE 1158, IEC 62751-1-2 and the component datasheet parameter, which signifies the novel output of this research work.

TABLE OF CONTENTS

LIST OF FIGURES

LIST OF TABLES

LIST OF ACRONYMS

AC	Alternating Current
BJT	Bipolar Junction Transistor
CEA	Constant Extinction Angle
CIA	Constant Ignition Angle
CTL	Cascaded Two-level Converter
DC	Direct Current
ESR	Equivalent Series Resistance
FWD	Freewheeling Diode
HVAC	High Voltage Direct Current
HVDC	High Voltage Alternating Current
IEC	International Electro-technical Commission
IEEE	Institute of Electrical and Electronics Engineers
IGBTs	Insulated Gate Bipolar Transistors
LCC	Line Commutated Converter
MMC	Modular Multilevel Converter
MOSFET	Metal-oxide-semiconductor Field-effect Transistor
PID	Proportional Integral Derivative
PLL	Phase Locked Loop
p.u.	Per unit
PWM	Pulse Width Modulation
RMS	Root Mean Square
ROW	Right of Way
SSOA	Switching Safe Operating Area
Std.	Standards
VSC	Voltage Source Converter

LIST OF SYMBOLS

Symbols	Definitions	Units
α	converter firing angle (alpha)	Degree (°)
β	converter ignition angle (beta)	Degree (°)
π	pi (3.142857143)	dimensionless
Ω	Unit of resistance	ohm
γ	converter extinction angle	Degree (°)
μ	overlap angle	Degree (°)
KW/MW	Unit of power	kilo watt (10^3)/ megawatt (10^6)
kV	Unit of voltage	kilo-volt (10^3)
km	Unit of distance	kilometre
kA	Unit of current	Kilo-Ampere
R_n	Effective resistance	Ω
n	Harmonic number	dimensionless
I_n	Harmonic current	kA
P_R	Reactor loss	kW
X_{Ln}	Reactor reactance	Ω
f	Frequency	Hz
Q_n	Quality factor	dimensionless
P_m	Magnetization loss	kW
P_o	Direct current losses	kW
P_h	Hysteresis loss component	p.u
P_e	Eddy-current loss component	p.u
I_o	dc current	Ampere
E_R	Capacitor bank rated voltage	V
R_C	Capacitor bank total resistance	Ω
P_C	Filter capacitor losses	Watt (W)
m	Modulation index	dimensionless
E_{on}	IGBT turn on switching energy	Watt (W)
E_{off}	IGBT turn off energy loss	Watt (W)
f_{sw}	PWM switching frequency	kHz
D	PWM duty factor	dimensionless
$V_{ce.sat}$	IGBT saturation voltage drop	Volt (V)
∅	Phase angle between output voltage and current	Degree (°)

CHAPTER 1
INTRODUCTION

1.1 Background

In power transmission systems, the evaluation of transmission losses is very imperative and it is essential that a transmission system with minimal power losses be designed. The optimization of the overall system performance can be achieved through the power loss estimation in transmission system by evaluating the economic and technical benefits of the system and understanding which of the components on the high voltage direct current (HVDC) network that contribute to maximum power losses. The estimations of losses provide the breakdown and calculation of losses that exist in the operating system for designers and operators to help estimate the economic and technical benefit of the project. For devices that produce large amount of losses, the suppliers need to know how and where losses are generated in order to determine the ratings of component and equipment and further increase operational efficiency of the transmission system by optimization design. Sufficient accurate loss figure is required by the customer which allows effective comparison of cost in a procedure of bid [1, 2].

It is important to study and critically analyze the losses including HVDC system to actually improve the economics of HVDC system [3]. The losses in an HVDC converter station are composed of the losses of various pieces of equipment, each of which has its own loss versus load relationship. The essence of this research work is to determine and calculate the overall losses of various topologies of high-voltage direct current (HVDC) converter stations utilizing both analytical and simulation approaches in order to validate the feasibility of HVDC technology loss study, giving confidence in the results for the converter stations losses that have been obtained. The HVDC technologies considered in this research work are LCC-based and VSC-based (two-level, three-level and modular multilevel topologies), and these losses are calculated during various operating conditions using the idealized mathematical representations stipulated in IEC 61803, IEEE 1158, IEC 62571-1-2 and the component datasheet parameters. It is worthy of note that LCC-based HVDC system uses Thyristor-valve and VSC-based HVDC uses IGBT as their switching electronic component, respectively. As such, the method of estimating their loss profile differs, because they are different electronic component entirely and their mode of operation is different. More so, it is difficult to determine converter stations losses by the traditional method of direct measurement, since losses are usually less than 1% of the power transferred, and it leads to inaccuracy of this method. Therefore, in accordance to the standard IEC 61803 (LCC-based) and IEC 62751-1-2 (VSC-based), loss calculation models for converter station equipment under different operational conditions are established [4], [6].

The loss calculation in this research work are precisely applicable to all parts of the converter stations and cover standby, partial-load, and full-load losses and methods of calculation and measurement [4, 5]. HVDC converter-stations consist of a number of various pieces of equipment, the loss calculation procedures vary among various pieces of equipment, and it is the agreement of the industry that the total losses cannot readily be obtained by either factory or field-testing alone [6].

1.1.1 LCC-based HVDC Converter Station Losses

The losses of HVDC system are mainly composed of converter station losses, HVDC transmission line and electrode line system. However, the line system losses are sometimes ignored because of its small quantity. The total losses of converter stations are the sum of all equipment losses [7]. The converter station equipment includes the valve, transformer, AC filters, shunt capacitor, DC reactor, DC filters and auxiliary equipment. The standards of IEC 61803 and IEEE 1158 ‘’Determination of power losses in high voltage direct current (HVDC) converter stations’’ list the calculation methods of each equipment in details. It is difficult to determine converter stations losses by the traditional method of direct measurement, since losses are usually less than 1% of the power transferred, and it leads to inaccuracy of this method [4, 6]. In accordance to the standard of IEC 61803, loss calculation models for converter station equipment under different operational conditions are established [8].

1.1.1.2 Classification of Losses of an LCC-based Converter Valve

The thyristor valve of LCC-based converter mainly consists of the following parts; they are thyristors, voltage-grading capacitor, damping capacitors, firing and detecting system of the thyristor and saturated reactors. Note that about 85%-95% of the thyristor valves losses occur at the damping resistors and the thyristors. The LCC-based thyristor valves have the following principal loss mechanisms, which are illustrated in figure 1-1 [3].

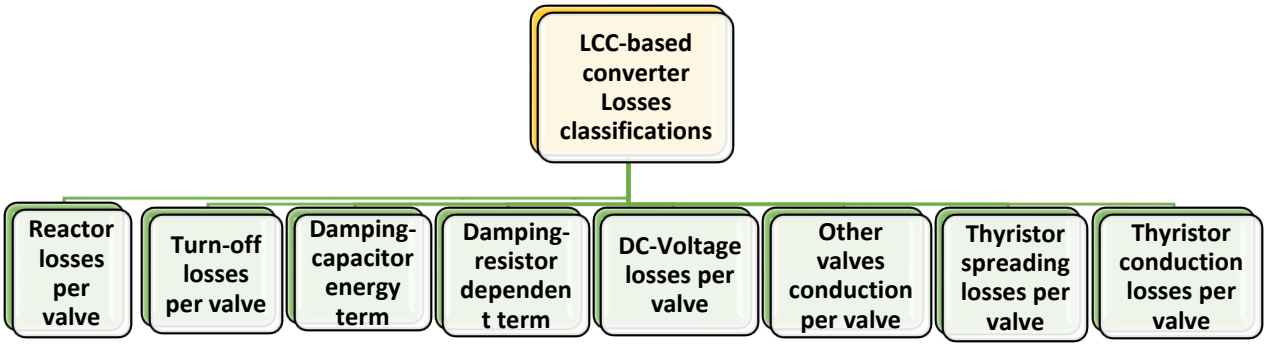

Figure 1-1: Classification of losses in an LCC-based converter valve unit [9]

Figure 1-1 shows the breakdown of the classification of the losses in an LCC-based converter valve unit. The summation of these losses results to the total loss contribution by the converter valves. The loss contribution of the converter valve is larger than any equipment on the converter station, so therefore, there is need to analyze these losses to know the actual losses generated by this equipment.

1.1.2 VSC-based Converter Valves Losses

Voltage source converter high voltage dc (VSC-based HVDC) transmission is popular and noticeable due to the recent innovation of controllable semiconductor devices and bulk power transmission for long distance of about 500 km and

above. VSC-HVDC is most superior to its counterpart, conventional HVDC (LCC) in applications, but the loss contributions of the system is relatively very high. Therefore, in respect of this, it would be an essential technique, practice and application value to determine and evaluate the losses of VSC-HVDC transmission [5, 10].

Therefore, it is worth noting that the VSC-based HVDC system configuration is similar to its counterpart technology, LCC- based HVDC and it includes the converter valves, AC filters, DC-Smoothing reactor and transmission lines etc. The analysis and calculation techniques of the losses in VSC-based HVDC transmission is not absolutely the same as the conventional HVDC transmission [1, 6]. The total losses of VSC-based HVDC technology is obtained by summing the losses of individual converter station equipment together utilizing the standards IEC 62751-1-2, "The power losses in voltage sourced converter (VSC) valves for high-voltage direct current (HVDC) systems" [5, 11]. The VSC-based topologies considered in the research work are 2-level, 3-level and modular multilevel converters. The mathematical representations of both 2-level and 3-level VSC-based converter topologies are well explained in these refs. [12, 13].

More so, an example of a unique voltage source converter (VSC) topology with immense potential for applications of high voltage direct current (HVDC) transmission is the modular multilevel converter (M2C). The M2C-based configuration has core features of low switching frequency and flexibly controlled so that its loss figures are smaller than that of the three-level and two-level VSC-based configuration [14]. Moreover, the detailed techniques adopted for estimating the power losses in the valves for a modular multilevel converter HVDC system are done in accordance with standards IEC 62751-1-2, "Power Losses in Voltage Source Converter (VSC) Valves for High-Voltage Direct Current (HVDC) Systems" [5, 15].

1.1.2.1 Classification of Losses of a VSC-based Converter Valve

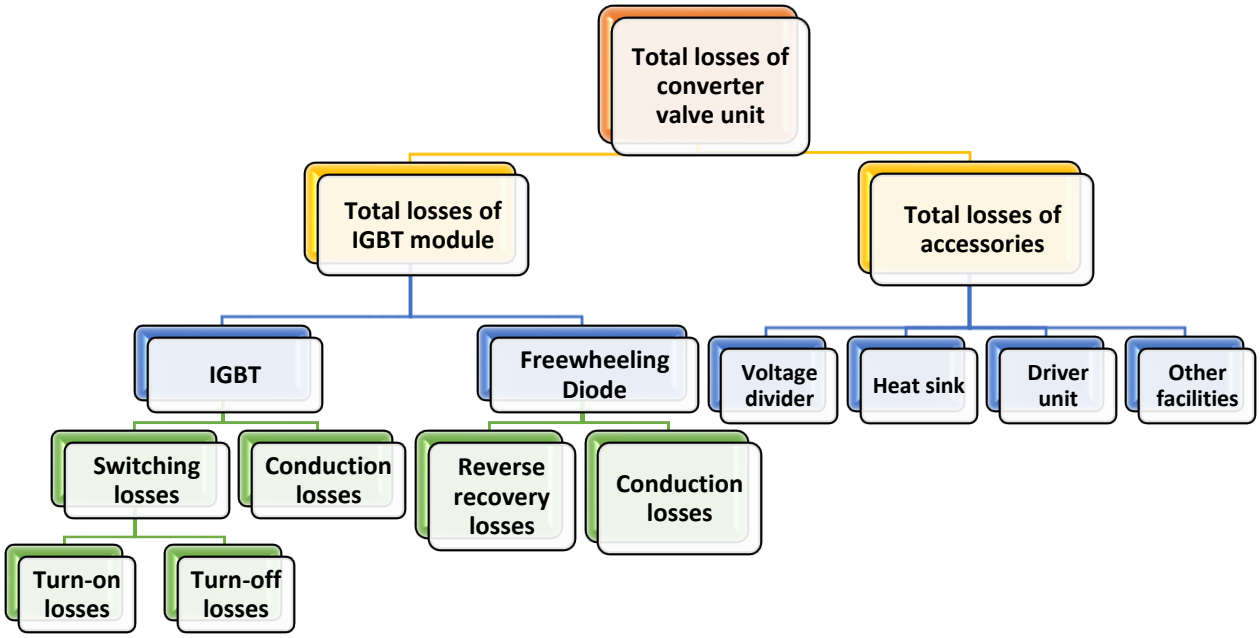

Figure 1-2: Classification of losses in a VSC-based converter valve unit [16]

Figure 1-2 shows the breakdown of the classification of the losses in VSC-based converter valve unit. The summation of these losses results to the total loss contribution by the converter valves. The loss contribution of the converter valve is larger than any equipment on the converter station due to his high switching frequency, so therefore there is need to analyze these losses to know the actual losses generated by this equipment.

In order to implement loss evaluation, the losses of converter valve would be segmented into various parts, as depicted in figure 1-2. The output characteristics curves are mostly used to calculate the IGBT and FWD steady state losses and are calculated based on the collector voltage-current characteristics in the transient state. More so, the conduction and switching losses of an IGBT device generate about half of the converter valve and the switching losses of the freewheeling diode (FWD) generates about one-third of the entire energy dissipation. An infinite proportion of losses results from the other parts of the module [17]. The proportion of the IGBT device and converter losses would reduce as the converter operates in the rectifier state, the reason being that the current flows through the freewheeling diode (FWD) most of the time, therefore, its losses are usually less than that of the IGBTs. Furthermore, changing the operating states and structure of the valves most of the time have an effect on the converter valve losses. The essential aspects to consider are the topology of the converter, types of the converter valve, scheme of valve driver, accessories of valve unit and temperature of the device, which are well explained in these references [18, 19].

The evaluation of power losses basically, provides the analysis and computation of losses that occur during the operating system in order for the designers and operators to assist in evaluating the technical and economic advantages of the project. Therefore, there is a dire need for the supplier to come to the knowledge of how and where the losses are generated in order to determine the equipment ratings and subsequently increase the operation efficiency of transmission system adopting the use of optimization design for the equipment that generates large losses [10, 20]. Power loss evaluation during the design stage of the VSC-based HVDC technology is very imperative, reason being that, it permits the designers to enhance the performance of the overall system through a compromise of various design indices [21].

1.1.3 Loss Characteristics of HVDC Technologies

In HVDC technologies, the main converter station equipment include converter transformer, converter valves, active power compensation equipment, smoothing reactor, DC capacitor filters etc. Firstly, the losses in a practical HVDC converter station are composed of equipment, each of which has its own loss versus load relationship. The valve losses are not proportional to the load current squared. More so, when the converter stations are energized, but in the standby state, the thyristor valves appear blocked, and for this reason, different loss mechanisms then apply from those that are found in normal operation. Secondly, during HVDC operation, a number of harmonics are generated both at the AC side as well as at the DC side of the converter station. Due to the flow of the harmonic current through the smoothing reactor, converter transformer, AC and DC filters, additional losses will be produced in the station. Lastly, note that, the loss varies because at different load levels, the equipment put into operation at converter stations is not exactly the same [6, 10]. As a result, the power loss calculations of the converter station are quite complex. Generally, the converter station losses are evaluated by means of randomly selecting various load points between no-load and

full-load conditions. Therefore, the converter station losses are most of the time analyzed or evaluated using two recommended losses, which are standby and total operating losses. [22, 23].

1.2 Research Motivation and Problem Statement

Recently, in transmission networks, when bulk of power is to be transmitted over a long distance, high voltage direct current (HVDC) systems have more advantages over high voltage alternating current (HVAC) systems. More so, the advancements in power electronics and reduction in costs serves as the major driving factors, subsequently, making high voltage direct current more reliable and attractive. The prospects of high voltage direct current (HVDC) transmission systems are even greater as the need for cross-country power lines and inter-country intensifies, although this already in existence in the Southern African region.

Globally, there is a constant search for various methods to reduce cost, improve reliability, minimizing the environmental impact of a power line and finally, minimum power loss during transmission. These have over the years increased challenges in the evolution of the design techniques to ensure to meet the problems the power industry faces today. The above problems could be addressed and solved if the transmitted power from the sending end could be monitored to prevent a large amount of power consumed by some of the equipment on the electrical networks.

It is most technically and economically expedient in many circumstances to introduce high voltage direct current (HVDC) links into electrical network during transmission of electrical power, which may be the only feasible technique of power transmission most especially when the distance between the station and load Centre is very far apart that is, a distance of 500 km and above. In application, DC transmission is given priority when the distance by cable or land is too long for economic and stable AC transmission, which results to the introduction of converter stations at both ends of the electrical supply systems. The inclusion of these converters produce a large amount of power losses, that is, they reduce the power transmitted from the rectifier converter to the inverter converter. More so, longer transmission distances lead to higher energy losses as well as higher investment costs [24-26].

However, the HVDC converter station losses are not only produced by the converters alone, some other equipment on the converter stations also produce power losses, some of the equipment are the converter transformer, the AC harmonic filters, the DC-smoothing reactor and the auxiliary equipment like cooling tank. However, the losses of the auxiliary equipment are infinitesimal compared to the losses generated by other station equipment [27].

Voltage source converter based on the HVDC system (VSC-based HVDC) are often used in transmission region and accomplished good operating results. On the other hand, the losses of VSC-based HVDC system are larger than the conventional HVDC, which tends to be the main hurdle to apply VSC-HVDC to high power transmission, in respect of this fact, the loss characteristics of VSC has become an important issue to investigate. The VSC-based HVDC losses have a large converter station loss proportion due to the low voltage level and most especially the high switching frequency characteristics of VSC.

Different methods are well known majorly for the prediction of losses in power semi-conduction circuit. One of the methods adopted by researchers is the complete numerical simulation of the circuit by special simulation programs with integrated or parallel running loss calculation. Another method that could be adopted is to estimate the electrical behavior of a typical circuit model analytically using the semiconductor device datasheet parameters given by the manufacturer (i.e. the voltage and current of the power semiconductors) and available standards to determine the loss contribution by the semiconductor device and the other station equipment losses at large. Moreover, extensive and complex mathematical analyzes are required for the computation of the station losses, for quick results and minimized calculation effort, some of these equations are further simplified for easy analysis. For this reason, it is of interest to analytically evaluate the power losses that occur in both VSC-based HVDC technology and the LCC-based HVDC technology and subsequently compare the results obtained with the results obtained using other loss simulation environment in order to draw conclusions based on their loss proportion [11, 28, 29].

1.3 Research Questions

Losses on the electrical network are detrimental to the perfect operation of the converter stations and other equipment on the electrical grid. Therefore, it is most pertinent to investigate the sources of these losses on the electrical power system and subsequently adopt critically analyses on the loss proportion of each of the sources of these losses. In respect of the above suggestion, these result to the following research questions.

- What are the necessary procedures to determine power losses in both LCC-based HVDC technology and VSC-based HVDC technology?
- What are the reasons why the losses of HVDC converter stations need to be accurately measured and evaluated?
- What are the loss contributions of each equipment of the LCC-based HVDC converter stations analytically?
- What are the loss contributions of each equipment of the VSC-based HVDC converter stations analytically?
- What are the other ways the results obtained analytically could be compared in order to validate the genuineness of the results obtained to justify the viability of the HVDC loss study?
- Based on the results obtained using other platforms, what are the percentage differences between the analytical approach and the software (simulation) approach?
- What are the conclusions drawn on the comparison of the technologies based on their loss measures?

1.4 Research Aims and Objectives

The overall aim of this study is to be able to predict the loss figure or profile of HVDC technologies most exactly, likewise to clearly show the loss dependency on some of the circuit parameters and operating point and besides to have a good basis for the comparison of both converter systems. Furthermore, the objective of this research work is to provide an analytical overview of power losses determination of HVDC converter stations using the following transmission technologies, voltage source HVDC converter and Line-commutated HVDC converter technologies. Furthermore, the feasibility of the loss study of HVDC technologies using standardized calculation method (analytical)

is therefore validated using other loss simulator environments such as Matlab-Simulink, Semisel and Melcosim. It is confirmed and accepted that the continuous development of power electronics present cost-effective opportunities for the utilities to exploit. So therefore, HVDC transmission system remains a key technology as far as bulk-power distant transmission is concerned.

In order to achieve these aims, the following objectives shall be accomplished, namely:

- Investigation and identification of the sources of power losses on HVDC electrical network.
- Evaluation of the loss contributions of each of the sources of LCC-based HVDC converter stations losses using datasheet parameters and the available standards.
- Estimation of the loss proportions of the individual components of VSC-based HVDC converter stations using datasheet parameters and available standards.
- Critical analytical assessments of the percentage losses of key equipment on the converter stations and subsequently comparing the results obtained with the results obtained from simulation environment.
- Evaluation of the losses of various HVDC technologies using other loss simulation platforms such as Matlab-Simulink, Melcosim and Semisel to validate the viability of the results obtained using standardized calculation methods (analytical). The feasibility of the loss study of various HVDC technologies was also investigated based on the results of these various loss calculation methods.
- Comparison of the various HVDC technologies using the loss mechanism of each technology to measure stability, reliability and efficiency of the power transmitted.

1.5 Structure of the Dissertation

This thesis presents an overview and progressive arrangement of chapters. Four Publications (P4) also support this thesis. The scientific contribution of the thesis is organized as follows:

Chapter 1 introduces the subject matter, and then gives an overview and background of the aim and objectives of the study. The LCC-based and VSC-based converter valves with respect to their various losses classifications were expressly discussed. Chapter 2 presents the literature review on loss taxonomy and losses of main equipment of both LCC-based and VSC-based HVDC technologies, the various methods of determination of power losses in converter stations with reference to standards IEC 61803, IEEE 1158, IEC 62571-1-2 and datasheet parameters and finally, a synopsis of the previous work done on similar studies. Chapter 3 presents the materials and the research methodology followed in the course of the study. Chapter 4 presents the results and analyses of power losses determination of LCC-based HVDC converter stations. Chapter 5 presents the results and analyses of power losses calculations of VSC-based HVDC converter stations. Chapter 6 presents the Model Simulation and results of power losses calculations of HVDC technologies. Chapter 7 concludes the dissertation and provides recommendations for further work applicable in the research field.

1.6 Summary

This section introduces the subject matters of the research work, and further discusses on the essence of the study, why it is very important to investigate and evaluate the transmission losses. More so, all the methods and the instruments utilized during the course of this research were discussed. Furthermore, it was stated that, in HVDC converter station, there is no single piece of equipment that produces dominating losses, unlike in AC substation where the transformer losses are the dominating factor. Thus, in respect of this, the losses in an HVDC converter station are composed of the losses of various pieces of equipment, each of which has its own loss calculation methods. Notwithstanding, there are some equipment that contribute large amount of losses such as converter transformer and the converter valves, but note that, the converter stations total losses is the sum of all the equipment losses of the converter station. Finally, the various types of HVDC converter stations and their classifications were fully explained. More so, the research motivation, problem statement, questions, aim and objectives were stated.

CHAPTER 2
LITERATURE REVIEW

2.1 Introduction to HVDC Technology

The advancement of HVDC technology is aided by the recent rapid development of power electronic components such as a thyristor, IGBT etc. in the power electronics field [30]. More so, it is of importance that the converters used during transmission process should be well configured. The reason why the converters are well configured is to increase power transfer capabilities, reduces harmonic, reduce transmission losses and increases reliability, in that, it offers high tolerance to fault along the line. Due to some of the essential benefits of long-distance transmission application, the high voltage direct current has a lot of attention over the past few years, as a result of its inherent benefits. It is widely used for bulk delivery of power over long distances, also for the stability of AC lines, renewable energy integration, power control, long submarine transmission and asynchronous systems interconnections. Furthermore, reduction in the right of way (ROW) is another merit over AC system. [31, 32].

South Africa currently has a single High Voltage Direct current (HVDC) system, which is the Cahora Bassa HVDC link that connects the hydroelectric scheme at the Cahora Bassa dam in Mozambique to the Apollo Station in South Africa. The scheme is rated to transmit 1920 MW at ±533 kV over a distance of 1420km and is predominantly used as a bulk power transmission tool into the South African grid [33]. Due to the following merits obtained from LCC-based HVDC, which are efficient and cost-effective power transmission for many applications and reliability provided from this advanced technology, the LCC-based HVDC will persist to be used for bulk power HVDC transmission over several hundred MW. [33, 34].

2.2 Loss Taxonomy of LCC-HVDC Technology

The losses of HVDC technology are mainly composed of the losses of converter stations, HVDC transmission line and electrode line system as shown in fig 2-1. Sometimes the line system losses are ignored because of its small quantity. The cross-section of the conductor and the length of the transmission line determine the loss of DC transmission lines. Therefore, for long distance transmission, the dc line loss is generally about 5%-7% of the rated transmission capacity, which accounts for the most part of the DC transmission system [35].

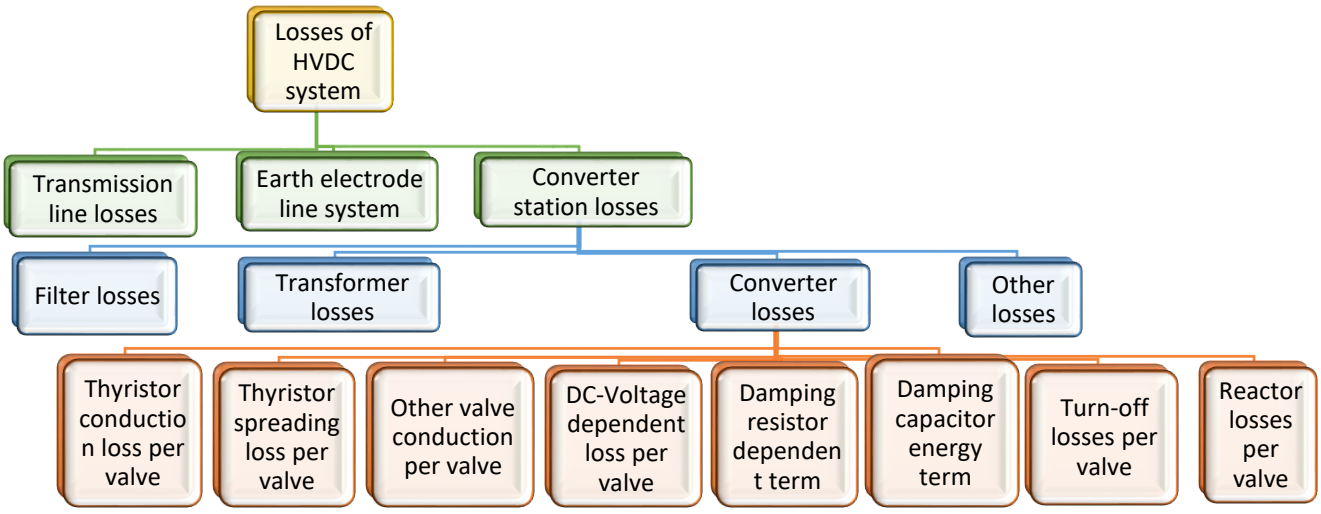

Figure 2-1: Loss taxonomy of an LCC-HVDC system [36]

Fig 2-1 shows the pictorial classification of losses of LCC-HVDC system. The converter stations equipment at both terminal points have several loss mechanisms and types. Therefore, to accurately determine the converter stations losses is quite difficult and complex analytically during the process of evaluating the loss of DC transmission systems. Note that, to determine the converter stations total losses, the converter station main equipment losses are measured and calculated respectively, the individual results of the losses are further added together to obtain the total losses. Generally, converter station loss is nearly 0.5%-1% of the rated transmission capacity of the converter stations [36, 37].

2.3 Loss of Main Equipment in LCC-based HVDC Converter Stations

The LCC-based HVDC converter stations are made up of some equipment such as AC filters, thyristor valves, smoothing reactors, converter transformers etc. Note that, to calculate the converter stations losses, the loss contributions of each equipment must be considered. Therefore, the loss compositions of each equipment are discussed below [6, 37].

2.3.1 Loss of Thyristor Valve

The thyristor valve is composed of saturated reactors, thyristor, damping capacitor, and resistor, DC voltage grading resistors, voltage-grading capacitors and the firing and detection system of the thyristor. The thyristors and damping resistors produce about 85%-95% of the thyristor valves losses. Currently, there is no suitable method available for direct thyristor valve measurement, since the waveform of thyristor valves in operation is quite complicated. As such, it is of common practice to compute the different loss components of the thyristor valves individually, then subsequently sum together the individual component losses to obtain the total thyristor valve losses [8, 38].

2.3.1.1 Sources of Thyristor Valve Losses

A valve consists of various components, meanwhile, most full-load losses (typically 85%-95%) are produced in just two components, which are the damping resistor and the thyristor. Firstly, the five principal loss mechanisms present in thyristor valves are, thyristor turn-on switching loss, spreading loss, on-state loss, turn-off switching loss, off-state and reverse leakage loss [9]. Secondly, the four principal loss components present in damping resistor are damping-resistor-dependent term, change of capacitor energy term, circuit inductance stored energy term, and damping resistor loss (dispersion effect). Furthermore, there are still other related losses, like current related losses (i.e. conductor losses, reactor core losses) and voltage related losses (i.e. dc grading circuit losses, water circuit losses and electronic losses) [9, 39, 40].

2.3.1.2 Loss Generation in Thyristor Valves

It is worthy of note that, whenever the integral of $V \times I$ product is taken over a full cycle, measured at the valve terminals, is not equal to zero, valve losses are generated. In application, practical valves losses are produced in each power frequency cycle during four distinct periods, at turn-on, during load current conduction, at turn-off, and during the blocking interval between conduction periods [16, 41]. Firstly, the valve is characteristically of a low (but not zero) impedance during the conduction periods and it is often times during these periods that load current flows, as a result of these load currents drift, subsequently leads to conduction losses in the valve. Secondly, the thyristors are fired into conduction most times by the application of a gate pulse at turn-on. Since thyristor valve exhibits very high impedance nature before conduction, at conduction, each thyristor switches to a low but finite impedance state in a time-scale feature of the thyristor adopted [42, 43].

2.3.1.3 Loss Determination Procedures of Thyristor Valves

The recommended procedures stated in IEC standard 61803, “Determination of Power Losses in High-voltage direct current (HVDC) Converter Stations” provide a total loss figure for valves based on the summation of each loss components. Therefore, the individual loss components are determined by applying standardized computation methods using the obtained data from confirmable sources [43]. Due to the fact that, the computations are done on key components of the thyristor valve, which contribute more losses during operating and standby modes, the answers obtained might not be precise. It is certain that all major loss mechanisms are determined and that in terms of accuracy, the results are more accurate than the alternative method of direct measurement at the site. More so, different loss components will assume difference significances [9, 44]. Note that, all losses are evaluated on a per-valve basis, in which a valve is taken to be one arm of a three-phase line commutated Converter Bridge. The equations used in this research work to calculate the eight principal thyristor power losses are elaborately stipulated in reference [9], the IEC standard 61803, “Determination of Power Losses in High-voltage Direct-Current (HVDC) Converter Stations”. The eight principal thyristor loss mechanisms include thyristor conduction loss per valve, thyristor spreading loss per valve, other valve conduction losses per valve, DC voltage-Dependent loss per valve, damping resistor loss per valve, damping-capacitor loss per valve, turnoff losses per valve and reactor losses per valve[16, 45].

2.3.2 Converter Transformer Losses

The converter transformer losses are of two kinds, which are load loss and no-load loss. The currents that flow through the converter transformers' windings contain harmonics whose magnitudes depend on the converter station operating parameters. The current-dependent load losses in the transformer due to the non-sinusoidal current wave shapes are greater than those that would occur with a sinusoidal current of the same RMS value at fundamental frequency [9]. No consensus has yet been reached recently, in the industry on how load losses in HVDC converter transformers should be estimated or measured. The major issue is how to account for the load losses caused by the harmonic currents, which vary with load, transformer leakage reactance, and converter fire angle [16, 43].

2.3.2.1 Sources of Converter Transformer Losses

When evaluating the losses of HVDC converter transformer, it is recommended that two types of losses be distinguished: standby losses and operating losses. During standby operation i.e. the transformers energized with the valve blocked, the applied voltage is the normal ac system voltage, which usually contains no appreciable harmonics [9, 46]. During operation with the valves unblocked, harmonic voltages, appear on the valve windings due to the flow of harmonic currents through the transformer. The magnitudes of the harmonic voltages vary with the operating parameters of the converter station. The harmonic voltages on the line windings are much lower in magnitude than those on the valve windings, and this is as a result of the low harmonic impedance of the ac filters. The converter transformer load losses consist of three main components, they are, winding dc resistance loss (I^2R loss), winding stray loss, and stray loss in the structure and external parts, such as the core, clamps, and tanks [16, 47]. Converter transformers load losses can be determined and measured by three methods, which are discussed below.

2.3.2.3 Method I

In this method, the converter transformers load losses are determined by measuring the converter transformer effective resistance at different harmonic frequencies, and subsequently estimating the total load losses as the sum of the losses due to each harmonic currents. The load loss admits expression as [48]:

$$Load\ loss = \sum_{n=1}^{n=49} I_n^2 R_n \tag{2-1}$$

where

R_n=The effective resistance, in ohms, at harmonic n.

I_n=The current, in amperes, at harmonic n

n= The harmonic number.

2.3.2.4 Method II

This is an approximate method of determining load losses, which do not require measurements at harmonic frequencies. It is based on a typical relationship between the effective resistance of converter transformers (in per unit of fundamental frequency resistance) and frequency. The relationship was developed from the measurement made in accordance with Method 1 on several converter transformers supplied on recent HVDC projects and then the effective

resistance is computed. Consequently, the converter transformer losses can be obtained by simply summing together the calculated losses of each harmonic orders.

The procedure consists of the following steps:

Measure the load loss of the converter transformer at power frequency in accordance with IEEE C57.12.90-1987.Calculate the effective resistance at the fundamental frequency (R_1) from the measurements [4]:

$$R_1 = \frac{P_L}{I^2} \tag{2-2}$$

where

P_L=The measured load loss in watts for one phase at current I in amperes

Determine the effective resistance at other harmonic frequencies

$$R_n = R_1(kn) \tag{2-3}$$

where

kn= relative resistance or harmonic factor.

2.3.2.5 Method III

This method only measures the converter transformers' losses under power frequency and a frequency higher than 150 Hz, such that it is needless to measure the loss at a frequency of the order of 1 KHz and the measurements are reduced to two. The converter transformer windings eddy-current losses and the stray losses of other structures are calculated by using the measured results, and some well-known equations are used to calculate the total load loss [48].

Method 1 is more precise than method 2, by the virtue of comparing the above three methods, but the required instrumentation and measuring technologies are not owned by all the manufacturers. Furthermore, the Method 1 accuracy is as a result of the measurement accuracy. The converter transformer's load loss of typical design is intended to be calculated approximately by Method 2. Note that, the accuracy of Method 2 may decrease, if the transformer design is greatly different from the typical design. Method 3 only requires measurement under two frequencies and eliminates the necessity of measuring the losses at frequency of the order 1 kHz. In spite of this, the required measuring accuracy can be achieved [34, 41].

The characteristic harmonic currents are calculated from the following:

$$I_n = \frac{3.F.E_{ph}}{\pi.n.X_t} \tag{2-4}$$

where

I_n= The current, in amperes, at harmonic n

n= The harmonic number.

X_t= The converter transformer reactance at fundamental frequency, in ohms

$$F = [k_1^2 + k_2^2 - 2k_1k_2\cos(2\alpha + \mu)]^{1/2} \tag{2-5}$$

$$k_1 = \frac{\sin\left[(n-1)\frac{\mu}{2}\right]}{n-1} \quad (2\text{-}6)$$

$$k_2 = \frac{\sin\left[(n+1)\frac{\mu}{2}\right]}{n+1} \quad (2\text{-}7)$$

E_{ph}= The equivalent line-to-neutral voltage on the valve side of the converter transformer calculated by multiplying the line-to-neutral voltage on the line side by the turns ratio (including the effect of tap position), in volts RMS

α= The firing delay angle, in degrees

μ= The commutation overlap angle, in degrees [44].

2.3.3 AC Filter Losses

The principal function of the alternating current filters in an HVDC converter station is to provide a low-impedance shunt for the harmonic currents generated by the converter. Typically, single-tuned, multiple-tuned, and high-pass filters are used in HVDC converter stations. For the purposes of loss determination, the AC system is assumed open-circuited so that all harmonic currents are considered to flow into the AC filters.

In the standby mode, AC filters are not connected to the AC system and, therefore, generate no losses.

The AC filters losses include losses of filter reactor, filter resistor and filter capacitor [49].

2.3.3.1 Filter Resistor Loss

The losses in the filter resistors are simultaneously calculated for the fundamental and harmonic currents together. The resistance value of the resistor is determined by factory measurements. The RMS current through the filter resistor is calculated. The losses in each resistor admits expression as [50] :

$$P_r = RI_R^2 \quad (2\text{-}8)$$

where

R=The resistor value, in ohms.

I_R= The rms current through the resistor, in amperes

P_r=The filter resistor losses, in watts

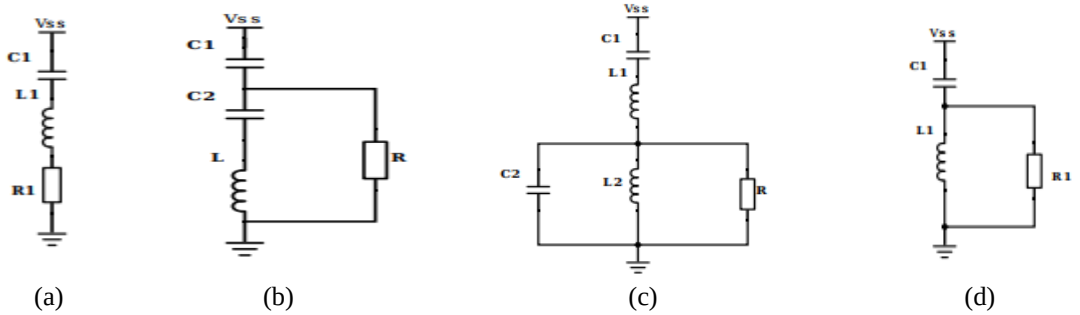

(a) (b) (c) (d)

Figure 2-2: Filters used for harmonics reduction and reactive power compensation [42].

Table 2-1: Types of AC Filters, functions and their mathematical expressions[50]

Filter types used	Functions	Expressions to Compute each element of the filter types
(a)Single-tuned band pass filter	This filter is used to eliminate 11th and 13th harmonic order.	$C_1 = \frac{Q}{2\pi f V^2}\left(1 - \frac{1}{n^2}\right)$ (2-9) $L_1 = \frac{1}{[2\pi f n]^2 C_1}$ (2-10) $R = \frac{2\pi f n L_1}{q}$ (2-11)
(b)C-type filter	This filter is used for low order high pass filter i.e. it is used to mitigate the 5th and 7th harmonic orders. It is used to provide reactive power and avoid parallel resonances. It can also allow filtering of low order harmonics such as 3rd order harmonic.	$C_1 = \frac{Q}{2\pi f V^2} \cdot \frac{\left[1-\frac{1}{n^2}\right]}{\left[1-\frac{1}{n_a^2}-\frac{1}{n_b^2}\right]}$ (2-12) $L = \frac{1}{[2\pi f n_a]^2 C_1}$ (2-13) $R = \sqrt{\frac{L}{C_1}}\Big/ q$ (2-14)
(c)Double-tuned filter	This filter is used to eliminate 17th and 19th harmonics.	$C_{1=} \frac{Q}{2\pi f V^2} \cdot \frac{\left[1-\frac{1}{n^2}\right]}{\left[1-\frac{1}{n_a^2}-\frac{1}{n_b^2}\right]}$ (2-15) $C_2 = \frac{1}{[2\pi f n_b]^2 L_2}$ (2-16) $L_1 = \frac{1}{[2\pi f n_a]^2 C_1}$ (2-17) $L_2 = \frac{1}{[2\pi f n_b]^2 C_2}$ (2-18)
(d)High pass filter	This filter is used to mitigate all harmonicc from the 23rd to 49th harmonic orders.	$C_1 = \frac{Q}{2\pi f V^2}\left(1 - \frac{1}{n^2}\right)$ (2-19) $L_1 = \frac{1}{[2\pi f n_a]^2 C_1}$ (2-20) $\mathrm{R} = \frac{2\pi \mathrm{f n L_1}}{\mathrm{q}}$ (2-21)

2.3.3.2 Filter Reactor Losses

The fundamental and harmonic currents in the filter reactors should be calculated when determining the losses of the filter reactors. The impedance of the reactor at fundamental frequency and the quality factors at the fundamental and harmonic frequencies should be measured and noted. The reactor losses admit expression as [4]:

$$P_R = \sum_{n=1}^{n=49} \frac{(I_{Ln})^2 X_{Ln}}{Q_n} \quad (2\text{-}22)$$

$$X_{Ln} = 2\pi f n L \quad (2\text{-}23)$$

where

n= The harmonic number

I_{Ln} = The calculated current through the reactor at nth harmonic, in amperes

X_{Ln} = The reactor reactance at nth harmonic, $X_{Ln} = nX_{L1}$, in ohms

Q_n =The average quality factor for all reactors of the same item measured at the nth harmonic

P_R = The filter reactor loss.

2.3.3.3 Capacitor Bank Losses (Filter Capacitor Losses)

Shunt capacitors are sometimes used in addition to harmonic filters to provide reactive support to the AC system. Shunt capacitor banks are made from a matrix of series- and parallel-connected capacitor cans. In the standby mode, shunt capacitor banks are not connected to the AC system and therefore generate no losses. When the converter station is operating, power losses in shunt capacitor banks should be determined for those load levels of the converter station at which such banks will be connected to the AC bus. Fundamental frequency losses of all capacitor units manufactured under the same contract should be measured during production tests according to IEEE Std 18-1980 and expressed in watts per kilovar. The losses due to harmonic currents can be taken to be infinitesimally small and most times should be ignored, as a result of the low power factor of the capacitor [4, 51].

The power losses of the entire bank, P, should then be calculated by:

$$P = P_1 S \quad (2\text{-}24)$$

where

P_1= The mean value of the losses of one capacitor unit averaged over all units manufactured under the same contract and expressed in watts per kilovar.

S = The three-phase kvar rating of the capacitor bank at nominal system voltage and frequency [10, 22].

2.3.4 DC Smoothing Reactor Losses

In HVDC converter stations, DC smoothing reactors are majorly utilized to filter the direct current and voltage, in order to limit the converter dc side over-currents during transient conditions, and to protect the converter from steep front overvoltages originating from the dc overhead line (in transmission systems) or from the other converter (in back-to-back systems) [52].

The DC reactor falls into two categories:

1. Air core, air insulated, naturally cooled, and mounted on a separate insulating support structure
2. Oil or gas cooled, oil/gas insulated, and mounted in a tank

The latter type of reactor may also have an iron shell core with an air gap, to limit the external stray magnetic field. The current flowing through the smoothing reactor is direct current with superimposed harmonic components, mainly characteristic harmonics. Particularly, when the AC system is unbalanced, small amounts of non-characteristic harmonics may also occur. The smoothing reactor load losses include harmonic and dc losses. Moreover, the hysteresis loss is evaluated, when the oil-immersed reactors with cores are utilized [22, 53].

2.3.4.1 Standby Losses

DC smoothing reactors are series connected to the converter dc terminal. Under standby conditions, the smoothing reactor current and voltage are both zero; therefore, losses do not occur [43].

2.3.4.2 Load Losses

The dc loss of the smoothing reactor should be established during factory tests according to IEC Pub 289 (1988) [54], and IEC Pub 76 using the direct current magnitude corresponding to the desired load level. Correction for the ambient temperature at the test should be made to relate the loss to the standard reference temperature. The winding loss due to harmonic currents was determined by calculation. The harmonic current amplitudes applicable to the appropriate load level and the corresponding harmonic resistance was used during the calculations. The harmonic resistance should be determined by bridge measurement. In smoothing reactors of a tanked construction, with an iron shell core, magnetization losses caused by harmonic currents may be a few percents of the total smoothing reactor losses. For a 6-pulse system, the magnetization loss was calculated with the following empirical procedure [4, 43]:

$$P_m = (0.125P_m + 0.125P_e)P_o \tag{2-25}$$

$$P_{hn} = \left(\frac{I_n}{I_o}\right) n \ (p.u) \tag{2-26}$$

$$P_{en} = \left(\frac{I_n}{I_o}\right)^2 n^{0.5} \ (p.u) \qquad (for\ n > 10) \tag{2-27}$$

$$P_{e2} = \left(\frac{I_n}{I_o}\right)^2 n^2 \ (p.u) \qquad (for\ n = 2) \tag{2-28}$$

where

P_m= The magnetization loss, in watts

P_o = The direct current losses, in watts

$P_h = \sum(P_{hn})$ = The hysteresis loss component, in per-unit

$P_e = \sum(P_{en})$ = The eddy-current loss component, in per-unit

I_n = The harmonic current of order n, in amperes

I_o = The dc current, in amperes

n = The harmonic number

2.3.5 DC-Filter Capacitor Losses

The losses in the dc filter capacitors are made up of losses in the dc voltage grading resistors and harmonic losses. The current harmonics losses are infinitesimally small and therefore, ignored due to the low power factor. The losses in the grading resistors are calculated by using the total resistance of the capacitor bank as determined from the mean value of all grading resistors per capacitor unit obtained from production tests, and the capacitor bank configuration, using [10, 55, 56];

$$P_C = \frac{(E_R)^2}{R_C} \tag{2-29}$$

where

E_R= Capacitor bank rated voltage, in volts

R_C = Capacitor bank total resistance, ohms

P_C = Filter capacitor losses, in watts.

2.4 Loss of Main Equipment of VSC-based HVDC Converter Stations

This section investigates the losses of key equipment of VSC-based HVDC converter stations that contribute a large amount of losses to the transmitted power. Losses determination of various equipment is based on the available standards. The losses evaluation of the main components of this HVDC technology utilized the formulas stipulated in standards IEC 62751-1-2. The losses of each equipment are separately estimated, hence, the total losses are the addition of the separate losses of individual component [4, 5]. VSC-based HVDC has various topologies such as two-level, three-level and modular multilevel converter which are well explained in references [12, 51].

The losses of voltage source converter have an immense proportion of the total losses of the converter stations due to the high switching frequency and low voltage level features of voltage source converter. Therefore, due to its characteristics of low switching frequency, low converter losses and flexibly controlled, the M2C has been vastly used in the HVDC transmission schemes. Therefore, it is of importance to conduct an investigation on the loss evaluation method in the flexible HVDC transmission system. However, the current loss computation technique can only be used for the three-level and two-level VSC-based HVDC technology [53, 57]. Moreover, the detailed techniques adopted for estimating the power losses in the valves for two-level, three-level and modular multi-level converter HVDC system are done in accordance with standards IEC 62751-1-2, “Power Losses in Voltage Source Converter (VSC) Valves for High-Voltage Direct Current (HVDC) Systems”.

The Modular Multi-Level Converter (MMC) and its closely related Cascaded two-level converter (CTL), have drastically changed the high power losses draw-back of a VSC-based technology of recent [5]. These converters allow the switching frequency to be minimized in magnitude, while at the same time achieving better harmonic performance than is feasible with the three and two-level converters. Therefore, adopting this VSC configuration, will result to the

overall losses per station should stand very close enough with LCC-based technology, for the two technologies to be able to compete in some applications [5, 14].

2.4.1 Loss Hierarchy of VSC-based HVDC System

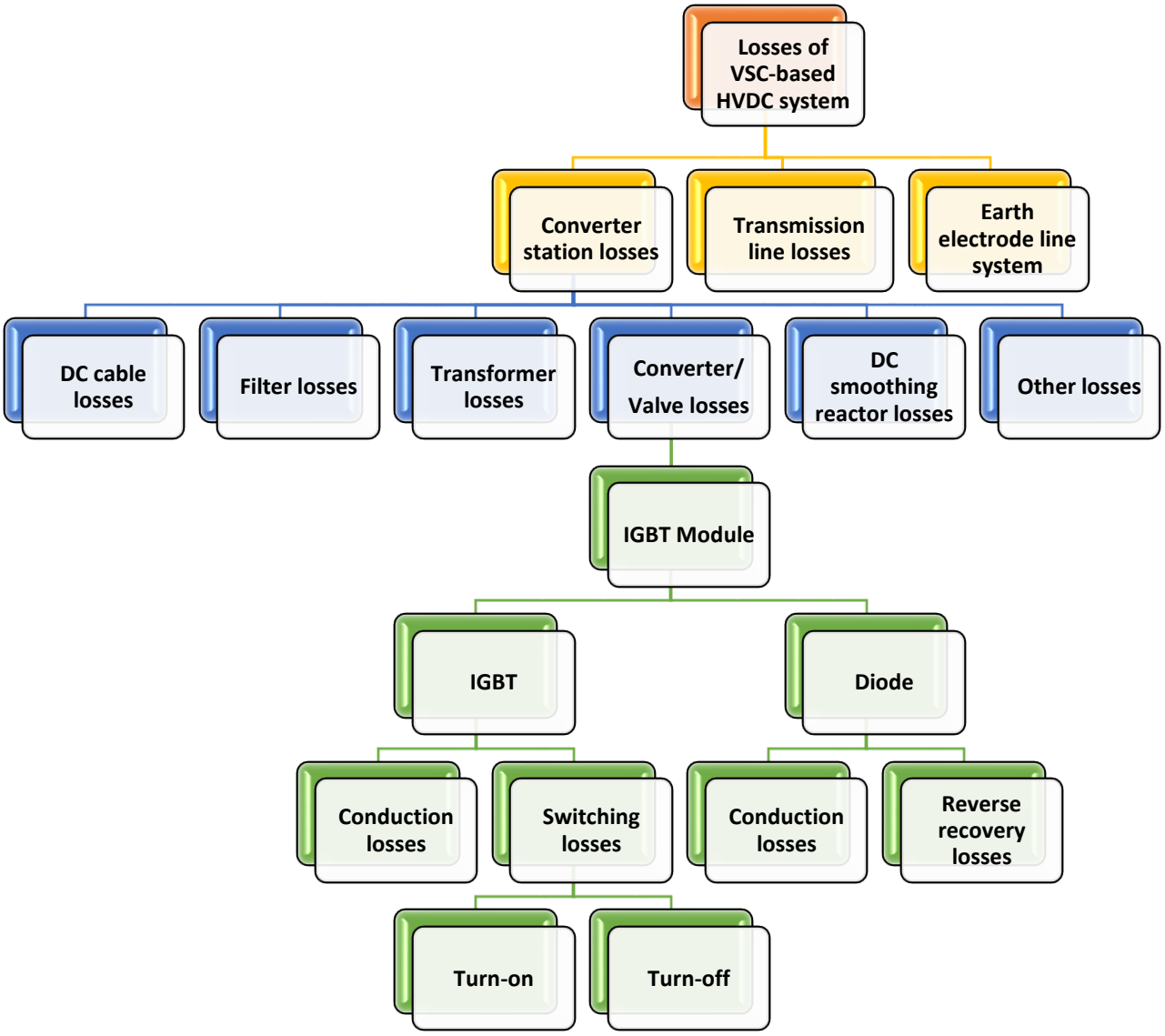

Figure 2-3: Loss taxonomy of VSC-based HVDC system [16]

Figure 2-3 depicts the various loss hierarchy of VSC-based HVDC technology, which consists of the converter losses, HVDC transmission line losses and the earth electrode. The valves losses consist of the losses due to IGBT and anti-parallel freewheeling diode, the loss contribution of these devices are added together to obtain the total valve losses.

2.4.2 Valve Losses

The main contributor to the overall VSC-based HVDC losses are the valve losses. The valves compose of IGBTs and diodes (FWD), which are collectively known as IGBT module, in an IGBT module there are various IGBT, and diode

die based on the module and the application requirements. When conducting or switching from one state to another, all chips dissipate power. However, it is expedient to consider each of the devices that make up the valve [58].

2.4.3.1 Estimating Power Losses of IGBTs

In thermal design, the first step is the computation of total power losses. An IGBT is a voltage-controlled device, which merges the merits of a BJT and a MOSFET. IGBT is a three terminal device; emitter, collector, and the gate terminal. IGBT can handle high currents and has a low forward voltage drop. It also has a voltage controlled capacitive gate, just like as in a MOSFET. IGBT chips are arranged in parallel in a sub-module, in order to increase the power handling capacity. Based on the application current rating, the number of sub-modules is selected [19]. In addition, it is a four-layer semiconductor that uses the voltage characteristics of BJT and the drive characteristics of a MOSFET. However, for high power IGBT modules operation, it is mandatory to provide a suitable heatsink, else, it may go into the thermal runaway. In power electronics circuit, which adopts the use of IGBTs, since IGBT operates in two states and produce losses in those states, it is imperative to consider the two most important sources of power dissipation, which are conduction losses and switching losses [59, 60]

2.4.3.2 Conduction Losses of IGBT

The losses in IGBT module that occur during the On-state of the IGBT or freewheeling diode when current is being conducted are known as conduction losses. The dissipated total power is estimated by multiplying the On-state saturation voltage and On-state current (current flowing through the collector or anode). Furthermore, in order to obtain the average power dissipation, the conduction losses, in PWM applications, must be multiplied by the duty factor. More so, the first order approximation of conduction losses can be obtained by multiplying the IGBT saturated voltage drop (Vce. sat) by the expected average device current [21, 45]. Conduction losses are the On-state losses or steady state losses. The average power dissipated by the IGBT admits expression as [61]:

$$P_{avg.cond} = \frac{1}{T}\int_0^T [Vce(t) \times I_{ce}(t)]dt \tag{2-30}$$

where

$P_{avg.cond}$ = Average conduction losses, in W.

Vce = the device forward voltage or On-state saturation voltage (IGBT), Volt.

I_{ce} = On-state current, in Ampere.

T= Conduction period, seconds.

The forward resistance R_o can easily be computed from the IGBT characteristic curve from the data sheet provided by the manufacturer.

$$R_o = \frac{\Delta V_{ce}}{\Delta I_C} = \frac{V_{ce2} - V_{ce1}}{I_{C2} - I_{C1}} \tag{2-31}$$

Description as above. Forward resistance R_f is the ratio between the difference of collector-emitter voltage and the collector current difference. The value of $V_{ce0}(t)$ is computed as follow [62, 63]

$$V_{ce.sat} = V_{ceo} + R_o i_c(t) \tag{2-32}$$

When the expression for the forward voltage is substituted from equation (2-32) into equation (2-30) yields:

$$P_{avg.cond} = V_{ce} I_{av} + R_f I_{rms}^2 \tag{2-33}$$

where

I_{av}= Average current through the device during conduction period, in Ampere.

I_{rms}^2 = rms current through the device during conduction period, in Ampere.

The average and RMS current through the device during conduction period are estimated as follows:

$$I_{av} = \frac{1}{T}\int_0^T i_a(t)dt \tag{2-34}$$

$$I_{rms}^2 = \frac{1}{T}\int_0^T i_a^2(t)dt \tag{2-35}$$

Note that, the V_{ce} value obtained from equation (2-32) should be approximately equal to the value in the datasheet to justify the correct computation from the graph. However, the average power losses in PWM sine wave switching admits expression as [64]:

$$P_{cond.IGBT} = \frac{1}{2} \times \left(V_{ceo} \times \frac{I_p}{\pi} + R_o \times \frac{I_p^2}{4}\right) + m \times \cos\emptyset \left(V_{ceo} \times \frac{I_p}{8} + R_o \times \frac{I_p^2}{3\pi}\right) \tag{2-36}$$

m= modulation index.

$\cos\emptyset$= power factor.

I_p=Peak value of sinusoidal output current, in Ampere.

Other descriptions as above.

Note that, from equation (2-30), time-period 'T' is inversely proportional to the frequency 'f'.

$$T = \frac{1}{f} \tag{2-37}$$

Which results to,

$$P_{avg\ IGBT} = f \int_0^T [P(t)]dt \tag{2-38}$$

From equation (2-38), it can be deduced that by simply integrating all the values of power losses over a period of time, the total average power losses incurred in the IGBT can be obtained. The conduction losses independent of the switching frequency f_{sw} , however, depends on duty cycle, whereas, switching losses depends on the switching frequency f_{sw} and at the same time, they are directly proportional to each other. The total average conduction loss can also be evaluated by alternative method if the values of I_{rms} and I_{avg} can be estimated for the system. Assuming that the load current admits expression as [63]:

$$i_a(t) = I_m \sin(\omega t - \theta) \tag{2-39}$$

Similarly, the leg phase voltage admits expression as:

$$V_a(t) = V_m \sin \omega t \tag{2-40}$$

Likewise, the duty cycle for the device switches (IGBT) admits expression as:

$$d_{T1} = \frac{1}{2}\,[1 + m \sin \omega t] \tag{2-41}$$

$$d_{T2} = 1 - d_{T1} = \frac{1}{2}\,[1 - m \sin \omega t] \tag{2-42}$$

Similarly, the average and RMS currents for IGBTs $T1$ and $T2$ are estimated using equation (2-34) and (2-35) alongside with the equation (2-41) and (2-42). The following expressions were obtained after applying various mathematical analytical measures [65]:

$$I_{T1,av} = \frac{1}{2\pi}\int_{\theta}^{\pi+\theta} d_{T1} i_a d\omega = I_m \left[\frac{1}{2\pi} + \frac{m \cos\theta}{8}\right] \tag{2-43}$$

$$I_{T2,av} = \frac{1}{2\pi}\int_{\theta}^{\pi+\theta} d_{T2} i_a d\omega = I_m \left[\frac{1}{2\pi} - \frac{m \cos\theta}{8}\right] \tag{2-44}$$

$$I^2_{T1,rms} = \frac{1}{2\pi}\int_{\theta}^{\pi+\theta} d_{T1} i_a^2 d\omega = I_m^2 \left[\frac{1}{8} + \frac{m \cos\theta}{3\pi}\right] \tag{2-45}$$

$$I^2_{T2,rms} = \frac{1}{2\pi}\int_{\theta}^{\pi+\theta} d_{T2} i_a^2 d\omega = I_m^2 \left[\frac{1}{8} - \frac{m \cos\theta}{3\pi}\right] \tag{2-46}$$

$$P_{cond.IGBT} = \left[I_{T1,av} * V_{ceo} + R_o * I^2_{T1,rms}\right] \tag{2-47}$$

2.4.3.3 Switching Losses of IGBT

Switching losses, in power electronic devices, usually contribute a substantial amount to the overall losses of the system. Thus, ignoring losses due to switching of the electronic devices in the computation or weighting the losses due to conduction of the devices with an estimated factor to actually consider switching losses, might lead to large errors. As touching the total losses, the power dissipated during the conducting (turn On) and non-conducting (turn Off) switching transitions are known as switching losses. Similarly, switching losses are simply total sum of on-state switching losses and turn-off switching losses, consequently, it depends on the switching frequency, device current and device characteristics. The switching losses occur due to the energy loss during the transition and switching frequency. It also depends on the junction temperature, dc link voltage, and load current. Losses will likewise be higher, If the switching frequency is higher [1, 7]. However, to compute the junction-temperature time behavior such that the reliability of the design is improved, it is essential to estimate accurately the switching losses. More so, to evaluate the average switching power losses, obtain the E_{on} and E_{off} values from the curve at the expected average operating current. Therefore, the average power dissipated admits expression as [45, 66]:

$$P_{sw.IGBT} = \left(E_{on} + E_{off}\right) \times \frac{f_{sw}}{\pi} \tag{2-48}$$

Based on the conditions provided for any application with respect to the datasheet nominal values, the switching power loss is required to be normalized, which admits expression as:

$$P_{sw.IGBT} = \frac{\left(E_{on}+E_{off}\right)\times I_p \times f_{sw} \times V_{dc}}{\pi \times I_{nom} \times V_{nom}} \tag{2-49}$$

The values of the energy loss E_{on} and E_{off} are given in the datasheet (Dynex), therefore, there is no need to compute these values. The switching energies are basically multiplied by the switching frequency resulting to the power loss for on and off time as illustrated by equation (2-48).

The total average power loss for the IGBT can be split into three parts:

- Turning on the device.
- Conducting period.
- Turning off the device.

$$P_{avg.IGBT} = P_{cond} + P_{on} + P_{off} \tag{2-50}$$

$$P_{avg.IGBT} = \frac{1}{T} \int_{tcond}^{T} P(t)dt + f \int_{ton}^{T} P(t)dt + f \int_{toff}^{T} P(t)dt \tag{2-51}$$

Total losses admits expression as [45]:

$$P_{avg.IGBT} = P_{cond.IGBT} + P_{sw.IGBT} \tag{2-52}$$

Nomenclature,

E_{on}= IGBT turn-on switching energy at I_c and T=125°C.

E_{off}= IGBT turn-off energy loss at I_c and T=125°C.

f_{sw} =PWM switching frequency.

D = PWM duty factor

$V_{ce.sat}$ = IGBT saturation voltage drop at I_c and T=125°C.

$\emptyset$ = Phase angle between the output voltage and current.

I_c = Peak value of sinusoidal output current [45].

2.4.3.4 Estimating the Power Losses of Freewheeling Diode

Power loss estimations of the freewheeling diodes are investigated under the following loss mechanisms:

2.4.3.5 Conduction Losses (Diode)

In power electronics, a diode is a two-terminal p-n junction device; whose two terminals are anode and cathode. It is an electronic device, which allows current to pass when it is forward biased in one direction (conduction state), whereas blocking current in the opposite direction (reverse direction).

The average total power losses in diode admits expression as [21]:

$$P_{avg.Diode} = P_{cond.Diode} + P_{rec.Diode} \quad (2\text{-}53)$$

The forward resistance R_D can easily be computed from the diode characteristic curve from the data sheet provided by the manufacturer.

$$R_D = \frac{V_{f2}-V_{f1}}{I_{f2}-I_{f1}} \quad (2\text{-}54)$$

From equation (2-54), the value of diode resistance, R_D can be obtained from the change of forward voltage and forward current. The forward voltage of a diode admits expression as:

$$V_f = V_{DO} + R_D \times I_C \quad (2\text{-}55)$$

Similarly, diode threshold voltage V_{DO} can be computed from the datasheet of the device, which is used for estimating the forward voltage as shown in equation (2-55). This forward voltage can be checked against the value on datasheet to confirm the validity of the calculation. The average power losses in diode when operating under PWM sinewave switching admits expression as [67]:

$$P_{cond.Diode} = \frac{1}{2} \times \left(V_{Do} \times \frac{I_p}{\pi} + R_D \times \frac{I_p^2}{4}\right) + m \times \cos\emptyset \left(V_{Do} \times \frac{I_p}{8} + R_D \times \frac{I_p^2}{3\pi}\right) \quad (2\text{-}56)$$

Parameters description as above.

2.4.3.6 Reverse Recovery Time

Basically, when switching a diode from the conduction mode to the blocking mode, a diode or rectifier tends to have stored charge, which must be firstly discharged, prior the reversed voltage is blocked by the diode. This discharge takes a limited amount of time known as Reverse Recovery Time, or t_{rr}. More so, during this time, diode current may drift in the reverse direction. However, when the device (diode) turns off, as a result of the discharging operation, which still permits the drifting action of the diode current in the reverse direction, losses are generated which is called recovery loss, and likewise, the time needed to recover is called the reverse recovery time. The recovery losses of a diode admit expression as [65, 68]:

$$P_{rec.Diode} = E_{rec} \times f_{sw} \tag{2-57}$$

Nomenclature,

E_{rec}= Diode reverse recovery energy (The turn-off energy of the diode due to reverse recovery current).

f_{sw} = Switching frequency.

I_{rr} = Diode reverse recovery current.

Q_{rr} = Diode reverse recovery charge.

T_{rr} = Diode reverse recovery time.

As previously stated, based on the conditions provided for any application with respect to the datasheet nominal values, the switching power loss is required to be normalized.

$$P_{rec.Diode} = \frac{E_{rec} \times I_p \times f_{sw} \times V_{dc}}{\pi \times I_{nom} \times V_{nom}} \tag{2-58}$$

Finally, the summation of equation (2-56) and equation (2-58) results to equation (2-53). Therefore, the sum of conduction loss and reverse recovery loss in diode result to the total average power loss for the diode.

Alternatively, if the values of I_{rms} and I_{avg} can be estimated for the system, the total average conduction loss can also be evaluated. Assuming that the load current admits expression as:

$$i_a(t) = I_m \sin(\omega t - \theta) \tag{2-59}$$

Similarly, the leg phase voltage admits expression as:

$$V_a(t) = V_m \sin \omega t \tag{2-60}$$

Likewise, the duty cycle for the device switches (Diode) admits expression as:

$$d_{D1} = d_{T2} = 1 - d_{T1} = \frac{1}{2}\left[1 - m \sin \omega t\right] \tag{2-61}$$

$$d_{D2} = d_{T1} = \frac{1}{2}\,[1 + m\sin\omega t] \tag{2-62}$$

It is worth noting that, the average and (Root mean square) RMS currents for the lower freewheeling diode are similar in terms of expression to that of the upper IGBT device, however the direction of flow is opposite. Therefore, the average and RMS currents admit expression as [11, 64]:

$$I_{D1,av} = -I_{T2,av} = -I_m\left[\frac{1}{2\pi} - \frac{m\cos\theta}{8}\right] \tag{2-63}$$

$$I_{D2,av} = -I_{T1,av} = -I_m\left[\frac{1}{2\pi} + \frac{m\cos\theta}{8}\right] \tag{2-64}$$

$$I^2_{D1,rms} = I^2_{T2,rms} = I^2_m\left[\frac{1}{8} - \frac{m\cos\theta}{3\pi}\right] \tag{2-65}$$

$$I^2_{D2,rms} = I^2_{T1,rms} = I^2_m\left[\frac{1}{8} + \frac{m\cos\theta}{3\pi}\right] \tag{2-66}$$

$$P_{cond.Diode} = \left[I_{D1,av} * V_{DO1} + R_D * I^2_{D1,rms}\right] \tag{2-67}$$

Similarly, the average (total) conduction losses of a per valve IGBT module admits expression as:

$$P_{total.cond} = [P_{cond.IGBT} + P_{cond.Diode}] \tag{2-68}$$

$$P_{total\ losses\ per\ device} = [P_{total\ IGBT\ losses} + P_{total\ Diode\ losses}] \tag{2-69}$$

$$P_{total.cond-per\ valve} = 6 * \left[I_{T1,av} * V_{ceo} + R_o * I^2_{T1,rms} + I_{D1,av} * V_{DO1} + R_D * I^2_{D1,rms}\right] \tag{2-70}$$

Note that for two-level converter, the total conduction and switching losses for the 6-valves becomes:

$$P_{total.cond,6-valves=} 6 * N_{IGBT\ valve} * [P_{cond.IGBT} + P_{cond.Diode}] \tag{2-71}$$

$$P_{total.sw,6-valves=} 6 * N_{IGBT\ valve} * [P_{sw.IGBT} + P_{rec.Diode}] \tag{2-72}$$

Where

$N_{IGBT\ valve}$ = Number of IGBTs connected in series in each valve [1, 66].

2.5 Loss Evaluation Method of Modular Multilevel Converters

The Modular Multilevel Converter (M2C) has popularly become the most promising converter topology for different medium and high power-converter applications, such as variable speed drive, propulsion system of electric ships, grid connection of energy storage systems, electric railway supplies and high-voltage dc (HVDC) transmission. Due to its miniaturization or compactness (small footprint), high modularity and the fact that the losses incurred during operation is very low compared to its counterpart and also it has shown that it is feasible to merge the excellent output voltage waveforms with very high frequencies [69, 70]. Therefore, M2C permits the decrease of the switching frequency down towards the fundamental frequency, meanwhile, the output voltage content of the harmonic is still kept low resulting to a large number of levels compared to the conventional two-level and three-level voltage source converters (VSCs) [68]. Apparently, the switching methods and semiconductor devices are determining factors when considering the efficiency of M2C-based stations. So therefore, there are various semiconductor devices and switching methods which are not covered in this research work, but well explained in [68, 71].

The M2C consist of submodules, which are otherwise known to be a number of series-connected half bridges with dc-capacitors. The individual phase leg consists of one positive (upper) arm and one negative (lower) arm, which is linked to the dc terminal points. More so, the number of submodules that are inserted in the positive (upper) and negative (lower) arms are changed in order to control the potential at the ac side connection point. However the case may be, the bypassing and the insertion of the submodules must be arranged in such a way that the capacitor voltages remain juxtapose to their nominal values [66, 72].

2.5.1 Topology of M2C HVDC Technology

The VSC-HVDC technology was reformed due to the advent of the MMC and its close related technology, the cascaded two-level converter by largely mitigating the need for harmonic filtering and further reducing the power losses of the converter drastically. The reduction of switching frequency made possible by the MMC results in the reduction of power losses of the converter. The MMC permits the magnitude of the switching frequency to be lower than two or three level converter. A very large dc capacitor is required in each submodule when the switching frequency is equal to the grid frequency, therefore, a more economic optimum is generally to have a switching frequency of around 100 Hz. Moreover, the dominant component of losses in two or three-level converters which happens to be switching losses, are now of secondary importance in the MMC, therefore, the power losses are dominated by the conduction losses in the diodes and IGBTs [5, 14, 73].

The circuitry of the M2C configuration is illustrated in fig. 2-5, M2C consists mainly of three-phases in which individual phase has the equal number of submodules (SMs or Cells) and a valve-reactor which is series connected in both the positive (upper) and negative (lower) legs. Therefore, individual submodule consists of two IGBTs, two freewheeling diodes (FWD) and a capacitor. This capacitor is an energy storage component and does not consume energy during the charge and discharge processes [53, 74]. Therefore, the losses of M2C mainly include the losses of valve reactor, FWD, and IGBT, the losses due to valve reactor accounts for a small proportion of losses, which can be ignored in most cases. Similarly, each phase of this topology consists of two arms, namely, upper (positive) and lower (negative) arms, which are connected from the positive and negative dc poles to the ac terminal, respectively [75, 76].

A series connection of N identical cells, and arm inductors L_{arm} are connected together to form each arm. Similarly, the resistance of the submodules and inductor in one arm, which is depicted as R. Note that, a submodule is said to be bypassed if the lower switch is closed and the upper switch is opened. Similarly, if the lower switch is opened and the upper switch is closed, then the submodule is said to be inserted. More so, the state of a submodule defined by the state signal S_k and it is defined in such a way that when submodule k is inserted S_k equals to one likewise, when submodule k is bypassed, S_k equals to zero. Furthermore, the submodules are arranged such that the first N submodules are positioned in the lower arm [66, 77].

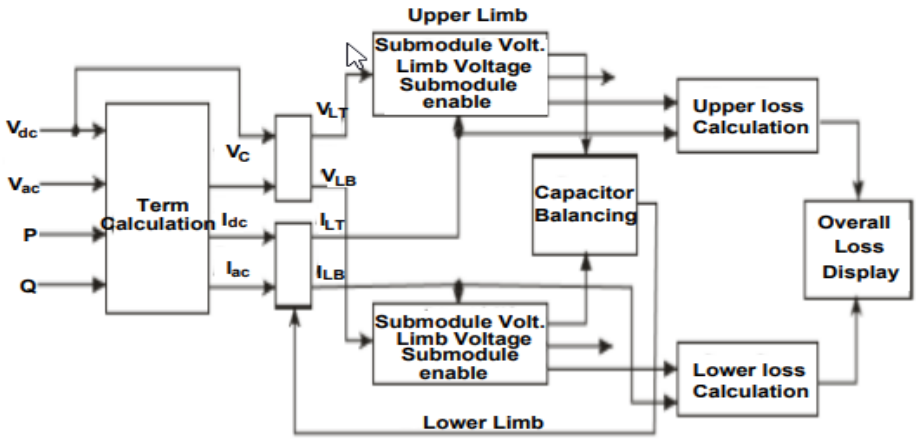

Figure 2-4: A typical illustration of loss calculation model structure [78]

Figure 2-4 shows a typical illustration of loss- calculation model structure, the loss calculation is based on the switching coming from submodule cell and the limb current. The submodule switching operation and hence, the converter loss, vary with the average capacitor voltage value. These individual losses are then added to give a total loss for the top and bottom converter arms [14, 76].

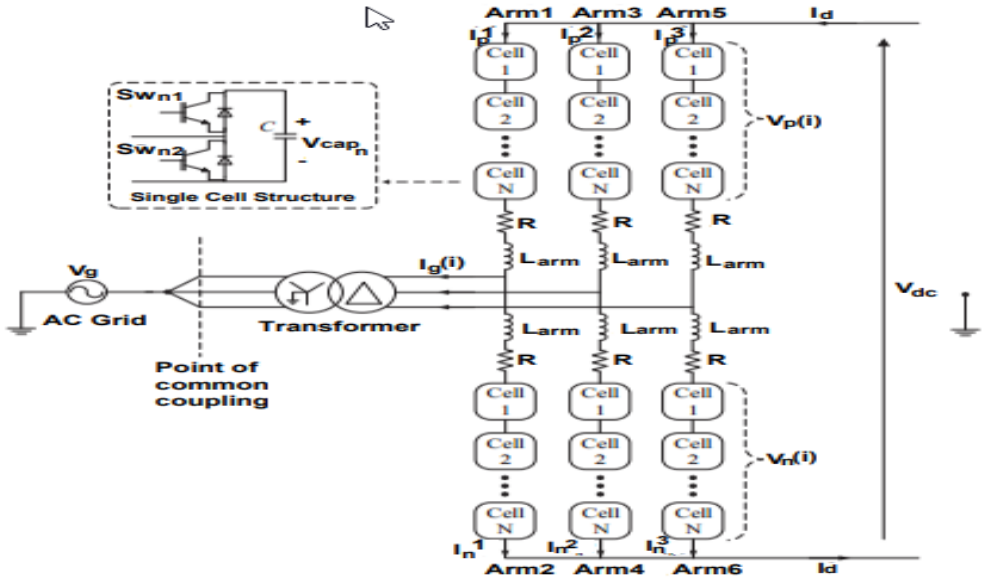

Figure 2-5: Three phase circuit schematic of M2C topology [79]

Varying the number of inserted and bypassed submodules in each arm, the ac side voltage is obtained. Most times this is done in a complementary manner, in such a way that one submodule is bypassed in the upper arm, when one module is inserted in the lower arm. As a result, the overall total number of inserted submodules in individual phase leg is mostly equal to N [80]. From figure 2-5, both the positive and negative arm current $I_p(i)$ and $I_n(i)$ admit expressions as [15, 51]:

$$I_p(i) = \frac{I_s(i)}{2} - \frac{I_d}{3} \tag{2-73}$$

$$I_n(i) = -\frac{I_s(i)}{2} - \frac{I_d}{3} \tag{2-74}$$

where

$I_s(i)$ = Converter phase current, in A.

I_d = Converter dc current, in A. Note that (i) denotes the arbitrary number of each phase.

Therefore, the converter phase current $I_s(i)$ can be obtained from solving equation (2-73) and equation (2-74) simultaneously which results to;

$$I_p(i) - I_n(i) = I_s(i) = \sqrt{2}\, I_s(i) \cos(\omega t + \delta_s(i) - \varphi(i)) \tag{2-75}$$

where

$I_s(i)$ = The phase current RMS value, in A.

$\delta_s(i)$ = Phase voltage angle, in degrees.

$\varphi(i)$ =The load angle, in degrees.

Similarly, replacing equation (2-75) into equations (2-73) and (2-74) respectively, this results to;

$$I_p(i) = \frac{\sqrt{2}\, I_s(i) \cos(\omega t + \delta_s(i) - \varphi(i))}{2} - \frac{I_d}{3} \tag{2-76}$$

$$I_n(i) = -\frac{\sqrt{2}\, I_s(i) \cos(\omega t + \delta_s(i) - \varphi(i))}{2} - \frac{I_d}{3} \tag{2-77}$$

Additionally, assuming an equal dc and ac side power, the dc current I_d can admit expression as a function of the converter power P_c and dc voltage V_{dc} as;

$$I_d = -\frac{P_c}{V_{dc}} = -\frac{3V_s(i)I_s(i)\cos\varphi}{V_{dc}} \tag{2-78}$$

where

$V_s(i)$ = Phase current RMS value in i^{th} phase, in V.

$I_s(i)$ = Phase current RMS value in i^{th} phase, in A.

Similarly, the modulation index $m(i)$ admits expression as;

$$m(i) = \frac{2\sqrt{2}\, V_s(i)}{V_{dc}} \tag{2-79}$$

Note that, solving for V_{dc} in equation (2-79) and replacing the result into equation (2-78) yields;

$$I_d = -\frac{3m(i)I_s(i)\ \cos\varphi}{2\sqrt{2}} \tag{2-80}$$

On replacing equation (2-80) into equations (2-76) and (2-77), the upper (positive) and lower (negative) arm currents admit expressions as;

$$I_p(i) = \frac{\sqrt{2}\, I_s(i) \cos(\omega t + \delta_s(i) - \varphi(i))}{2} + \frac{3m(i)I_s(i)\ \cos\varphi}{2\sqrt{2}} \tag{2-81}$$

$$I_n(i) = -\frac{\sqrt{2}\, I_s(i) \cos\left(\omega t + \delta_s(i) - \varphi(i)\right)}{2} + \frac{3m(i)I_s(i)\ \cos\varphi}{2\sqrt{2}} \tag{2-82}$$

The total number of cells admits expression as;

$$N = \frac{V_d}{V_{cap}^{nom}} \tag{2-83}$$

where

V_{cap}^{nom} = The nominal converter cell capacitor voltage.

For instance, considering the positive arm in an arbitrary phase, the number of inserted $n_p^{in}(i)$ and $n_p^{by}(i)$ bypassed cells admit expressions as;

$$n_p^{in}(i) = \frac{\frac{V_{dc}}{2} - V_s(i)}{V_{cap}^{nom}} \tag{2-84}$$

$$n_p^{by}(i) = N - n_p^{in}(i) \tag{2-85}$$

Therefore, on ignoring the voltage drop over arm inductor, L_{arm} and applying the Kirchhoff's voltage law, more so, replacing the sinusoidal representation of;

$$v_s(i) = \sqrt{2}\, V_s(i) \cos\big(\omega t + \delta_s(i)\big) \tag{2-86}$$

Substituting equation (2-83) and equation (2-84) into equation (2-85), the number of inserted and bypassed cells for the positive arm admit expressions as;

$$n_p^{in}(i) = \frac{N}{2}\big(1 - m(i)\cos\big(\omega t + \delta_s(i)\big)\big) \tag{2-87}$$

$$n_p^{by}(i) = \frac{N}{2}\big(1 + m(i)\cos\big(\omega t + \delta_s(i)\big)\big) \tag{2-88}$$

Note that, since the dc side voltage can be expressed by summing up the upper (positive) and lower (negative) arm output terminal voltages of N number of cells, the negative arm insertion and bypass number admit expressions as;

$$n_n^{in}(i) = \frac{N}{2}\big(1 + m(i)\cos\big(\omega t + \delta_s(i)\big)\big) \tag{2-89}$$

$$n_n^{by}(i) = \frac{N}{2}\big(1 - m(i)\cos\big(\omega t + \delta_s(i)\big)\big) \tag{2-90}$$

Consequently, controlling the number of inserted and bypassed cells in each converter arm, the desired currents and voltages at the dc and ac terminal points of M2C can be created. Therefore, an appropriate switching method can control the M2C in various operating modes and therefore, accomplish the system requirements [68, 81, 82].

2.6 Summary

Several works on loss study of HVDC system have been reported in literature, LI Zhan-ying et al [6], quantitatively calculated the losses of HVDC system using IEC 61803 standard, in his work, the loss calculation models for converter station equipment under different operational conditions were established. Based on basic theory and specific models, loss calculation program for HVDC converter station was developed using Visual Basic programming language. Microsoft's Access was adopted as database for data storage and ADODC method is adopted to realize the connection between database and program. Phil S Jones et al [14], presented a mathematical analysis for estimating both the switching and conduction losses for VSC-based HVDC stations adopting the MMC topology. The total converter losses are subsequently determined by summing up the switching and conduction losses of all the converter valves. Additionally, H. Peter Lips et al [37], analyzed the power losses of each component of the HVDC thyristor valve using

mathematical tool stipulated in IEC 61803 standards. Finally, G. Daelemans et al [35], verified the feasibility, technical as well as economic, of VSC HVDC on loss minimization in meshed networks. The losses of the different components of a VSC HVDC link are studied and the impact of the installation on the overall system losses in the mesh network was verified through simulations.

As earlier said, there have been numerous studies done on loss determination of HVDC converter stations. Most of which utilized either Matlab-Simulink method of loss calculations or loss calculation program in Visual Basic 6 to evaluate the HVDC converter losses [6]. Moreover, some authors used PSCAD to analyze the loss contributions of various converter equipment [83]. Meanwhile, these results obtained by simulations were not validated by other methods of loss calculations. Conceptually, the loss calculation method using standardized mathematical representations illustrated in the standards are complex and rigorous to analyze. In respect of this, most authors prefer to analyze the losses of HVDC converter stations using simulation approach. It is worthy of note that using only one method to calculate the losses of HVDC converter stations would not validate the results obtained and the feasibility of the HVDC loss study. Based on these gaps mentioned, a novel approach was used to evaluate the losses of various HVDC technologies using analytical loss calculation method and subsequently validated the results obtained by simulation method. More so, to further validate the results obtained, some commercialized loss-simulation environments (Semisel and Melcosim) were used to calculate the loss mechanisms of HVDC technologies, which signify the significance and contributions of this research work. The next chapter explains the various methods utilized in subsequent chapters to obtain the results shown.

In conclusion, the difficulty of HVDC transmission system loss calculation falls in the loss calculation of the converter station. To understand the loss proportion of equipment in HVDC converter station and to decrease the losses of the HVDC system, analysis based on the formulas stipulated in the standard of IEC 61803 “Determination of power losses in LCC-based high-voltage direct current (HVDC) converter stations” and IEC 62751-1-2 “Determination of power losses in VSC-based high-voltage direct current (HVDC) converter stations” were used to calculate the losses of each equipment in the converter stations.

CHAPTER 3
METHODOLOGY

3.1 Introduction

Theoretically, the converter station losses of an HVDC system can be investigated and determined either by direct measurement of both the input and the output powers or by means of component characteristics, utilizing suitable mathematical models of the converter individual component. This chapter invariably discussed the methods adopted in this research work. In order to satisfy the objectives and answer the research questions of this dissertation, a quantitative research based on the estimation and analyses of various equipment losses of different HVDC technologies were fully investigated based on the following outlines: research approach and methods, research procedure and process, research instrument, research layout, and research strategy and limitations.

3.2 Research Approach and Methods

The purpose of this research is to discuss the methods of identifying and determining the various equipment that produces a large amount of power losses on HVDC converter stations during power transmission. Subsequently, the loss contributions of the individual equipment on the converter stations are investigated, determined and calculated for both HVDC technologies (i.e. the LCC-based and VSC-based HVDC technologies), during operating and standby mode. However, being that there are various interconnected equipment on the converter stations at both end of each technology, the author limited the scope of this research to investigate key equipment such as converter transformer, thyristor converter valves, DC-smoothing reactors, AC filters and DC capacitor. However, the loss contributions from auxiliary power equipment such as valve cooling system, transformer cooling system, converter control, and protection, switch-yard equipment cooling system switch-yard equipment control and protection system to mention but few are neglected because their loss contributions are infinitesimal compared to those converter station equipment being investigated which can be ignored. These results will give the author a good overview of the loss mechanisms of each of the equipment of the HVDC converter stations under investigation. In order to fully investigate and determine these losses, there is need to identify some variables to carry out this research. These variables include the following, the dc voltage at the rectifier output, the on-state power loss, the harmonic currents, junction temperature, firing angle, overlap angle, advanced angle, dc current, average thyristor stored charge, RMS source voltage, the transformer rating, the transformer resistance. Other variables include transformer reactance, the converter rating, the number of valves at each station for both technologies, number of IGBTs connected in series for two-level, three-level and multi-level VSC configurations etc.

These variables mentioned above alongside with the datasheet parameters from the manufacturer of the electronic devices, which are used as power converter at each stations of both technologies, are very useful in loss calculations. Most significantly, the standards IEC 61803 and IEC 62751-1-2, “IEEE recommended practice for determination of power losses in high-voltage direct-current (HVDC) converter stations”, are used to determine the power losses in the converter valve, converter transformer, DC smoothing reactor and so on [4].

The essence of determining and analyzing the loss mechanisms of converter stations equipment for both technologies, is to be able to predict exactly, the loss profile of both HVDC technologies according to the standards stipulated in IEC 61803 and IEC 62751-1-2, "Determination of Power Losses in High-voltage Direct-Current (HVDC) Converter Stations". This subsequently, shows the dependency of the losses on circuit parameters and operating point and besides to have a good basis for the comparison of the loss mechanisms for both HVDC-converter technologies. Therefore, after the determination and the computations of the various losses of each converter stations equipment for both HVDC technologies, the percentage loss proportion will then be calculated based on the loss values obtained previously. Thus, this is done in order to allow conclusions to be drawn on which of the converter stations equipment that produces the highest amount of losses and at what percentage proportion. Furthermore, the losses of all the stations' equipment will be added together to obtain the total power losses produced by the converter stations of both HVDC technologies. The ultimate aim is to compare the loss profile of LCC-based HVDC technology, two-level, three-level and multi-level VSC-based technology and make conclusions on which of these technologies transmit power efficiently based on the loss profile. More so, in order to further conclude this research work, the author deems it fit to validate the results obtained using physical analyses from the data obtained from the datasheet of the electronic component and the formulas stipulated in the IEC 61803 standards with the results obtained when the same system is modeled on a simulation environment. The author further validated these results not only with the Matlab environment but also with Melcosim software and some online loss simulation environment such as Semisel.

3.3 Research Procedure and Process

In this research work, four HVDC technologies were considered, LCC-based, two-level VSC-based, three-level VSC-based, and multi-level VSC-based technologies. The loss contributions of each converter stations for different HVDC technologies were fully investigated and calculated. For LCC-based technology, a typical model was investigated whose transformer rating was 500/440 kV at the rectifier terminal and 350/230 kV at the inverter terminal, with a power capacity of 1000 MVA. This model adopts 6-pulse thyristor valve HVDC system, which operates at a frequency of 50 Hz [4, 5].

Firstly, the testing of the rectifier circuit was carried out, and this was done on the basis of measuring the output dc voltage at the rectifier terminal when the delay angle was being varied, thorough steps were taken to ensure that the values obtained tallied with the theoretical values using the respective formulas stated in various pieces of literature reviewed. The control adopted was constant current at the rectifier terminal and constant extinction angle (CEA) at the inverter terminal. Afterward, the testing of the inverter was also carried out for the same quantities as above.

Secondly, the standards "IEC 61803, IEEE recommended practice for determination of power losses in high-voltage direct-current (HVDC) converter stations" was fully studied and investigated. The various equipment losses on the converter stations were determined and evaluated based on the formulas stipulated in this standard. For instance, the thyristor valve losses are divided into eight groups such as the thyristor conduction loss per valve, thyristor spreading loss per valve, other valve conduction losses per valve, DC voltage-dependent loss per valve, damping-resistor loss per valve, damping-capacitor loss per valve, turn-off losses per valve and reactor losses per valve. These losses were

carefully analyzed with the available system parameters and the datasheet parameters given by the manufacturer of the thyristor valves adopted in the LCC-based technology. The losses of other equipment on the converter stations were also investigated and calculated, for instance, the losses of converter transformers, AC filter losses, DC smoothing reactor losses and DC capacitor losses. Finally, the sum of the loss contributions of all these equipment were obtained to give the total losses produced by the converter stations as a whole. More so, the percentage losses of this equipment were also investigated and calculated.

On the other hand, the losses of VSC-based technology was also investigated and calculated using standards IEC 62751-1-2. Note that, this standard is mainly used to evaluate the converter valves losses. The loss mechanisms of the other equipment like converter transformers, AC filters etc. still adopt the standardized calculation methods stipulated in standard IEC 61803 for their loss evaluations. However, the publication of standards IEC 62751-1-2 allows objective comparisons to be made between the power losses of VSC and LCC stations. Here, the converter valve consists of IGBT and freewheeling diode device, which are collectively called IGBT module. The losses of the converter valve are divided into two, namely, the conduction losses and the switching losses, these losses were fully investigated and calculated based on the available system parameters and the datasheet parameters given by the manufacturer of IGBT module adopted in two-level, three-level and multi-level VSC configurations. Likewise, the losses of other equipment were also investigated and calculated as stipulated above, then finally, the sum of the losses of all this equipment were obtained to give the total loss contributions by converter stations as a whole. More so, the percentage losses of this equipment were also estimated for further conclusions.

More so, the HVDC technologies such as LCC-based, two-level, three-level, and multi-level VSC-based were also simulated on Matlab environment, Melcosim, and Semisel online loss simulator, and the losses were calculated accordingly.

Finally, the losses of the various HVDC technologies were compared to draw and reach conclusion as to which technology is more reliable, stable and efficient for power transmission system.

3.4 Research Instruments

This research made use of a software-based tool known as SimPowerSystem tools of Matlab. The Simulink package of this tool was used to model a typical HVDC model to investigate the variation of some parameters like the dc output voltage when the delay angle is varied. This was done to have an overview of how a typical HVDC system works. This environment was also used in the analysis and calculation of power losses in the converter stations of HVDC system. Various HVDC technologies were modeled using Matlab environment, the various loss equations were modeled into a block and interfaced accordingly on the modeled system to calculate the losses of various equipment on the converter stations. Subsequent to this Simulink model, matlab codes were written for the loss function of the formulas necessary to calculate the loss values of all the equipment on the converter stations using all the formulas stipulated in the standards IEC 61803, “IEEE recommended practice for determination of power losses in high-voltage direct-current (HVDC) converter stations”. These codes prompt the user to input variables according to his or her

design specifications, this makes it flexible such that various loss profile of the converter stations equipment can be obtained by varying the parameters used in the Matlab codes. These codes were used to calculate the power losses of HVDC converter stations at both the rectifier and inverter terminals, and most especially for the two HVDC technologies at large.

More so, in order to fully investigate and accurately calculate the losses of various equipment on converter stations, especially power electronics components like thyristors, IGBT modules etc. that makes up the valve, there are some operating parameter that can only be obtained on the datasheets, which are always given by the manufacturers of these electronic devices. For instance, the threshold voltage, the slope resistance, the nominal RMS on-state current, the junction-coolant thermal resistance, the form factor, junction temperature, all these are thyristor valve operating parameters. On the other hand, for IGBT modules, the operating parameters include the IGBT turn-on switching energy, IGBT turn-off switching energy, IGBT saturation voltage drop, diode reverse recovery energy, the thermal resistance of both IGBT etc. All these datasheet parameters are very important when calculating power losses in converter valves.

Finally, Melcosim software and an online loss simulator known as semisel were used to further validate the results obtained from using Matlab environment.

3.5 Research Layout

Organizing this research study really involve the use of set out goals and defined activities. Technical investigation, determination, and computation of power losses were carried out on a typical Simulink model with respect to the various HVDC technologies i.e. the LCC-based, two-level, three-level and multi-level VSC-based HVDC systems. The various step taken to meet up with the research objectives are highlighted below.

An extensive literature review was carried out on loss determination and calculations of various HVDC technologies such as LCC-based, two-level, three level and multi-level VSC-based. This is majorly to get a vast-based knowledge of the loss mechanisms of different converter stations equipment and the overall loss contributions of the converter stations as a whole on the electrical network, in order to know which of the equipment on the power grid that produce more power losses. This research contains the topologies, different configuration, applications and methods of calculating the power losses with all the formulas necessary for the execution and completion of the research objectives. These areas stipulated above were researched to really understand the concept of this research work. This process gives the overview of the loss percentages of various equipment on HVDC converter stations so as to have a theoretical guide towards my results.

3.5.1 Losses of HVDC System

When evaluating the losses of HVDC converter stations, it is recommended that two types of losses be distinguished: standby losses and total operating losses.

3.5.1.1 Standby Losses

These are the losses generated with the HVDC converter-station energized but with the valves blocked. Under this condition, the ac filters and shunt compensating equipment are not required, and they are not connected to the ac bus. Smoothing reactors and dc filters, if any, are also not energized. However, the station service and cooling equipment are connected as required for immediate pickup of the load. Standby losses can be considered as being equivalent to "no-load" losses in conventional ac substation practice [10].

3.5.1.2 Total Operating Losses

These are the total station losses produced with the converter station energized and the valves operating. When the converter valves are operating, the dc current is not permitted to drop below a defined minimum current, which is design-dependent and varies from project to project. Operating losses may be required to be evaluated at any load current between the minimum and maximum values. It is important to keep in mind that some of the equipment in the HVDC station is not used at all load levels; the ac filters are an example. Therefore, the calculation of the losses for a particular station loading must specify which apparatus is online for that load condition. In general, all equipment should be assumed to be connected, which is required to meet the specified performance at the particular load level. Total operating losses minus the standby losses can be considered as being equivalent to "load losses" in conventional AC substation practice [1, 10].

3.5.2 Methods of Converter Loss Evaluation

The efficiency of an HVDC converter station is most advantageous and less accurate to be determined by a direct measurement of its energy losses, which is taken as a general principle. However, it is imperative that any effort to compute the converter station loss by the method of subtracting the measured output power from the measured input power should realize that such measurements in application have an inherent inaccuracy, particularly if implemented at a very high voltage [2, 84]. In addition, HVDC converter power losses at full load are generally less than 1% of the power transmitted from the sending end of the network. Therefore, the actual power losses measured as a small difference between two large quantities is not likely to be an indication of adequately accurate measurement. For instance, a temporary test arrangement may be possible in some situations, such that two converters are operated from the same AC source and likewise connected together via their dc terminals. In this connection, the power drawn from the AC source equals the losses in the circuit. However, the ac source must also provide commutating voltage and var support to the two converters. Once again, there are practical difficulties in measurement [8, 85]. In order to avoid the problems described above, these standards standardize a method of calculating the HVDC converter station losses by summing the losses calculated for each item of equipment[10, 22].

Therefore, there are several techniques to analyze and estimate the power losses in HVDC converter stations.

3.5.2.1 Practical Measure or Direct Measurement Method

Determining the converter losses directly by simply finding the difference between the measured output power and the measured input power looks realistic, reasonable and accurate. However, the losses of the system are generally less than the transmitted power, if the scheme is carried out at high voltage and power, therefore, the actual power losses measured as a small difference between two large quantities is not likely to be an indication of an adequately accurate loss measurement. Moreover, at high voltage, the measurement is difficult to be carried out so the implementation of this technique is very applicable in situation of the small power [6, 13].

3.5.2.2 Test and Measure

Alternatively, the losses are essentially determined by the method of test and measure, which build up a sub-system by several thyristor valves and run it, at the same time the current and voltage curves of valves are measured by special facilities, subsequently, the power losses are computed from the record derived from measurement. In certain condition, the method gets the energy dissipation easily and precisely mainly by suitable apparatus and exact records for switching currents and voltages. However, the need for special facilities for valve voltage and current measurement are not that essential since this method also has inherent inaccuracy of loss measurement. Therefore, scheme comparison through characteristic values is performed by the method which is only used in some laboratory and manufacture [1, 13].

3.5.2.3 Software Model Method

One of the most efficient and accurate methods to illustrate the LCC-HVDC transmission is Computer simulation. Based on basic theory and specific models, the currents, voltages and losses in each individual components can be estimated by loss calculation program for LCC-HVDC transmission system model, which is built using software simulation program. In addition, depending on the accuracy of the built model (approximate model), the technique requires an exact model of the device considering the precision of loss calculation of the LCC-HVDC system. The more accurate the built model, the more the loss is closed to the actual result [3, 13].

3.5.2.4 Analytical Method

The power losses of each component are derived from Numerical equations. In this research work, estimation of the losses due to conversion process in the LCC converters are done by using a relationship that is based on the root mean square and the average value of the current that flows in the LCC converter. Meanwhile, the conventional equations are used for calculating losses in AC filter, converter transformer, converter valves, dc capacitors and the smoothing reactors. The only major demerit of this method results from the parameters which may differ from the actual operating parameters used in a real application [1, 36].

Table 3-1: Typical breakdown of HVDC converter station losses [6, 10]

No.	Equipment in the converter station		Total loss proportion of the various equipment on converter station (%)
1	Converter transformer	No-load losses or fixed losses	$12 - 14$
		Load losses or Variable losses	$27 - 39$
		Total losses	$39 - 53$
2	Thyristor converter valve		$32 - 35$
3	DC-Smoothing reactors		$4 - 6$
4	AC filters		$7 - 11$
5	Other Losses		$4 - 9$

Table 3-1 depicts the converter stations' equipment loss distributions. The converter transformer and thyristor valves losses account for a major portion of the converter stations' total losses which are illustrated by the given loss data on the table. These losses are approximately within the range of 71%-88%. Therefore, in order to reduce the converter stations' total losses, it is essential to reduce both the converter transformers and thyristor valves losses.

3.5.3 Power Losses Evaluation of Two-Level and Three-Level Converter Topologies

The two-level converter power losses admit expressions as equations (2-71) and (2-72), therefore, the sum of both the two equations result to the total power losses in the entire IGBT modules. As regards losses, there is difference between the two topologies. A two-level converter for a high DC voltage requires many series-connected IGBTs. With respect to the high switching frequencies used in two-level converter, the switching losses are relatively very high. Conversely, for the three-level topology, each valve only switched half the number of times and at half the voltage. Subsequently, the switching losses for a three-level converter tends to be about half of the two-level converter. Due to the lower forward voltage drop, conduction losses are also lower. As a result of the lower switching frequency in three-level converter, it generates a smoother voltage with little harmonics, also lowers losses in other components of the converter station [86].

3.5.3.1 Power Losses Calculations in Three-Level Converter

3.5.3.2 Conduction Losses

The conduction losses P_{con} consist of losses in the IGBTs and the freewheeling diodes. However, the conduction losses for each switches can be estimated by the following expression:

$$P_{con} = V_o I_{avg} + R_f I_{rms}^2 \tag{3-1}$$

Consequently, in a three-level converter configuration, there are four IGBTs and six diodes in each phase.

The load current and the phase leg voltage are the same as the two-level configuration. However, the duty cycle across the switching devices admit expressions as follows [12, 66]:

$$d_{T1} = \begin{cases} m \sin \omega t\,, & 0 \le \omega t \le \pi \\ 0, & \pi \le \omega t \le 2\pi \end{cases} \tag{3-2}$$

$$d_{T2} = \begin{cases} 1, & 0 \le \omega t \le \pi \\ 1 + m \sin \omega t\,, & \pi \le \omega t \le 2\pi \end{cases} \tag{3-3}$$

$$d_{T3} = 1 - d_{T1} \tag{3-4}$$

$$d_{T4} = 1 - d_{T2} \tag{3-5}$$

Therefore, the average and RMS currents that flow in the IGBT T_1 and T_4 admit expressions as follows:

$$I_{T1,av} = I_{T4.av} = \frac{1}{2\pi}\int_{\theta}^{\pi} d_{T1} i_a d\omega t = \frac{mI_m}{4\pi}\,[(\pi - \theta)\cos\theta + \sin\theta] \tag{3-6}$$

$$I_{T1,rms}^2 = I_{T4,rms}^2 = \frac{1}{2\pi}\int_{\theta}^{\pi} d_{T1} i_a^2 d\omega t = \frac{mI_m^2}{12\pi}[3 + 4\cos\theta + \cos 2\theta] \tag{3-7}$$

where

I_m= The peak of the output voltage, in Ampere.

θ= The phase difference between the output voltage and current.

m= modulation index.

Similarly, the currents for T_2 and T_3 admit expressions as [12]:

$$I_{T2,av} = I_{T3.av} = \frac{1}{2\pi}\left[\int_{\theta}^{\pi} i_a d\omega t + \int_{\pi}^{\pi+\theta} d_{T2} i_a d\omega t\right] = \frac{I_m}{4\pi}[4 + \theta m\cos\theta - m\sin\theta] \tag{3-8}$$

$$I_{T2,rms}^2 = I_{T3,rms}^2 = \frac{1}{2\pi}\left[\int_{\theta}^{\pi} i_a^2 d\omega t + \int_{\pi}^{\pi+\theta} d_{T2} i_a^2 d\omega t\right] = \frac{I_m^2}{12\pi}\,[3(\pi - m) + 4m\cos\theta - m\cos 2\theta] \tag{3-9}$$

Likewise, the average and RMS currents that flow in the freewheeling diodes admit expressions as:

$$I_{Da1,av} = I_{Da2,av} = I_{Da3,av} = I_{Da4,av} = \frac{1}{2\pi}\int_{0}^{\theta} d_{a1} i_a d\omega t = \frac{mI_m}{4\pi}\,[\theta\cos\theta - \sin\theta] \tag{3-10}$$

$$I_{Da1,rms}^2 = I_{Da2,rms}^2 = I_{Da3,rms}^2 = I_{Da4,rms}^2 = \frac{1}{2\pi}\int_{0}^{\theta} d_{T1} i_a^2 d\omega t = \frac{mI_m^2}{4\pi}\,[3 - 4\cos\theta + \cos 2\theta] \tag{3-11}$$

Similarly, the average and RMS currents that flow in the clamped diodes admit expressions as:

$$I_{Ta5,av} = I_{Ta6,av} = \frac{1}{2\pi}\left[\int_{\theta}^{\pi} d_{da3} i_a d\omega t + \int_{\pi}^{\pi+\theta} d_{da2} i_a d\omega t\right] = \frac{I_m}{\pi} - \frac{mI_m}{4\pi}\left[(\pi - 2\theta)\cos\theta + 2\sin\theta\right] \quad (3\text{-}12)$$

$$I^2_{sa5,rms} = I^2_{sa6,rms} = \frac{1}{2\pi}\left[\int_{\theta}^{\pi} d_{sa3} i_a^2 d\omega t + \int_{\theta}^{\pi+\theta} d_{sa2} i_a^2 d\omega t +\right] = \frac{I_m^2}{12\pi}\left[3\pi - 6m - 2m\cos 2\theta\right] \quad (3\text{-}13)$$

Subsequently, the above listed formulas can be used in equation (2-89) to compute the total conduction per valve of IGBT module.

3.5.3.3 Switching Losses

Practically, there are only two commutations per output in IGBTs T_2 and T_3, so therefore, the switching losses of these IGBTs are most of the time excluded, however, ideal case is being considered in this research work, so the switching losses are computed for a qualitative analysis.
Furthermore, the switching losses in the IGBTs T_1 to T_4 for a three-level neutral point clamped converter admit expressions as:

$$P_{T1,sw} = P_{T4,sw} = \frac{f_s}{2\pi}\int_{\theta}^{\pi} k_1 I_m \sin(\omega t - \theta) d\omega t = \frac{k_1 f_s I_m}{2\pi}\left[1 + \cos\theta\right] \quad (3\text{-}14)$$

$$P_{T2,sw} = P_{T3,sw} = \frac{f_s}{2\pi}\int_{\theta}^{\pi+\theta} k_1 I_m \sin(\omega t - \theta) d\omega t = \frac{k_1 f_s I_m}{2\pi}\left[1 - \cos\theta\right] \quad (3\text{-}15)$$

More so, the switching losses of the diodes considering the fact that there is only switch off energy (recovery energy) can be obtained using equation (2-77).

3.5.3.4 Power Losses Estimation in the DC-Link Capacitor

The ESR (Equivalent series resistance) value and the current through the capacitor can be used to determine the DC-link capacitor losses. Similarly, the ESR values can be obtained from the capacitor datasheet, more so, the current can be estimated with the assistance of charging and discharging times of the capacitor using SKN 130 capacitor datasheet. When the charge and discharge current are estimated, the current that drifts through the capacitor can be evaluated from the expression of charge and discharge currents [54, 87].

$$I_{rms} = \sqrt{I^2_{crms} + I^2_{dcrms}} \quad (3\text{-}16)$$

where

I_{crms}= rms value of charging current.

I_{dcrms}= rms value of discharging current.

Most of the power losses associated with the converter valve occurs in the switches, but there is also some power losses in the DC-link capacitor. The total power loss of the valve admits expression as:

$$P_{total\ losses\ per\ device+Pcap} = 6 * N_{IGBT\ valve}[P_{total\ IGBT\ losses} + P_{total\ Diode\ losses}] + P_{cap\ losses} \quad (3\text{-}17)$$

3.5.4 Evaluation of the Average Junction Temperature

Conduction and switching power losses are expected to surface when operating the power device contained in IGBT and intelligent power modules. Therefore, the heat generated due to these losses has to be dissipated away from the power chips and likewise the environment using a heat sink. However, the power device will over-heat, if an adequate thermal system is not adopted or put in place, which could leads to modules failure. Conversely, the system thermal design in many applications is limited by the maximum useable power output of the module. So therefore, in getting maximum output from the device, it is very essential to design accurate thermal system [21],[88].

3.5.4.1 Calculation of Case Temperature

$$T_C = T_f + P_{total} \times R_{th(c-f)} \quad (3\text{-}18)$$

where

T_f= Heat sink temperature, in $°C$

$R_{th(c-f)}$= Thermal impedance between case to fin, in $°C$/W.

3.5.4.2 Calculation of IGBT Junction Temperature

$$T_{j-IGBT} = T_C + P_{total-IGBT} \times R_{th(j-c)IGBT} \quad (3\text{-}19)$$

where

$R_{th(j-c)IGBT}$= Thermal impedance between junction to case, $°C$/W.

3.5.4.3 Calculation of Diode Junction Temperature

$$T_{j-diode} = T_C + P_{total-diode} \times R_{th(j-c)diode} \quad (3\text{-}20)$$

3.5.4.4 Thermal Model

The junction temperature T_j admits expression as:

$$T_j = P \times \left[R_{th(j-c)} + R_{th(c-hs)} + R_{th(hs-a)}\right] + T_a \quad (3\text{-}21)$$

where

T_j= Junction temperature.

P= Module power loss.

$R_{th(j-c)}$= Thermal Resistance junction to case.

$R_{th(c-hs)}$= Thermal Resistance case to heat sink.

$R_{th(hs-a)}$= Thermal Resistance heat sink to ambient.

The number of IGBTs connected in series in each, $N_{IGBT\ valve}$ valve admits expression as:

$$N_{IGBT\ valve} = \frac{V_{dc}*(V_{dc-max,99.9})*(V_{dc-max,SSOA})}{V_{IGBT,SSOA} - V_{miss-distr}} \quad (3\text{-}22)$$

where

$V_{dc-max,99.9}$ = Voltage factor.

$V_{dc-max,SSOA}$ = Switching safe operating area voltage factor.

$V_{miss-distr}$ = Voltage miss distribution.

$V_{IGBT,SSOA}$= Switching safe operating area voltage factor for IGBTs.

The margin between the maximum and rated SSOA voltage is as a result of the voltage spike caused by the reverse recovery action of diode current [60, 89]. However, with respect to the series connected IGBT modules, it is imperative that a single component failure does not result to a mal-function of the entire device. Therefore, there are also redundant IGBTs made available should in case there is a fault event in one of the IGBTS [90]. The standard values for a two-level configuration are given in table 2 (provided by the ABB Corporate Research Sweden) [91].

Table 3-2: Standard values to determine the number of series IGBT's in a valve [12]

V_{dc}	2800 V
$V_{dc-max,99.9}$	1.05 V
$V_{dc-max,SSOA}$	1.15 V
$V_{miss-distr}$	325 V
$V_{IGBT,SSOA}$	336.3 V
Redundant IGBT's	2

Therefore, using the values on table 3-2 into equation (3-22), the number of series connected IGBTs are 300. It is worthy of note that, since the diode turns on as soon as the forward voltage emerges, the diode has negligible turn-on losses. The turn-off loss due to diode recovery is not negligible. The freewheeling diode is switched on or off rapidly compared to the switching action of IGBTs, due to this singular reason, its switching losses are relatively small compared to that in an IGBTs, therefore, in calculation of losses, they are not considered [90, 91].

3.5.5 Semiconductor Power Loss Evaluation in M2C VSC-based HVDC Topology

The semiconductor losses are discussed by considering the switching losses and conduction losses [5]. However, the total converter loss includes some other sources like transformers and reactors, gate drive units that are not estimated most often, because their loss impact is insignificant. For a half-bridge M2C cell, the semiconductor losses are subdivided into four parts, the upper leg IGBT (T1) and diode (D1) losses, and the lower leg IGBT (T2) and diode (D1) losses [76]. The directions of the converter arm currents (positive arm I_p and negative arm I_n) flowing through the M2C cells are very imperative in the switching on and off states or cell operating modes. For instance, considering the positive arm, reference [42] explains the four M2C converter cell-operating modes. Note that the same mode analysis is also applicable to the negative arm. For easy evaluation of the conduction and switching losses, the following discrete formulas are utilized in the analysis which are further explained in standards IEC 62751-1-2 [15, 70].

3.5.5.1 Analytical Calculations of M2C Conduction Losses

All Submodules contribute to the conduction losses in a converter limb, since currents always flow through one semi-conduction device in each submodule. Based on the conducting current and on-state resistance of the device in each time step, the IGBT and diode conduction losses are determined. For instance, the submodule (cell) conduction loss of IGBT and diode in an arbitrary positive arm admit expressions as [68, 92]:

$$P_{I1cond}^{in}(t) = (1-k)P_{I1cond}^{in}(t-1) + k(V_{ceo} + R_o I_p(t))I_p(t) \quad (3\text{-}23)$$

$$P_{I2cond}^{by}(t) = (1-k)P_{I1cond}^{by}(t-1) + k(V_{ceo} + R_o I_p(t))I_p(t) \quad (3\text{-}24)$$

$$P_{D1cond}^{in}(t) = (1-k)P_{D1cond}^{in}(t-1) + k(V_{do} + R_d I_p(t))I_p(t) \quad (3\text{-}25)$$

$$P_{D2cond}^{by}(t) = (1-k)P_{D2cond}^{by}(t-1) + k(V_{do} + R_d I_p(t))I_p(t) \quad (3\text{-}26)$$

where

$P_{I1cond}^{in}(t)$= The IGBT conduction loss in T_1.

$P_{I2cond}^{by}(t)$ = The IGBT conduction loss in T_2.

$P_{D1cond}^{in}(t)$= The Diode conduction loss in D_1.

$P_{D2cond}^{by}(t)$ = The Diode conduction loss in D_2.

$I_p(t)$ = The arm current at t instant.

R_d = The Diode on-state resistor.

V_{do} = The Diode threshold voltage.

V_{ceo} = The IGBT threshold voltage.

R_o = The IGBT on-state resistor.

$k = \frac{\Delta t}{T_{filter}}$ = The filter constant.

Note that Δt and T_{filter} are simulation time steps and filter time constant, respectively which can be adjusted based on the design specifications [15, 68, 74].

3.5.5.2 Analytical Calculations of Switching Losses

The dissipation of energy at each switching mode is relative to both the current level and the junction temperature at that instance. Therefore, the maximum junction temperature of $125°C$ is assumed for both conduction and switching loss estimation. Note that, for each current level at each switching instants, the switching power loss is extracted using the datasheet of the electronic device. Similarly, the switching loss evaluation can be determined in time domain study by adopting the following formulas [12, 74, 76];

$$P_{I-sw}^{in}(t) = (1-k)P_{I-sw}^{in}(t-1) + kE_{on-I}I_p(t) \quad (3\text{-}27)$$

$$P_{I-sw}^{by}(t) = (1-k)P_{I-sw}^{by}(t-1) + kE_{off-I}I_p(t) \quad (3\text{-}28)$$

$$P_{D-sw}^{in}(t) = (1-k)P_{D-sw}^{in}(t-1) + kE_{on-D}I_p(t) \quad (3\text{-}29)$$

$$P_{D-sw}^{by}(t) = (1-k)P_{D-sw}^{by}(t-1) + kE_{off-D}I_p(t) \quad (3\text{-}30)$$

where

$P_{I-sw}^{in}(t)$ = The IGBT turn on power loss.

$P_{I-sw}^{by}(t)$ = The IGBT turn off power loss.

$P_{D-sw}^{in}(t)$ = The Diode turn on power loss.

$P_{D-sw}^{by}(t)$ = The Diode turn off power loss.

$E_{on-D}I_p(t)$ =The diode turn on energy loss at $I_p(t)$.

$E_{on-I}I_p(t)$ = The IGBT turn on energy loss at $I_p(t)$.

$E_{off-D}I_p(t)$ = The Diode turn off energy loss at $I_p(t)$.

$E_{off-I}I_p(t)$ = The IGBT turn off energy loss at $I_p(t)$.

$k = \frac{\Delta t}{T_{filter}}$ = The filter constant.

3.6 Research Strategy and Limitations

Various techniques are adopted in the industry for making an economic evaluation of the cost of losses in electrical equipment; in particular, several methods have been suggested for use with HVDC converter station. In respect of this, the research conducted with respect to this dissertation was based on real analysis on the determination and calculations of power losses in HVDC converter stations, limiting the scope to LCC-based, two-level, three-level and multi-level VSC-based technologies. The proposed research took the form of a new research but on an existing research subject. Based on the formulas stipulated in the standards IEC 61803, "IEEE recommended practice for determination of power losses in high-voltage direct-current (HVDC) converter stations, necessary steps were taken to further simplify some of these formulas to ease the calculations of some of the equipment losses. The scope of this

research is limited to investigation, determination, calculation and system simulation of power losses in HVDC converter stations of the following technologies, LCC-based, two-level, three-level and multi-level VSC-based technologies.

3.7 Research Assumptions

- The HVDC system operation uses constant current at the rectifier terminal and constant extinction angle at the inverter terminal.
- For an optimal and proper operation of the HVDC system, the delay (firing), angle, α and the overlap (commutation) angle, μ were taken as 19° and 10° respectively.
- A six-pulse converter whose valve side winding are in star and delta configuration equipped with separate converter transformer was adopted in the HVDC model.
- It is important to keep in mind that some of the equipment in the HVDC station is not used at all load levels, the ac filters are typical examples. Therefore, the calculation of the losses for a particular station loading must specify which apparatus is online for that load condition. This research considered the general case, where all equipment are assumed to be connected, which is required to meet the specific performance at the particular load level.

3.8 Summary

As a general principle, it would be expedient to evaluate the HVDC converter station's efficiency by the direct measurement of its energy losses. However, the practical difficulty that prevents such measurement include the attempt to determine the station losses using an intuitive method of obtaining the converter station power losses by subtracting the measured output power from the measured input power. However, the difference between these two measured values is small, and a good accuracy will be difficult to reach. For most cases, therefore, the losses have to be estimated from component characteristic using suitable mathematical models of the converter station equipment. This chapter presented the methods, IEEE standards, the software programs and the document (datasheet) used for the investigation, determination and calculations of the HVDC converter stations equipment losses. The IEEE standard that contains the various formulas required for the accurate computation of the individual losses of the converter stations' equipment were briefly mentioned. The software program used to code the loss profile functions for each converter station's equipment was as well mentioned. Finally, the datasheet used to check the operating parameter values, which are only given by the manufacturer of the electronic devices, was also stated in this chapter. Therefore, the methods, IEEE standards, the software programs and the document (datasheet) were used to actualize the results in the subsequent chapters.

CHAPTER FOUR
RESULTS AND ANALYSES OF POWER LOSS DETERMINATION OF LCC-BASED HVDC CONVERTER STATIONS

4.1 Introduction

It is the consensus of the manufacturers, industries and researchers at large that the HVDC converter station total losses should be determined as the sum of the losses of various equipment on the converter station. It is imperative to understand that the actual losses of various equipment on the converter stations actually depend on the operating conditions or duty cycles to which it is applied as well as on the ambient conditions under which it operates. Therefore, the operating and ambient conditions for various equipment on the converter station must be defined, in order for the summation of the individual losses to be an adequately accurate depiction of the actual HVDC converter station total losses, based on the operating and ambient conditions of the whole HVDC converter station. In addition, losses or electrical features are measured at the factory under standardized operating and ambient conditions for some equipment or components. In these cases, some well-recognized calculation procedures were adopted to relate the results to the actual conditions in the HVDC converter station [52, 93]. The equipment losses were determined based on standardized calculation method stipulated in IEC 61803, IEEE 1158 and the component datasheet parameters, which is the fundamental principle of the recommended practice. Therefore, the entire HVDC converter station, which is mostly obtained by the summation of the various equipment losses, does give a dependable measure of the station losses. In addition, note that the two converters at the converter station can be connected to operate in a back-to-back manner that is, transmitted from one converter to the converter station and then returns from the other converter to the AC system. At this time, the active power delivered to the converter station by the AC compensating system is taken as the loss of the converter stations. However, for commutation purposes, it is required that the AC system has to supply the reactive power to the converters, therefore, seems to affect the measuring accuracy[23, 94]. As such, the converter stations' losses are not measured directly, but the acceptable loss calculation method it's obtained by calculating the loss of each piece of equipment in the converter station and subsequently, summing the losses together to obtain the total converter station losses [7, 22].

In this chapter, the results and analyses of loss profiles of individual equipment of LCC-based HVDC converter stations were explicitly illustrated with illustrative tables, charts (i.e. bar chart and pie chart). The research aims and objectives were carried out as well as some of the research questions stipulated in chapter 1 of this dissertation were fully answered in this section.

4.2 Results and Analyses

In this research work, thorough determination and analyses of the power losses of LCC-based HVDC converter stations were carried out. The analyses of some of the key equipment on converter stations that contribute large amount of losses were done in accordance with the standards IEC 61803, IEEE recommended practice for Determination of

Power Losses in High-Voltage Direct-Current (HVDC) Converter Stations along side with the power electronic device datasheet. Subsequent to these analyses, the following results were obtained.

4.2.1 Thyristor Valve Loss Calculations

Valve losses are complex and controversial issue, which needs immediate consideration in HVDC transmission systems. Reason been that, the magnitude and distribution of individual loss components are not that easy to predict and are somehow difficult to verify by measurement alone. This poses an urgent attention to other loss calculation methods, which are adopted in this research work. This study utilized two approaches towards loss calculations of HVDC converter valves, first is the analytical approach utilized in this chapter to evaluate the loss mechanisms of the thyristor valves. The second method is the simulation technique used in the subsequent chapter. The eight loss mechanisms of thyristor valves losses are:

4.2.1.1 Thyristor Conduction Loss per Valve W1 Calcculations

Table 4-1: Thyristor conduction loss per valve calculations

Data sheet parameters Of phase control thyristor type: DCR3030V42.	V_{TO}	R_O	I_T	$R_{\theta J}$	$R_{\theta C}$	T_C
	0.98V	0.198mΩ	4760 A	0.0130k/w	0.004k/w	125℃
	A	B	C	D		
	0.417877	0.1200233	6.308007×10^{-4}	-7.297986×10^{-3}		
μ (overlap angle)	10°					
n (number of thyristor level connected in series)	2					
I (dc current)	2000 A					
W_j (on state power loss)	3050.3 W					
T_j (junction temp)	176.86℃					
V_T(thermal voltage)	3.933 V					

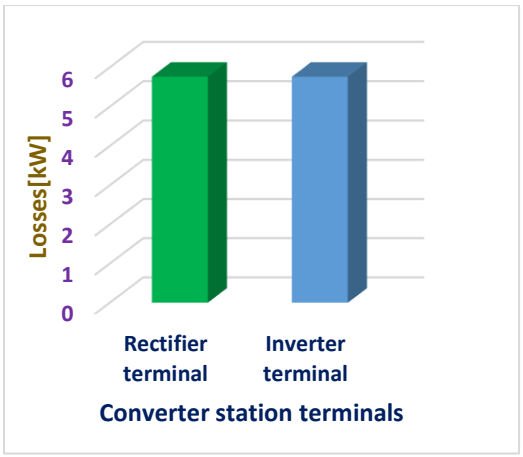

Figure 4-1: Thyristor conduction loss per valve

Table 4-1 and Figure 4-1 show the results from the calculation of the thyristor conduction loss per valve of both the rectifier and inverter terminals. The on-state voltage (i.e. the thermal voltage) was first calculated, using set of constants A, B, C and D whose values are given in the datasheet, subsequently, the junction temperature and on-state power loss were estimated. Lastly, the conduction per valve of the thyristor was calculated. Note that the formulas used to calculate the above quantities are stipulated in the standards IEC 61803 [4]. From the above results, the conduction loss per valve at the rectifier terminal of the converter station is the same as that of the inverter terminal, which shows that both the station terminals have equal power loss contributions on the transmitted power. Note that the threshold voltage,V_{TO}, the thermal resistance, R_O, the nominal rms on-state current, I_T, the junction thermal resistance, $R_{\theta J}$, case thermal resistance, $R_{\theta C}$, and case temperature, T_C are given in the device datasheet.

4.2.1.2 Thyristor Spreading Loss per Valve W_2 Calculations

Table 4-2: Thyristor spreading loss per valve calculations

Given parameters	n	f	v_1	v_2	α	μ	i
	2	50Hz	3.53	3.528	19°	10°	4760 A

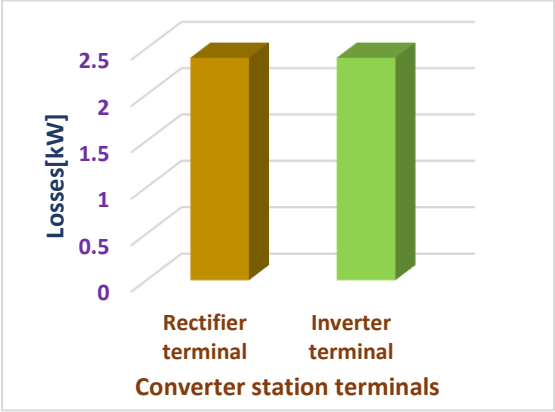

Figure 4-2: Thyristor spreading loss per valve

Table 4-2 and figure 4-2 show the results from the calculation of the thyristor spreading loss per valve of both the rectifier and inverter terminals using the set of equations in the standards. The spreading loss per valve of the thyristor at both terminals was calculated using the parameters given on table 4-2. Likewise, from the above results, the thyristor spreading loss per valve at the rectifier terminal of the converter station is the same as that of the inverter terminal, which shows that both the station terminals have equal power loss contributions on the transmitted power. Note that, the mean value of instantaneous on-state voltage drop of the thyrstor v_1 was calculated. Likewise, v_2, the instantaneous on-state voltage of the average thyristor was predicted with little discrepancies using. Note that all the above results indicated on table 4-2 and figure 4-2 were obtained using the stipulated formulas in standards IEC 61803. The nominal RMS on-state current was also obtained from the datasheet of the device, lastly, the firing angle, α and overlap angle, μ were chosen as 19° and 10° respectively for optimal operation of the HVDC system.

4.2.1.3 Other Valve Conduction Losses per Valve W_3 Results

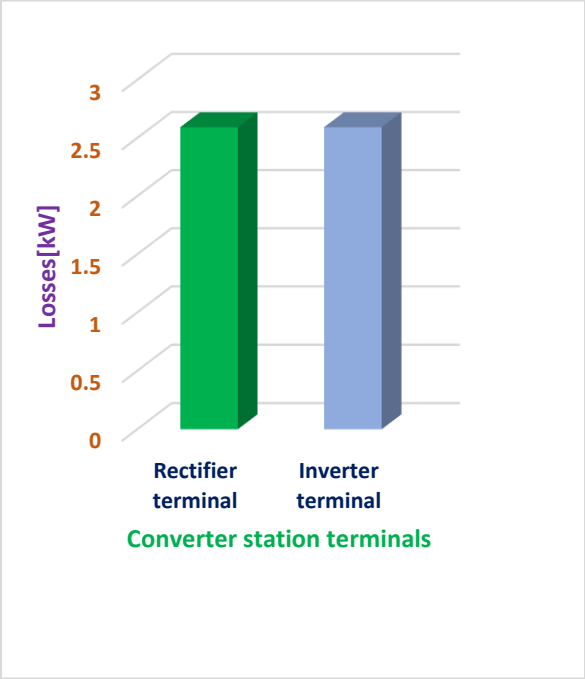

Figure 4-3: Other conduction loss per valve

Figure 4-3 shows the results from the calculation of the other conduction loss per valve of both the rectifier and the inverter terminals using the standardized mathematical representations. The overlap angle was taken as 10°, the value of dc resistance between two ends of the thyristor valve was taken from the datasheet and finally the dc current that flows through the bridge arm of the thyristor was taken to be 2000 A. Since the HVDC system is operating on constant current at the rectifier terminal and constant extinction angle at the inverter terminal. From the above results, the other conduction loss per valve at the rectifier terminal of the converter station is the same as that of the inverter terminal, which shows that both the station terminals have equal power loss contributions on the transmitted power.

4.2.1.4 DC Voltage-Dependent Loss per Valve (DC voltage-related loss) W_4 Calculations

Table 4-3: DC voltage-dependent loss per valve calculations

Parameters needed for calculations.	m	α	μ	V_L	$V_{rms=\frac{V_L}{\sqrt{2}}}$
	0	19°	10°=0.1745rad	440/350 kV	311.13 kV
$V_{DC-offset}$	800 V				
$I_{DC-offset}$	0.0001 A				
$R_{DC} = \frac{V_{DC-offset}}{I_{DC-offset}}$	8 MΩ				

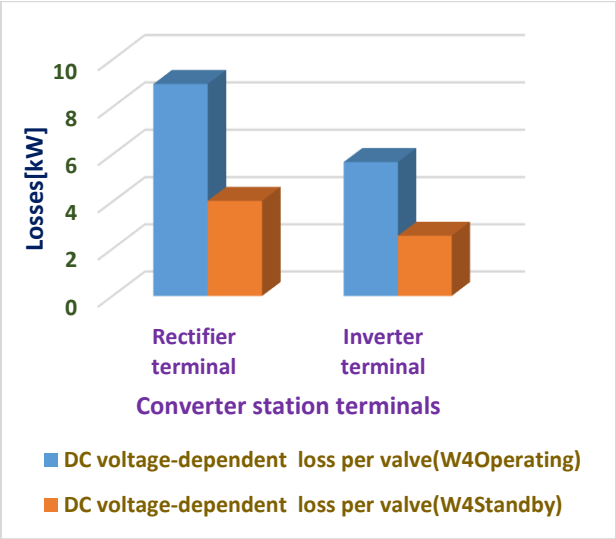

Figure 4-4: DC voltage-dependent loss per valve

Table 4-3 and figure 4-4 show the results from the calculation of the DC-Voltage dependent loss per valve using the set of equations in the standards used for this research (IEC 61803). It was noted that the DC offset voltage of a thyristor is quite large due to its high value of its DC resistance and low DC offset current, which are readily available in the datasheet of the thyristor. Note that one of the research assumptions, a six-pulse converter whose valve side winding are in star and delta configuration equipped with separate converter transformer was adopted in the HVDC model. Due to this configuration, the inductance between the commutation voltage source and the common coupling point of star and delta configuration on the valve side, L_1=0, therefore, the mutual inductance, m=0. More so, the RMS line-to-line voltage is also obtained by dividing the source line-to-line voltage, finally the delay and the overlap angle remain the same. The power loss, when the thyristor is in standby mode was also calculated for both converter station terminals. From the above results, the other conduction loss per valve is higher at the rectifier terminal of the converter station than at the inverter terminal, which shows that the rectifier station terminal has larger power loss contributions on the transmitted power.

4.2.1.5 Turn- off Loss of Thyristor Valve W_7 Results

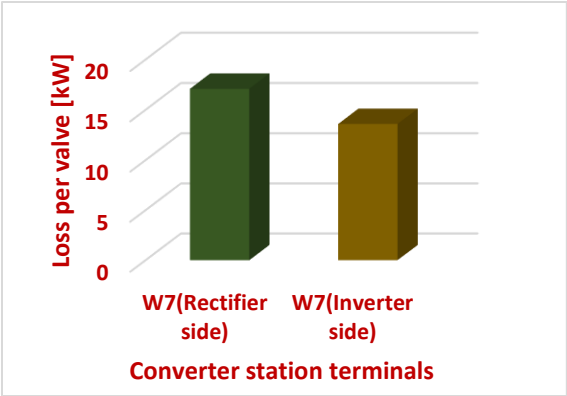

Figure 4-5: Turn-off loss per valve at the converter terminals

Figure 4-5 shows the results from the loss calculations of turn-off loss per valve using standardized mathematical model in IEC 61803. The delay and overlap angles remain 19° and 10° respectively, the frequency of operation is 50Hz, the rms line-to-line commutation voltage is calculated to be 311.13kV, the commutation di/dt measured at the instance of zero crossing, $\left(\frac{di}{dt}\right)_{i=0}$ and the average value of thyristor-stored charge measured at the junction temperature, Q_{rr} are readily available in the device datasheet. Subsequently, the time, t_0 was obtained using the formula in the standards. From the above illustrated chart results, the turn-off loss per valve is higher at the rectifier terminal of the converter station (17.093 kW) than at the inverter terminal (13.596 kW), which shows that the rectifier station terminal has larger power loss contributions on the transmitted power.

4.2.1.6 Reactor Losses per Valve (Saturable Reactor Hysteresis Loss of Thyristor Valves) W_8

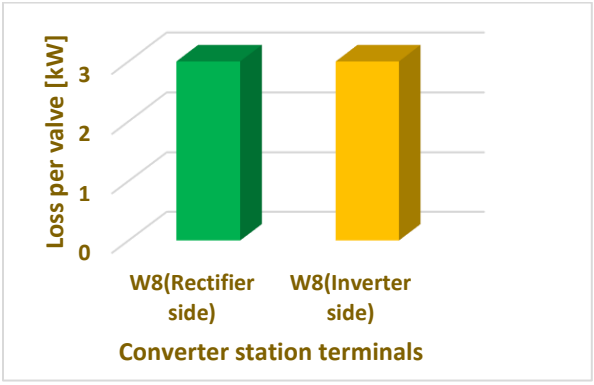

Figure 4-6: Reactor loss per valve at station terminals

Figure 4-6 shows the results from the loss calculation of the reactor loss per valve using the idealize mathematical representations stipulated in standards IEC 61803. The number of reactor cores in a valve is 3, the mass of each core is 5kg, the characteristics of hysteresis loss is 4J/kg and the frequency of operation is 50 Hz. Likewise, from the above results, the reactor loss per valve at the rectifier terminal of the converter station (3 kW) is the same as that of the inverter terminal (3 kW), which shows that both the station terminals have equal power loss contributions on the transmitted power.

4.2.1.7 Damping Loss per Valve (Loss of Damping Resistor) W_5 Results

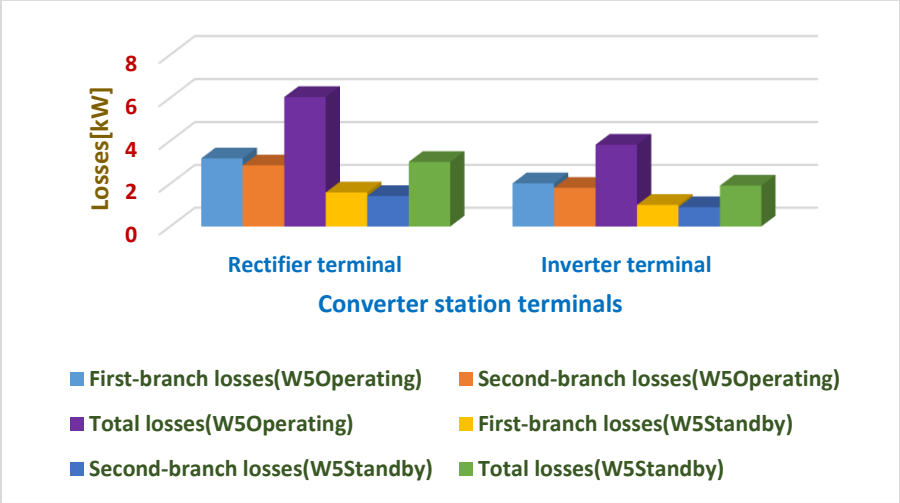

Figure 4-7: Damping loss per valve (loss of damping resistor)

Figure 4-7 shows the results from the calculation of the damping resistor loss per valve. The loss contribution of each branch-damping resistor of the grading network was calculated using the standardized calculation method stipulated in IEC 61803. For instance, the damping resistor dependent loss component of the first branch was calculated, with R_1=5kΩ, the result was added separately with that of the second branch following the same procedure as the first branch and are subsequently added together for each of the station terminals respectively. More so, the mutual inductance, m=0, the delay and overlap angles are 19° and 10° respectively. Furthermore, the thyristor valve loss of each of the branches of the grading network during standby mode was also calculated at both converter station terminals. From the above results, the other conduction loss per valve is higher at the rectifier terminal of the converter station than at the inverter terminal, which shows that the rectifier station terminal has larger power loss contributions on the transmitted power.

4.2.1.8 Loss Due to Charging and Discharging of Capacitors W_6

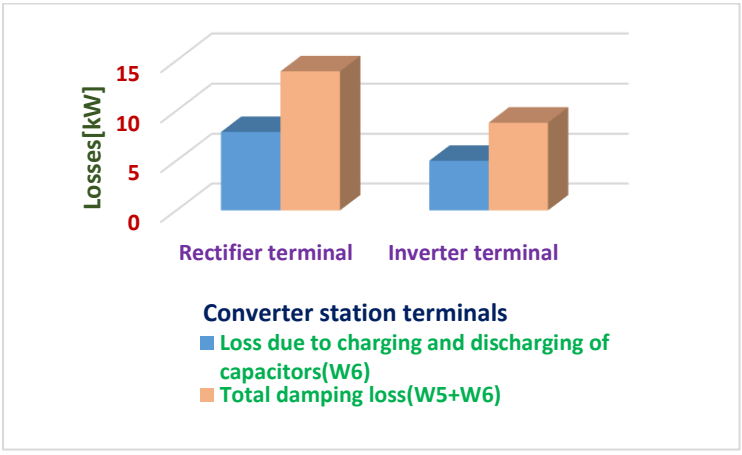

Figure 4-8: Loss due to charging and discharging of capacitor and total damping losses

Figure 4-8 shows the loss calculation due to charging and discharging of capacitors. The total capacitance of the voltage grading and damping circuits inside the thyristor valve,C_{hf}, which is the sum of all the damping capacitances, C_1 and C_2, which are the damping capacitances, C_3, which is the dc grading capacitance and C_s, which is the stray capacitance mainly for fast voltage distribution. The mutual inductance, m, delay angle, α, overlap angle, μ, frequency of operation and rms line-to-line voltage are still the same as previously stated. The loss contribution of each branches due to charging and discharging of capacitors of the grading network was calculated. Note that the above calculations were done using the standardized calculation method stipulated in standards IEC 61803. More so, figure 4-8 shows the total damping loss of the valve, which is the summation of the loss of damping resistor and the loss due to charging and discharging of capacitors. Likewise from the results, the loss at the rectifier terminal is also higher than that of the inverter, which shows that the rectifier station terminal has larger power loss contributions on the transmitted power [39].

4.2.1.9 Total Valve Losses W_T Results

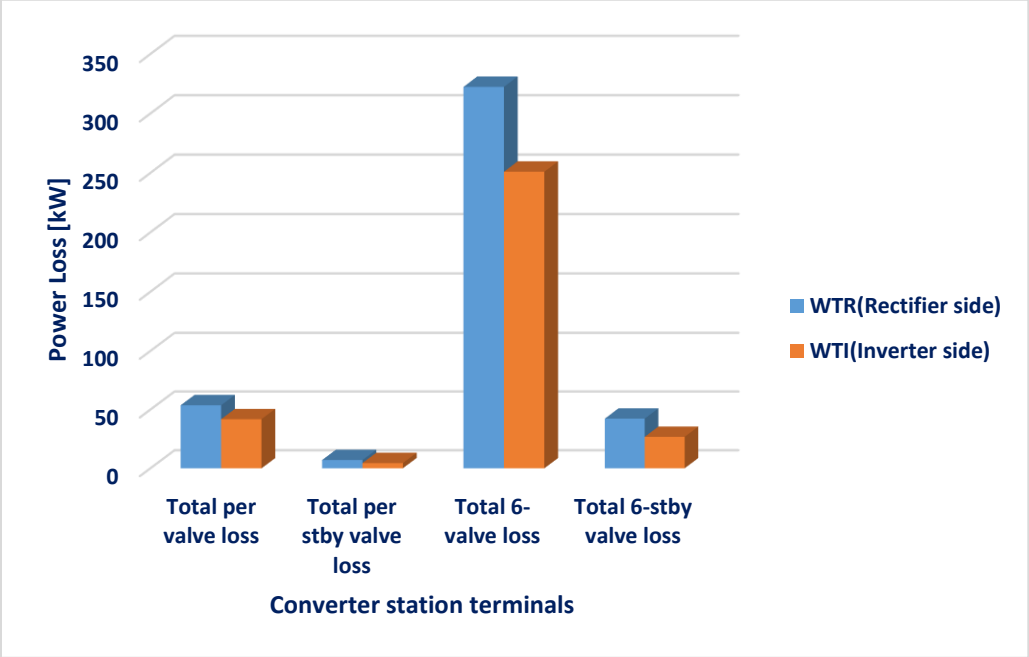

Figure 4-9: Total valve loss per valve, standby loss and 6-valve loss at station terminals

Figure 4-9 shows the chart illustration of the loss calculations of total valve loss by summing up all the losses associated with the thyristor valve and consequently multiplying the result by 6 to give the total valves losses for 6-pulse thyristor valves. Likewise, the total thyristor valves losses during the standby mode were also calculated. The chart illustrates the results in two ways, the total losses per valve of both operating and standby modes at the rectifier terminal (53.734 kW and 7.052 kW respectively) and at the inverter terminal (41.830 kW and 4.462 kW respectively). Likewise, the total losses for 6-thyristor valves of both operating and standby mode at the rectifier terminal (322.404 kW and 42.308kW respectively) and the inverter terminal (250.982 kW and 26771 kW) are also depicted on the chart.

From the above results, the total valve loss is higher at the rectifier terminal of the converter station than at the inverter terminal, which shows that the rectifier station terminal has larger power loss contributions on the transmitted power.

4.2.2 Losses of Converter Transformers

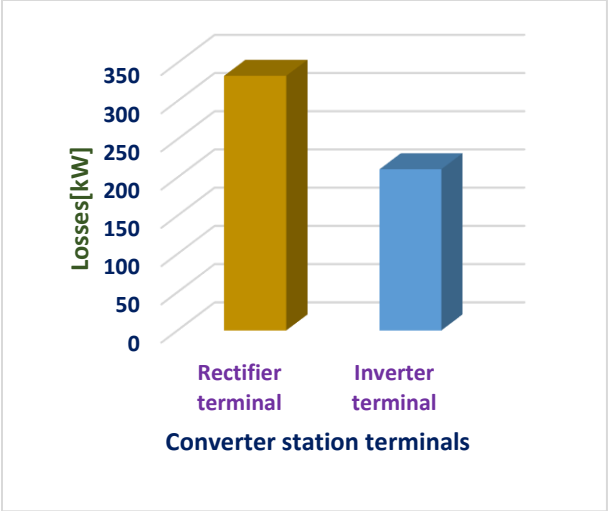

Figure 4-10: Converter transformer losses using method 1 (transformer effective resistance at various harmonic frequencies).

Figure 4-10 shows the loss calculation result of the rectifier station transformer using Method 1. The analysis starts with the computations of the characteristic harmonic currents using equation (2-4), then a constant parameter, F, k_1 and k_2 were calculated using equations (2-5), (2-6) and (2-7) respectively. Therefore, with these calculated parameters, the harmonic currents were calculated using equation (2-4). Subsequently, the effective resistance, R_n, was calculated using equation (2-3) and the variation of transformer resistance with frequency table stipulated in the standard IEC 61803, IEEE recommended practice for Determination of Power Losses in High-Voltage Direct-Current (HVDC) Converter Stations, finally, the square of the harmonic currents were multiplied by the effective resistance to obtain the losses due to converter transformer operations.

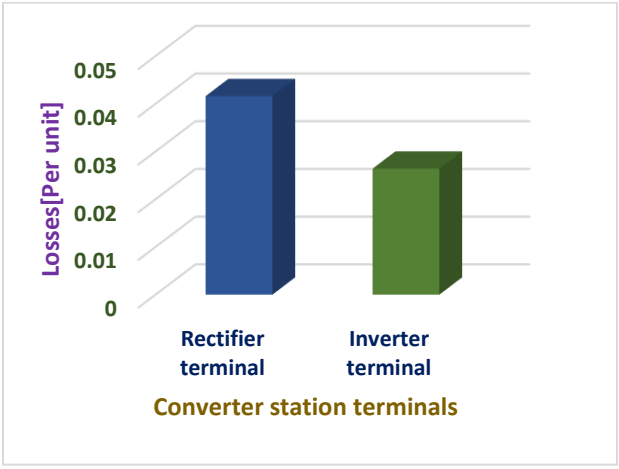

Figure 4-11: Converter transformer losses using per unit method

Figure 4-11 shows an alternative method of calculating the converter transformer losses using per unit method, the same procedures as described above, as the conventional method of calculation still applies but the results are calculated in per unit. Thus, the results is multiplied by the base value parameters of the transformer to obtain the actual value, which must tally with the conventional method. The loss contribution becomes quite small at the higher harmonics with characteristic harmonics from the 35th order to 49th order, contributing less than 1% to the load loss.

Table 4-4: A breakdown of the converter transformer losses using per unit method

1 p.u loss=$I^2R_{effective}$		8 MW
I=rms value of full load current		2 kA
R_{eff} =Effective resistance at 50Hz		2 kΩ
Loss in per unit	Rectifier terminal	0.0416 p.u
Loss in per unit	Inverter terminal	0.0264 p.u
DC resistance per phase referred to the valve winding side, $R_{dc}(1.2\Omega)$ =I^2R_{dc}× loss in p.u		199.84 kW
Stray losses if there were no harmonics=$I^2(R_{eff}-R_{dc})$ × loss in p.u		133.23 kW
Total load loss= 1 p.u loss × loss in p.u	Rectifier terminal	333.07 kW
	Inverter terminal	210.75 kW

Table 4-4 shows the total breakdown of the converter transformer losses using the per unit method of loss analysis

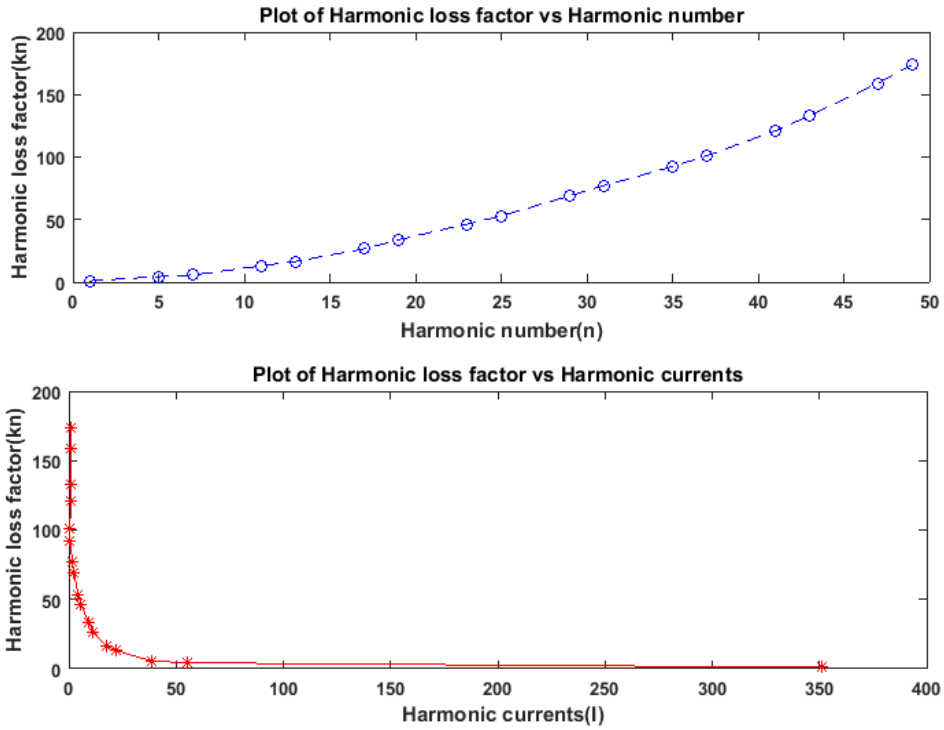

Figure 4-12: Harmonic loss factor versus harmonic number (n) /harmonic current (I)

From the above results, the converter transformer loss at the rectifier terminal of the converter station is higher than that of the inverter terminal, which shows that the rectifier station terminal has larger power loss contributions on the transmitted power. From figure 4-12, which shows the plot of harmonic loss factor against harmonic number and harmonic current respectively, it can be deduced from the plot that the harmonic loss factor is directly proportional to the harmonic number i.e. increase in harmonic loss factor will result to a corresponding increase in harmonic number. On the other hand, it can also be deduced from the other plot that the harmonic loss factor is inversely proportional to the harmonic current to a certain value of the harmonic current, and then afterwards becomes constant throughout the transformer operation.

4.2.3 AC Filter Losses

4.2.3.1 Filter Resistor Loss Results

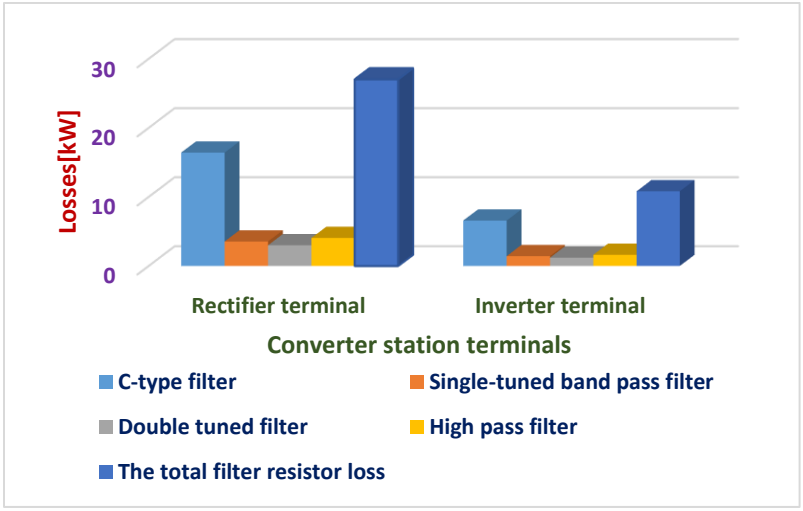

Figure 4-13: Filter resistor losses

Figure 4-13 show the results from the loss calculation of the filter resistor loss of various filter types used, using equation (2-8) to equation (2-21). Starting from the C-type filter which is mainly used for low order high pass filtering (i.e. was used to mitigate the 5th and 7th harmonic orders). The currents due to these harmonic orders, $I_5 + I_7$, were added together at both converter station terminals, the q-factor of low order high pass filters is always between the ranges of 45-50, so 50 was selected for this filter design, the values of C_1, R, and L were calculated for both station terminals using equations (2-12), (2-14) and (2-13) respectively. Therefore, having known the above stated parameters, the filter resistor losses due to C-type filter was calculated using equation (2-8).

Secondly, with the single-tuned band pass filter, which is mainly used to mitigate the 11th and 13th harmonic orders. Therefore, the currents due to these harmonic orders, $I_{11} + I_{13}$, were added together at both converter station terminals, the q-factor of band pass filters is always between the ranges of 15-20, so 20 was selected for this filter design, the values of C, R, and L were calculated for both station terminals using equations (2-9), (2-11) and (2-10) respectively.

Therefore, having known the above stated parameters, the filter resistor losses due to single-tuned band pass filter was calculated using equation (2-8).

Thirdly, with the double-tuned filter which is mainly used to eliminate the 17th and 19th harmonic orders. Therefore, the currents due to these harmonic orders, , $I_{17} + I_{19}$, were added together at both converter station terminals, the q-factor of this tuned filter is always between the ranges of 2-4, so 4 was selected for this filter design, the values of C_1, C_2, R, L_1, and L_2 were calculated for both station terminals using equations (2-15), (2-16), (2-14), (2-17), (2-18) respectively. Therefore, having known the above stated parameters, the filter resistor losses due to double-tuned filter was calculated using equation (2-8).

Lastly, with the high pass filter which is mainly used to mitigate all the harmonics from the 23rd to 49th harmonic orders. Therefore, the currents due to these harmonic orders, $I_{23} + I_{25} + \cdots \ldots \ldots + I_{49}$, were added together at both converter station terminals, the q-factor of band pass filters is always between the ranges of 1-2, so 2 was selected for this filter design, the values of C, R, and L were calculated for both station terminals using equations (2-19), (2-21) and (2-20) respectively. Therefore, having known the above stated parameters, the filter resistor losses due to high pass filter was calculated using equation (2-8). From the above results, the filter resistor loss is higher at the rectifier terminal of the converter station than at the inverter terminal, which shows that the rectifier station terminal has larger power loss contributions on the transmitted power.

4.2.3.2 Filter Reactor Losses

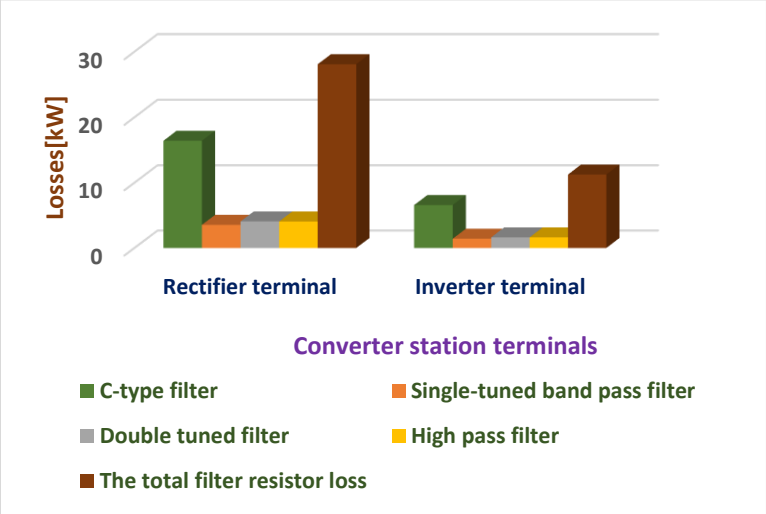

Figure 4-14: Filter reactor losses

Figure 4-14 show the results from the loss calculation of the filter reactor loss of various filter types used, using equation (2-22). The procedures used to calculate the filter resistor losses can also be similarly used to calculate the filter reactor losses. The only parameter needed to obtain is the harmonic inductive reactance,X_{Ln}, which is calculated using equation (2-23). Therefore, having known the above stated parameters, the filter reactor losses due to the various

filter types were calculated using equation (2-22). From the above results, the filter reactor loss is higher at the rectifier terminal of the converter station than at the inverter terminal, which shows that the rectifier station terminal has larger power loss contributions on the transmitted power.

4.2.3.3 Capacitor Bank Losses (Filter Capacitor Losses)

The average loss/kVar designs of the capacitors are given below;

Low dielectric loss = 0.1 w/kVar.

Paper, oil impregnated* =2.0 – 2.5 w/kVar.

Paper, PCB impregnated* = 3.0 – 3.5 w/kVar.

Plastic file/paper, PCB impregnated* = 0.5 – 1.0 w/kVar.

Metallized film = under 0.5w/kVar.

The asterik type are not manufactured anymore due to the non-biodegradability of the poly-chlorinated biphenyle (PCBs). Note that the Q_C used was 200MVar, then the power loss or shunt capacitor bank loss admits expression as equation (2-52), using low dielectric loss of 0.1w/kVar then ;

Capacitor bank losses at each of the converter station terminals admit expressions as:

Filter capacitor losses at the rectifier terminal = P = $\frac{0.1W}{kVar} \times kVar$

Filter capacitor losses at the inverter terminal = P = $\frac{0.1W}{kVar} \times kVar$

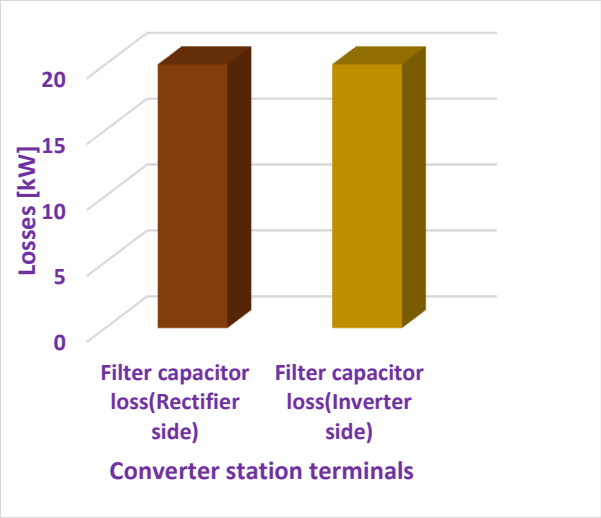

Figure 4-15: Filter capacitor loss calculations at station terminals

Figure 4-15 shows the results from the loss calculation of the filter capacitor loss using equation (2-24). From the above results, the filter capacitor loss at the rectifier terminal of the converter station is the same with that at the inverter terminal, which shows that both the station terminals have equal power loss contributions on the transmitted power.

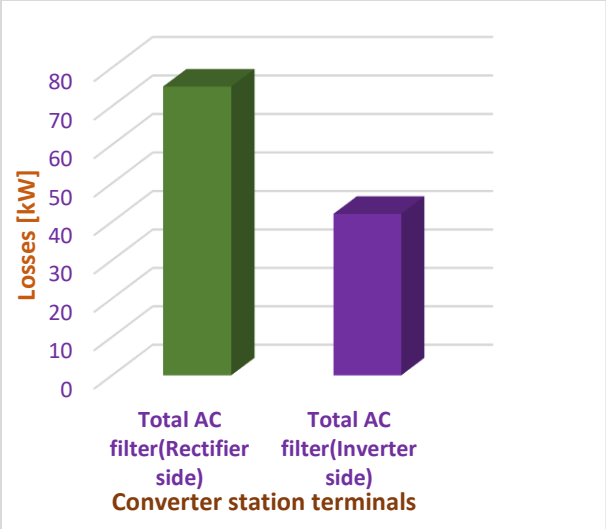

Figure 4-16: The total AC filter loss calculations at converter station terminals

Figure 4-16 shows the loss calculations of total AC filter losses, which is obtained by summing up all the losses associated with the AC filters installed at each of the converter stations to give the total AC filter loss contribution to the overall system network. The total AC filter losses of the rectifier terminal is 75.105 kW and that of the inverter terminal is 42.066 kW. From the above results, the total AC filter loss is higher at the rectifier terminal of the converter station than at the inverter terminal, which shows that the rectifier station terminal has larger power loss contributions on the transmitted power.

4.2.4 DC Smoothing Reactor Losses

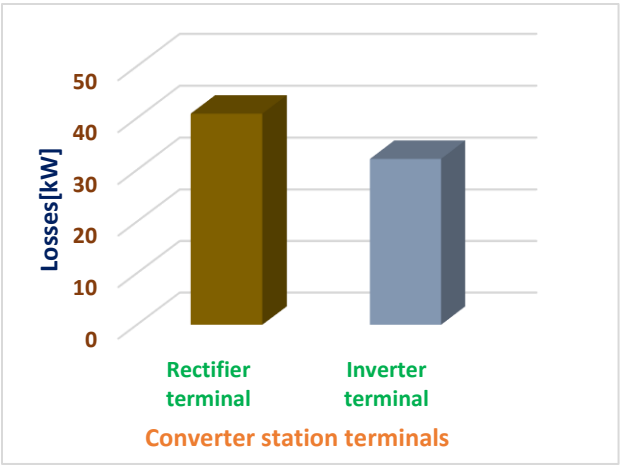

Figure 4-17: DC-Smoothing reactor losses

Figure 4-17 shows the result from the loss calculations of the DC-Smoothing reactor loss of both the rectifier and inverter terminals using equation (2-25) to equation (2-28). Firstly, the hysteresis loss component,P_{hn}, was calculated for all the harmonic orders using equation (2-26), afterwards, the eddy-current loss component, P_{en}, was evaluated for

harmonic orders greater than 10, using equation (2-27). More so, the eddy-current loss component, P_{e2}, was as well evaluated for harmonic orders less and equal to 2 using equation (2-28), finally, the sum of the results was put in equation (2-25) to obtain the magnetization loss, P_m. Similarly, the value of the direct current losses was also estimated using some conventional equations written on the table. From the above results, the DC-Smoothing reactor loss is higher at the rectifier terminal of the converter station than at the inverter terminal, which shows that the rectifier station terminal has larger power loss contributions on the transmitted power.

4.2.5 DC-Filter Capacitor Losses

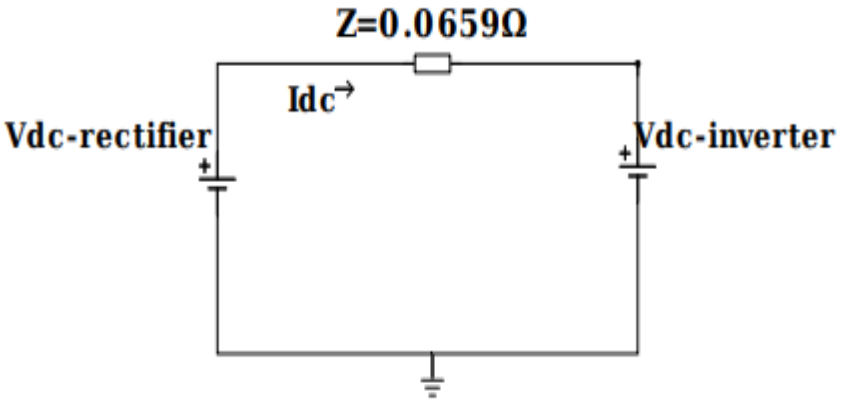

Figure 4-18: Simplified equivalent circuit of a typical HVDC system

Table 4-5: DC-filter capacitor loss parameters

Parameters required for loss calculations	Z	α	V_L	C_{cap}
	0.0659 Ω	19°	440 kV	0.3 nF
V_{dcr}(The input DC voltage to the rectifier converter).	561.64 kV			
V_{dci} (The input DC voltage to the inverter converter).	561.51 kV			
$R_{cap} = X_{cap}$ (Capacitive reactance)	10.610 MΩ			
P_{dc-cap} (DC-filter capacitor losses)	29.715 kV			

$$V_{dcr} = 1.35V_L \cos\alpha \quad (4\text{-}1)$$

Applying KVL to the above circuit of figure 4-18,

$$V_{dcr} = I_{dc}Z + V_{dci} \quad (4\text{-}2)$$

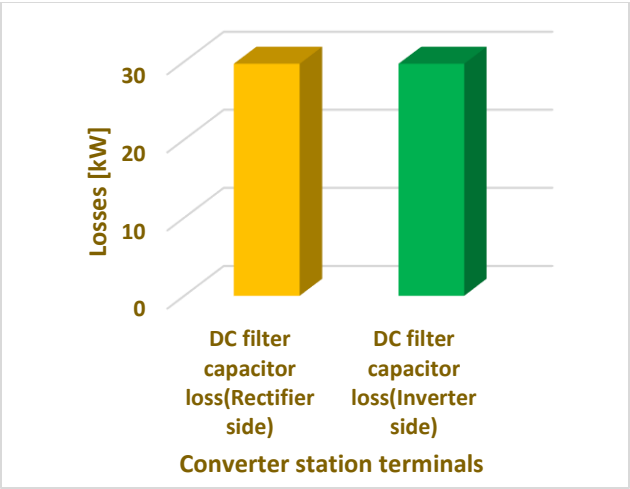

Figure 4-19: DC-filter capacitor loss calculations at converter station terminals

Table 4-5 and Figure 4-19 show the results from the loss calculations of the DC-filter capacitor losses using equation (4-1), equation (4-2) and equation (2-29). The first step was to calculate the rectifier dc voltage using equation (4-1), afterwards, the above result was used in equation (4-2) to compute the inverter dc voltage, finally, the value obtained above was used in equation (2-29) to evaluate the dc filter capacitor losses. From the above results, it can be deduced that the filter capacitor loss at the rectifier terminal of the converter station is the same with that at the inverter terminal, but not the same in all cases, it depends on the converter configurations and system operations.

4.2.6 Percentage Loss Calculations of Each Converter Station Equipment

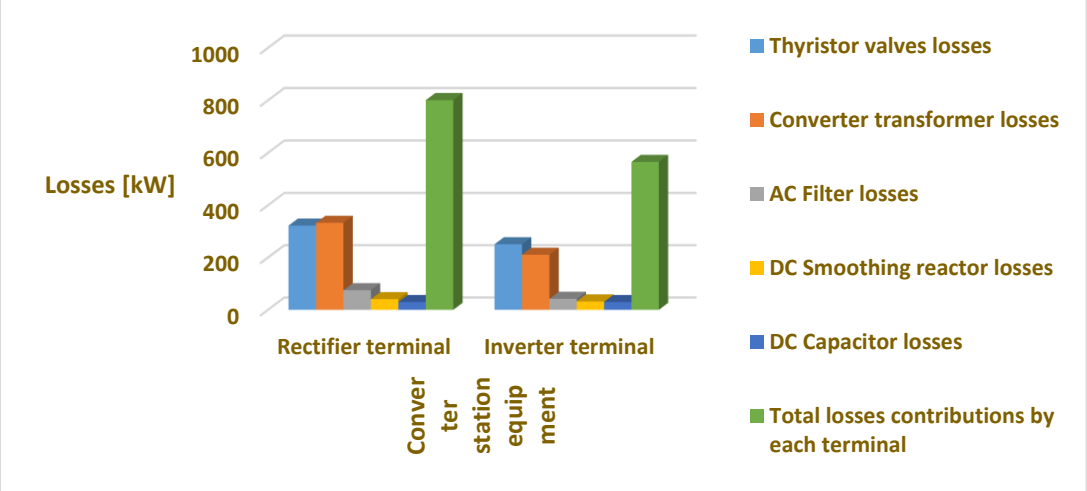

Figure 4-20: The total loss calculations of all the component of the converter stations

Figure 4-20 show the analysis of the total loss proportion of each converter station equipment both at the rectifier and inverter terminals. From these illustrations, it can be deduced that the loss proportion of each equipment at the rectifier

terminal is higher than that of the inverter side, likewise, the loss of the converter transformer and the thyristor valves have the highest losses contributions at both converter station terminals.

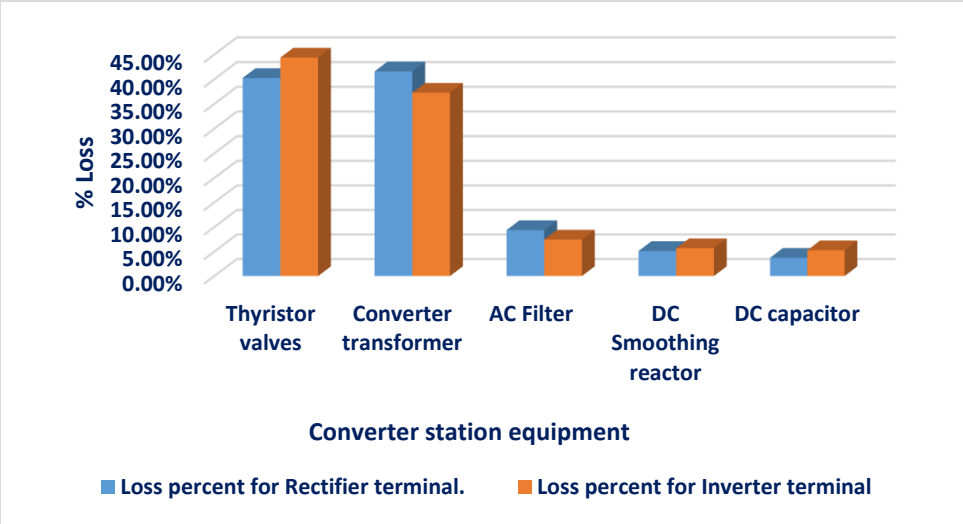

Figure 4-21: Percentage loss calculations of each converter station component

Figure 4-21 show the percentage loss analysis of each converter station equipment both at the rectifier and inverter terminals. From these illustrations, it can be deduced that the loss-percent proportion of the equipment at the rectifier terminal is higher than that of the inverter side, likewise, the percentage loss of the converter transformer and the thyristor valves have the highest loss-percent contribution at both converter station terminals.

4.3 Summary

The losses of each equipment in converter station fall with the decrease of the transmission power under bipolar operational conditions. The losses of each equipment in the converter station increase with the decrease of the DC voltage under different single operartional conditions. The losses of each equipment in inverter station are lower than those in rectifier station. The loss proportion of each equipment in converter station under the operartional mode condition of bipolar rated transmission power is seen on figure 4-20.

It can be seen from figure 4-20 and 4-21, that the losses of converter station are mainly composed of the losses of valve and converter transformer. To decrease the total losses of HVDC system, the losses of valve and converter transformer should be consider first. In view of all the analyses stipulated in this section, this justified that the aims and objectives of this research have been carried out to the last letter, more so, the results ontained answered all the research questions.

In conclusion, the difficulty of HVDC transmission system loss calculation falls in the loss calculation of the converter station. To understand the loss proportion of equipment in HVDC converter station and to decrease the losses of the HVDC system, analysis based on the formulas stipulated in the standard of IEC 61803, Determination of power losses in LCC-based high-voltage direct current (HVDC) converter stations were used to calculate the losses of each equipment in the converter stations [6, 56].

CHAPTER FIVE
RESULTS AND ANALYSES OF POWER LOSS CALCULATIONS OF VSC-BASED HVDC CONVERTER STATIONS

5.1 Introduction

The previous chapter described the method for determining power losses for line-commutated converter HVDC stations, which is well documented in standards IEC 61802. Moreover, the VSC HVDC systems adopt the same standardized calculation method of loss determination for various VSC-HVDC topologies such as 2-level, 3-level and modular multilevel converter using standards IEC 62751-1-2. Note that, for most converter stations equipment in VSC-HVDC system, the method of loss calculation of individual equipment is nearly the same to that described in standards IEC 61803. Hence, the major difference comes from the loss calculations of the converter valves, as a result, the method of loss determination is covered in the standards IEC 62751-1-2. The valve losses are divided into a number of categories and the losses due to each categories are calculated separately then subsequently, summed to obtain the total losses [14],[4].

5.2 Results and Analyses

In this research work, comprehensive determination and analyses of the power losses of VSC-based HVDC converter stations were carried out. The investigation of some of the key equipment on converter stations that contribute large amount of losses were done in accordance with the standards IEC 62751-1-2, IEEE recommended practice for Determination of Power Losses in Voltage Source Converter High-Voltage Direct-Current (HVDC) Converter Stations, alongside with the power electronic device datasheet.

The purpose of this chapter is to calculate the loss mechanisms of the popular VSC-based HVDC technologies. The topologies considered in this chapter are two-level, three-level and modular multilevel converter configurations. The total loss figure of the these VSC-based technologies are calculated based on the summation of individual loss components, and the individual component losses are determined by applying standardized calculation methods. Subsequent to these calculations, the following results were obtained:

5.2.1 Power Losses Calculations of Two-Level VSC-based HVDC Converter Stations

5.2.1.1 IGBT Conduction Losses Calculations

Table 5-1: System parameters

Components	Actual value	
	Rectifier side	Inverter side
Transformer rating	500/440 kV, 1000 MVA	350/230 kV
Transformer resistance	2 Ω	2 Ω
Transformer reactance	55.5 mH	55.5 mH
Coupling reactor	41.8 mH	41.8 mH
VSC converter rating	1000 MVA	1000 MVA
DC cable resistance	0.05Ω/km(500km long) =25 Ω	0.05Ω/km(500km long) =25 Ω
V_{ce-dc}	2800 V	2000 V
DC link voltage	561.64 kV	561.51 kV
$N_{IGBT\ valve}$(number of IGBTs connected in series)	300	300
Number of valves at each station.	6	6

Table 5-2: Calculations of IGBT power conduction losses

Results	IGBT	
Power conduction losses in IGBT (W)	Rectifier terminal	Inverter terminal
	1836.45 W	2686.11 W

Table 5-2 shows the results of the calculations of IGBT power conduction losses using equation (2-36). The modulation index, m, the power factor and the peak value of sinusoidal output current are shown on table 5-1, similarly, the forward voltage at no-load, V_{ceo}, and the forward resistance, R_o, of the IGBT are readily available on the datasheet. From the above results, the IGBT conduction losses at the inverter terminal of the converter station is larger than that of the rectifier terminal, which shows that the inverter station terminal has larger power loss contributions on the transmitted power.

5.2.1.2 IGBT Switching Losses Calculations

Table 5-3: Calculations of IGBT power switching losses

Results	IGBT	
Power switching losses in IGBT (W)	Rectifier terminal	Inverter terminal
	5463.86 W	4906.24 W

Table 5-3 shows the results of the calculations of IGBT power switching losses using equation (2-49). The peak value of sinusoidal output current, I_p, the switching frequency, f_{sw}, and the dc IGBT saturation voltage, V_{dc-sat}, are given on table 5-1. Similarly, the IGBT turn on switching energy, E_{on}, the IGBT turn off energy loss, E_{off}, and the nominal values of current, I_{nom}, and voltage, V_{nom}, to normalize the switching power loss are readily available on the IGBT datasheet. From the above results, the IGBT switching losses at the rectifier terminal of the converter station is larger than that of the inverter terminal, which shows that the rectifier station terminal has larger power loss contributions on the transmitted power.

5.2.1.3 Total IGBT Power Losses Calculations

Table 5-4: Total power loss in IGBT calculations

Results	IGBT	
Total Power losses in IGBT (W)	Rectifier terminal	Inverter terminal
$P_{avg.IGBT} = P_{cond.IGBT} + P_{sw.IGBT}$	7300.31 W	7592.35 W

Table 5-4 shows the results of the calculations of IGBT total power losses using equation (2-52). From the above results, the IGBT total power losses at the inverter terminal of the converter station is larger than that of the rectifier terminal, which shows that the inverter station terminal has larger power loss contributions on the transmitted power.

5.2.1.4 Diode Conduction Losses Calculations

Table 5-5: Calculations of diode conduction losses

Results	Freewheeling Diode	
Power conduction losses in Diode (W)	Rectifier terminal	Inverter terminal
	418.32 W	587.92 W

Table 5-5 shows the results of the calculations of Diode power conduction losses using equation (2-56). The modulation index, m, the power factor and the peak value of sinusoidal output current are shown on table 5-1, similarly, the diode threshold voltage, V_{Do}, and the diode forward resistance, R_D, of the diode are readily available on

the datasheet. From the above results, the diode conduction losses at the inverter terminal of the converter station is larger than that of the rectifier terminal, which shows that the inverter station terminal has larger power loss contributions on the transmitted power.

5.2.1.5 Diode Switching Losses Calculations

Table 5-6: Calculations of diode switching losses

Results	Freewheeling Diode	
Power switching losses in Diode (W)	Rectifier terminal	Inverter terminal
(Reverse recovery energy loss)	1845.9 W	1657.51 W

Table 5-6 shows the results of the calculations of diode power switching losses using equation (2-58). The peak value of sinusoidal output current, I_p, the switching frequency, f_{sw}, and the dc diode saturation voltage, V_{dc-sat}, are given on table 5-1. Similarly, the diode reverse recovery energy, E_{rec}, and the nominal values of current, I_{nom}, and voltage, V_{nom}, to normalize the switching power loss are readily available on the IGBT datasheet. From the above results, the diode switching losses at the rectifier terminal of the converter station is larger than that of the inverter terminal, which shows that the rectifier station terminal has larger power loss contributions on the transmitted power.

5.2.1.6 Total Diode Power Losses Calculations

Table 5-7: Total diode power losses calculations

Results	Diode	
Total Power losses in Diode (W)	Rectifier terminal	Inverter terminal
$P_{avg.Diode} = P_{cond.Diode} + P_{rec.Diode}$	2264.22 W	2245.43 W

Table 5-7 shows the results of the calculations of diode total power losses using equation (2-53). From the above results, the diode total power losses at the rectifier terminal of the converter station is slightly larger than that of the inverter terminal, which shows that the rectifier station terminal has larger power loss contributions on the transmitted power.

5.2.1.7 Total Losses per IGBT Module Calculations

Table 5-8: Calculations of total losses per IGBT module

Results	IGBT module ($P_{IGBT} + P_{Freewheeling-Diode}$)	
Total Power losses per IGBT module (W)	Rectifier terminal	Inverter terminal
$P_{total\ losses\ per\ device} = [P_{total\ IGBT\ losses} + P_{total\ Diode\ losses}$	9564.54 W	9837.78 W

Table 5-8 shows the results of the calculations of total power losses per IGBT module using equation (2-69). From the above results, the total power losses per IGBT module at the inverter terminal of the converter station is slightly larger than that of the rectifier terminal, which shows that the inverter station terminal has larger power loss contributions on the transmitted power.

Figure 5-1: Total power losses at the converter station terminals

Figure 5-1 shows the calculations of total power losses of a 300-series connected 6-valve IGBT modules, note that, using the values on table 3-2 in equation (3-22), the number of series connected IGBTs is calculated to be 300. Therefore, the overall total power losses of the IGBT module is obtained by multiplying the number of series connected IGBTs with the total losses per IGBT module, which results to 17.22 MW at the rectifier terminal and 17.71 MW at the inverter terminal. From the calculation, it is obvious that the power losses at the inverter terminal is higher than that of the rectifier terminal, so therefore, the loss contributions of the inverter terminal is higher than that of the rectifier terminal.

5.2.1.8 Power Losses Estimation of the DC-Link Capacitor for Two-Level Configuration

Table 5-9: Charge and discharge currents, ESR, losses per unit and total loss. In the calculation of total loss, the amount of capacitors used in two-level VSC HVDC is six

Configuration	$I_{crms}(A)$	$I_{dcrms}(A)$	$I_{rms}(A)$	ESR (mΩ)	Loss/unit (W)= $I_{rms}^2 ESR$	Total Losses(W)
Two-Level VSC-configuration	31.6	26.9	41.5	65	112	672

Table 5-9 shows the required parameters needed to compute the total losses of DC-link capacitor. The RMS current was obtained using equation (3-16). The RMS value of charging current of the capacitor, I_{crms}, rms value of discharging current of the capacitor, I_{drms} and the equivalent series resistance value are readily available in SKN 130 capacitor datasheet. The number of capacitors in a two-level configuration are always 6 in number. Moreover, when the configuration of DC-link capacitance is considered, the total losses of capacitors are estimated to be 672W in two-level configuration.

Most of the power losses associated with the converter valve occurs in the switches, but there is also some power losses in the DC-link capacitor. The total power loss of the valve was calculated including the DC link capacitor total losses using equation (3-17), the results were 17.221 MW and 17.711 MW for both rectifier and inverter station terminals respectively.

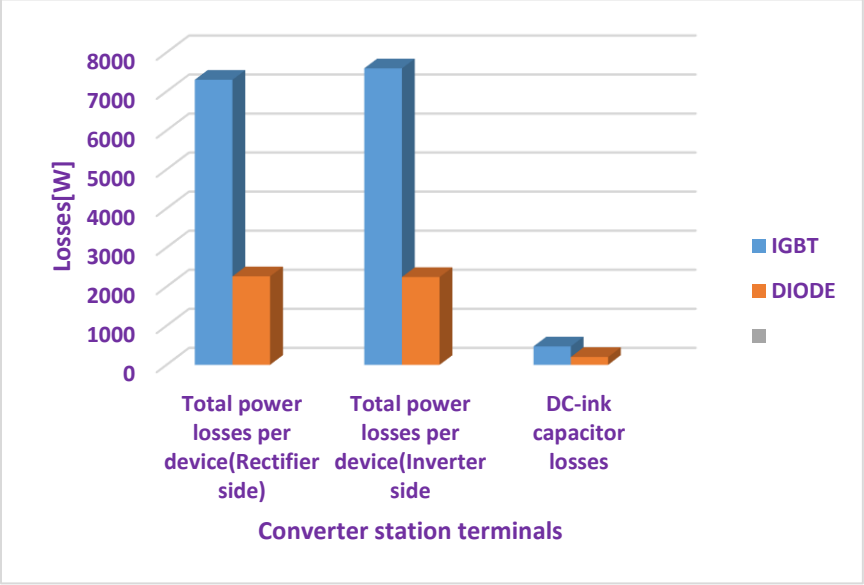

Figure 5-2: The overall total power losses per device at each converter terminals

Figure 5-2 shows the chart illustration of the loss calculations of the overall power losses per IGBT module including DC link capacitor losses at both the rectifier terminal and inverter terminal of a two-level VSC HVDC technology.

5.2.1.9 Evaluation of the Average Junction Temperature

Table 5-10: Calculations of junction temperature of both IGBT and freewheeling diode

Results	IGBT		FREEWHEELING DIODE	
Junction temperature, $T_j(°C)$.	Rectifier terminal	Inverter terminal	Rectifier terminal	Inverter terminal
	315.5°C	325.74°C	139.25°C	138.6°C

Table 5-10 shows the calculations of junction temperature, T_j, of both IGBT and freewheeling diode at both converter terminal. These results were obtained using equation (3-21). Note that most of the equation parameters are readily available on device datasheet.

5.2.2 Power Losses Calculations of Three-Level VSC-based HVDC Converter Stations

5.2.2.1 IGBT Conduction Losses Calculations

Table 5-11: Calculations of the IGBT conduction power losses of the both terminals of the three-level converter stations

Results	Rectifier terminal	Inverter terminal	Rectifier terminal	Inverter terminal
	T_1 and T_4	T_1 and T_4	T_2 and T_3	T_2 and T_3
I_{avg}	689.06 A	866.24 A	1167.42 A	1467.58 A
I_{rms}^2	1070.44 kA	1691.66 kA	1714.78 kA	2709.96 kA
P_{con}	2787.38 W	4084.3 W	4556.78 W	6657.92 W

Table 5-11 shows the IGBT conduction losses calculations of both rectifier and inverter terminals of a three-level VSC-based HVDC technology. Equation (3-6) to equation (3-9) were used to calculate the average and RMS currents that flow in the IGBT T_1 to T_4 respectively. The results from this analysis were used in equation (3-1) to calculate the conduction losses of IGBT, whose results are stipulated on table 5-11.

5.2.2.2 Total IGBT Conduction Power Losses Calculations

Table 5-12: Calculations of total IGBT conduction losses

Results	Rectifier terminal	Inverter terminal
Total IGBT conduction Losses ($P_{total-IGBT-cond-loss}$ (W))	T_1 to T_4	T_1 to T_4
	7344.16 W	10742.22 W

Table 5-12 shows the results of the calculations of IGBT total conduction losses at both terminals of the converter stations of three-level VSC-based HVDC technology. The above results on table 5-12 were obtained by summing the conduction losses of the four IGBTs together at both station terminals.

5.2.2.3 IGBT Switching Losses Calculations

Table 5-13: Calculations of the switching power losses of both station terminals of the three-level converter stations

Results	Rectifier terminal	Inverter terminal	Rectifier terminal	Inverter terminal
	T_1 and T_4	T_1 and T_4	T_2 and T_3	T_2 and T_3
P_{SW}	10108.14 W	9076.54 W	819.58 W	735.936 W

Table 5-13 shows the IGBT switching losses calculations of both rectifier and inverter terminals of a three-level VSC-based HVDC technology. Equations (3-14) and (3-15) were used to calculate the IGBT switching losses, noting that k_1, which is the switching energy is equal to $E_{on} + E_{off}$ as used in two-level configuration. Meanwhile, the equation was also normalized since some parameters were taken from the datasheet, so the peak current and dc saturation voltage are normalized and their values are readily available in the datasheet of the device.

5.2.2.4 Total IGBT Switching Power Losses Calculations

Table 5-14: Calculations of total IGBT switching losses

Results	Rectifier terminal	Inverter terminal
Total IGBT Switching power Losses ($P_{total-IGBT-sw-loss}$ (W))	T_1 to T_4	T_1 to T_4
	10927.72 W	9812.476 W

Table 5-14 shows the results of the calculations of IGBT total switching losses at both terminals of the converter stations of three-level VSC-based HVDC technology. The above results on table 5-14 were obtained by summing the switching losses of the four IGBTs together at both station terminals.

5.2.2.5 Total IGBT Power Losses Calculations

Table 5-15: Total power loss in IGBT calculations

Results	IGBT	
Total Power losses in IGBT (W)	Rectifier terminal	Inverter terminal
$P_{avg.IGBT} = P_{cond.IGBT} + P_{sw.IGBT}$	18271.88 W	20554.696 W

Table 5-15 shows the results of the calculations of IGBT total power losses using equation (2-52). From the above results, the IGBT total power losses at the inverter terminal of the converter station is larger than that of the rectifier terminal, which shows that the inverter station terminal has larger power loss contributions on the transmitted power.

5.2.2.6 Diode Conduction Losses Calculations

Table 5-16: Calculations of the diode conduction power losses of both terminals of the three-level converter stations

Results	Rectifier terminal	Inverter terminal	Rectifier terminal	Inverter terminal
	D_1 to D_4	D_1 to D_4	Clamped diodes	Clamped diodes
			D_5 and D_6	D_5 and D_6
I_{avg}	27.924 A	35.104 A	478.348 A	601.348 A
I_{rms}^2	42.176 kA	66.652 kA	644.352 kA	1018.304 kA
P_{con}	99.2 W	140.62 W	1608.2 W	2264.76 W

Table 5-16 shows the results of the diode conduction losses calculations of both rectifier and inverter terminals of a three-level VSC-based HVDC technology. Equation (3-10) to equation (3-13) were used to calculate the average and RMS currents that flow in the diodes D_1 to D_6 respectively. The results from this analysis was used in equation (3-1) to calculate the conduction losses of diodes, whose results are stipulated on table 5-16.

5.2.2.7 Total Diode Conduction Power Losses Calculations

Table 5-17: Calculations of total diode conduction losses

Results	Rectifier terminal	Inverter terminal
Total Diode conduction Losses ($P_{total-diode-cond-loss}$ (W))	D_1 to D_6	D_1 to D_6
	1707.4 W	2405.38 W

Table 5-17 shows the results of the calculations of diode total conduction losses at both terminals of the converter stations of three-level VSC-based HVDC technology. The above results on table 5-17 were obtained by summing the conduction losses of the six diodes together at both station terminals.

5.2.2.8 Diode Switching Losses Calculations

Table 5-18: Calculations of the diode switching power losses of both station terminals of the three-level converter stations

Results	Rectifier terminal	Inverter terminal
	$D_1\ to\ D_6$	$D_1\ to\ D_6$
P_{SW}	11075.4 W	9945.06 W

Table 5-18 shows the diode switching losses calculations of both rectifier and inverter terminals of a three-level VSC-based HVDC technology. Equation (2-49) was used to calculate the diode switching losses, noting that k_1, which is the switching energy is equal to $E_{on} + E_{off}$ as used in two-level configuration. Meanwhile, the equation was also normalized since some parameters were taken from the datasheet, so the peak current and dc saturation voltage are normalized and their values are readily available in the datasheet of the device.

5.2.2.9 IGBT Module Conduction Losses Calculations

Table 5-19: Calculations of total conduction losses per IGBT module

Results	IGBT module ($P_{IGBT} + P_{Freewheeling-Diode}$)	
Total conduction Power losses per IGBT module (W) $P_{t-cond\ losses\ per\ device} = [P_{t.IGBT-cond-\ losses} + P_{total-cond\ Diode\ losses}$	Rectifier terminal	Inverter terminal
	9051.56 W	13147.6 W

Table 5-19 shows the results of the calculations of total conduction power losses per IGBT module using equation (2-68). From the above results, the total power losses per IGBT module at the inverter terminal of the converter station is slightly larger than that of the rectifier terminal, which shows that the inverter station terminal has larger power loss contributions on the transmitted power.

5.2.2.10 IGBT Module Switching Losses Calculations

Table 5-20: Calculations of total switching losses per IGBT module

Results	IGBT module ($P_{IGBT} + P_{Freewheeling-Diode}$)	
Total switching Power losses per IGBT module (W) $P_{t-sw\ losses\ per\ device} = [P_{t.IGBT-sw-\ losses} + P_{total-sw\ Diode\ losses}$	Rectifier terminal	Inverter terminal
	22003.12 W	19757.536 W

Table 5-20 shows the results of the calculations of total switching power losses per IGBT module using equation (2-69). From the above results, the total power losses per IGBT module at the rectifier terminal of the converter station is slightly larger than that of the inverter terminal, which shows that the rectifier station terminal has larger power loss contributions on the transmitted power.

5.2.2.11 Power Losses Estimations of DC-Link Capacitor for Three-Level Configuration

Table 5-21: Charge and discharge currents, ESR, losses per unit and total loss. In the calculation of total losses, the amount of capacitors used in three-level VSC HVDC is four

Configuration	$I_{crms}(A)$	$I_{dcrms}(A)$	$I_{rms}(A)$	ESR (mΩ)	Loss/unit (W)= $I_{rms}^2 ESR$	Total Losses(W)
Three-Level VSC-configuration	73.2	62.3	96.1	14	129.3	517.2

Table 5-21 shows the required parameters needed to compute the total losses of DC-link capacitor. The rms current was obtained using equation (3-16). The rms value of charging current of the capacitor, I_{crms}, rms value of discharging current of the capacitor, I_{drms} and the equivalent series resistance value are readily available in SKN 130 capacitor datasheet. The number of capacitors in a three-level configuration are always 4 in number. Moreover, when the configuration of DC-link capacitance is considered, the total losses of capacitors are estimated to be 517 W in three-level configuration.

Most of the power losses associated with the converter valve occurs in the switches, but there is also some power losses in the DC-link capacitor. The total power loss of the valve was calculated including the DC link capacitor total losses using equation (3-17), the results were 9.317 MW and 9.872 MW for both rectifier and inverter station terminals respectively.

5.2.2.12 Total Power Losses for 100 Series Connected IGBT Modules in Three-Level Configuration

Table 5-22: Total power losses for 100 series connected IGBT modules in three-level configuration

Results	Rectifier terminal	Inverter terminal
	$3 \times 100\ (P_{cond.IGBT+Diode} + P_{SW.IGBT+Diode}) + P_{DC-link-cap}$	$3 \times 100\ (P_{cond.IGBT+Diode} + P_{SW.IGBT+Diode}) + P_{DC-link-cap}$
Total power losses for 100 series connected IGBT modules including the DC-link capacitor losses ($P_{Overall-losses}$)	9.317 MW	9.872 MW

Table 5-22 shows the results of the calculations of the total power losses for 100 series connected IGBT modules in three-level VSC-HVDC technology. The above results were obtained by simply adding the IGBT module conduction power losses and IGBT module switching power losses together, then the result was multiplied by 3 and 100, the three signifies the number of levels while the hundred signifies the number of series connected IGBTs. Finally, the result obtained was added to the DC-link capacitor losses.

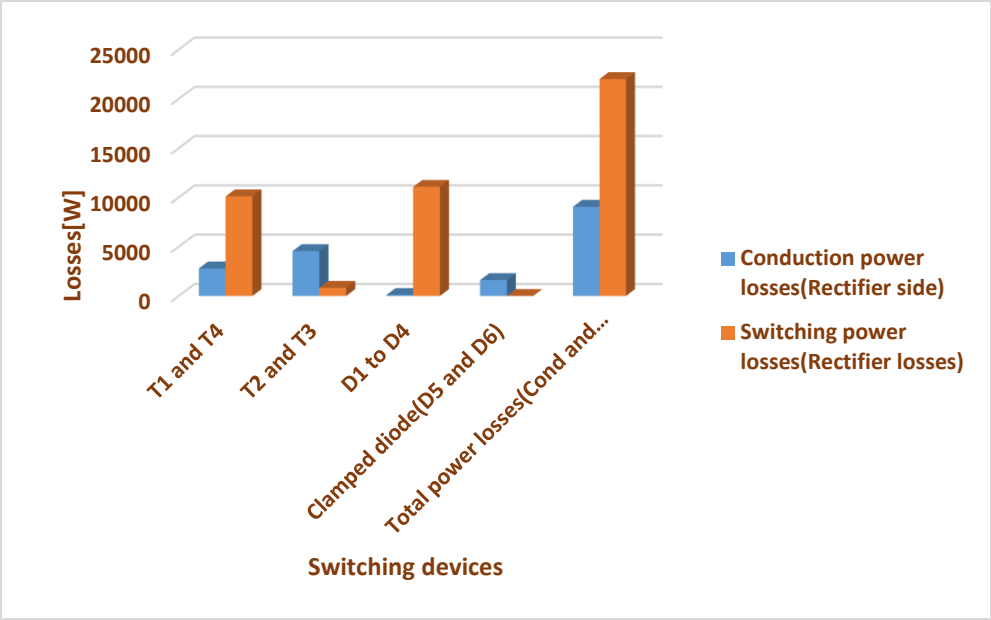

Figure 5-3: The Conduction and switching power losses at the rectifier terminal

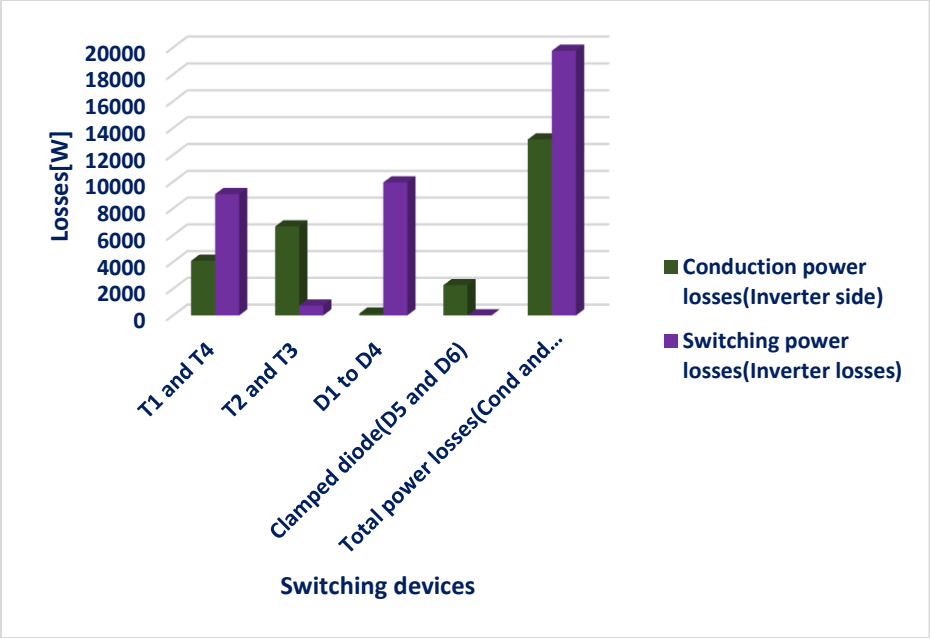

Figure 5-4: The Conduction and switching power losses at the Inverter terminal

Figure 5-3 and 5-4 show the power losses analysis at the converter stations, from the above figures, it could be deduced that the switching losses are the dominating contributor of losses in the converter valves. The switching losses at the rectifier and inverter terminals are extremely high due to the high switching frequency used by the converter topologies, however, due to this high switching frequency, it results to high switching power losses at both converter stations.

5.2.2.13 Power Losses Comparison Between the VSC-based HVDC Technologies

Table 5-23: Total power losses for 100 series connected IGBT modules in three-level configuration

Results	VSC-based HVDC technologies.			
	Two-level configuration		Three-level configuration	
	Rectifier terminal	Inverter terminal	Rectifier terminal	Inverter terminal
Overall total power losses of IGBT modules	17.221 MW	17.711 MW	9.317 MW	9.872 MW

Table 5-23 Compares the overall power losses of two-level and three-level converter configurations at the converter station terminals. It could be clearly seen that the overall power losses of the three-level converter is lower in amount compared to its counterpart, two-level converter configuration, reason being that for a high DC voltage two-level converter, a lot of series connected IGBTs is required. More so, the two-level converter requires a very high switching frequency, due to this singular fact, the switching losses are relatively very high compared to its counterpart, three-

level converter configuration. Subsequently, the switching losses of for a three-level converter configuration tend to amount to the half of a two-level converter. Due to the lower forward voltage drop, conduction losses are very low compared to the two-level converter. As a result of these lower power losses, the three-level topology generates a smoother voltage with fewer harmonics, therefore, lowering the losses in other equipment of the converter station. The merits of increasing the number of levels include decrease in the blocking voltage of the valve, also the switching frequency of the valve drops, therefore, lowering the switching losses.

5.2.3 Loss of Converter Transformers

The losses of converter transformers can be obtain using the same methods adopted during LCC-based HVDC technology, using equations (2-1) to (2-7).

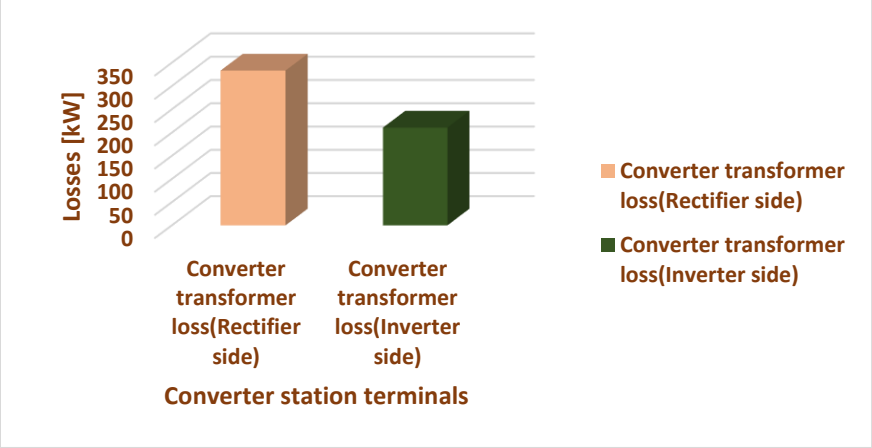

Figure 5-5: Converter transformer losses at the station terminals

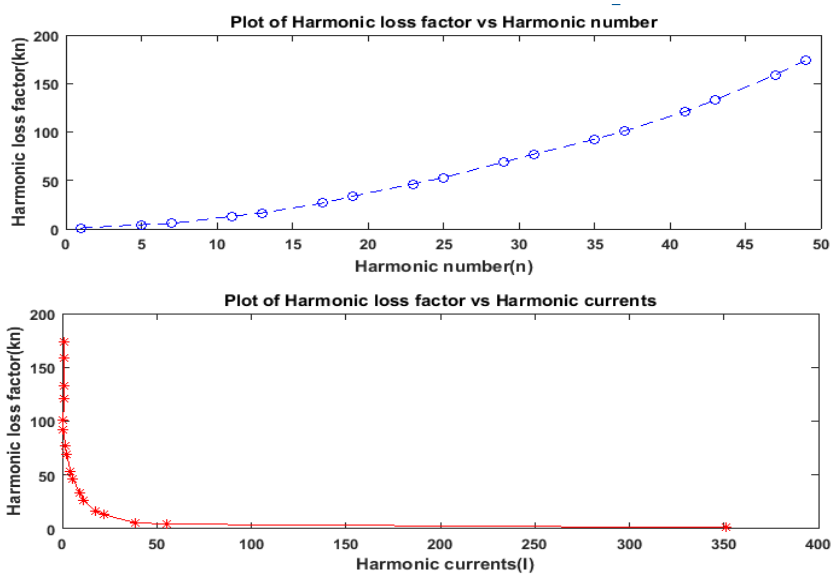

Figure 5-6: Harmonic loss factor vs harmonic number (n) /harmonic current (I)

Figure 5-5 show the chart representation of the loss calculation result of converter transformer at both station terminals using Method 1 of IEC standard 61803. The analysis starts with the computations of the characteristic harmonic currents using equation (2-4), then a constant parameter, F, k_1 and k_2 were calculated using equations (2-5), (2-6) and (2-7) respectively. Therefore, with these calculated parameters, the harmonic currents were calculated using equation (2-4). Subsequently, the effective resistance, R_n, was calculated using equation (2-3) and the variation of transformer resistance with frequency table stipulated in the standard IEC 61803, IEEE recommended practice for Determination of Power Losses in High-Voltage Direct-Current (HVDC) Converter Stations, finally, the square of the harmonic currents were multiplied by the effective resistance to obtain the losses due to converter transformer operations. From the above results, the converter transformer loss at the rectifier terminal of the converter station is higher than that of the inverter terminal. From figure 5-6, which shows the plot of harmonic loss factor against harmonic number and harmonic current respectively, it can be deduced from the plot that the harmonic loss factor is directly proportional to the harmonic number i.e. increase in harmonic loss factor will result to a corresponding increase in harmonic number. On the other hand, it can also be deduced from the other plot that the harmonic loss factor is inversely proportional to the harmonic current to a certain value of the harmonic current, and then afterwards becomes constant throughout the transformer operation.

5.2.4 AC Filter Losses

5.2.4.1 Filter Resistor Loss

The filter resistor losses can be obtain using the same methods adopted during LCC-based HVDC technology, using equations (2-8) to (2-21).

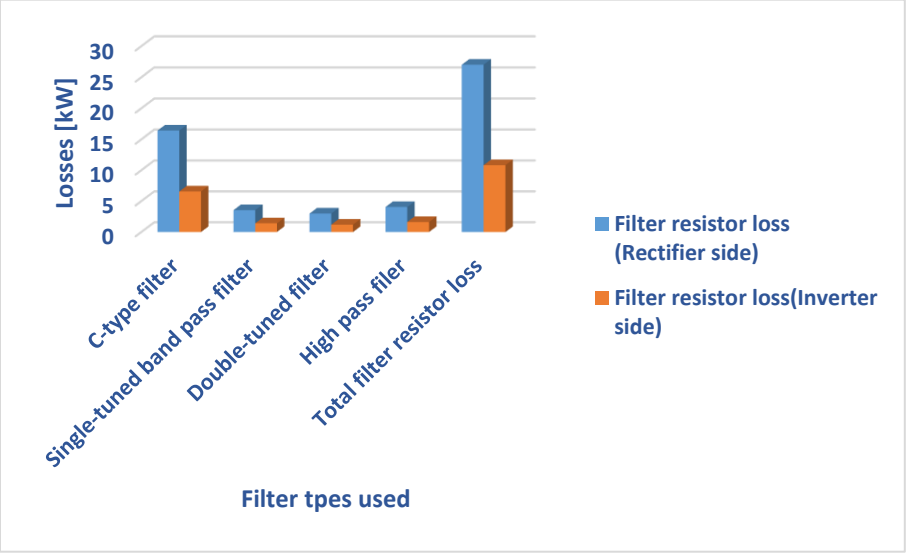

Figure 5-7: Filter resistor loss at station terminals

Figure 5-7 shows the chart representation of the results from the loss calculation of the filter resistor loss of various filter types used, using equations (2-8) to equation (2-21). Starting from the C-type filter which is mainly used for low order high pass filtering (i.e. was used to mitigate the 5th and 7th harmonic orders). More so, the currents due to these harmonic orders, $I_5 + I_7$, were added together at both converter station terminals. The q-factor of low order high pass filters is always between the ranges of 45-50, so 50 was selected for this filter design. The values of C_1, R, and L were calculated for both station terminals using equations (2-12), (2-14) and (2-13) respectively. Therefore, having known the above stated parameters, the filter resistor losses due to C-type filter was calculated using equation (2-8).

Secondly, with the single-tuned band pass filter which is mainly used to mitigate the 11th and 13th harmonic orders, therefore, the currents due to these harmonic orders, $I_{11} + I_{13}$, were added together at both converter station terminals. The q-factor of band pass filters is always between the ranges of 15-20, so 20 was selected for this filter design. The values of C, R, and L were calculated for both station terminals using equations (2-9), (2-11) and (2-10) respectively. Therefore, having known the above stated parameters, the filter resistor losses due to single-tuned band pass filter was calculated using equation (2-8).

Thirdly, with the double-tuned filter which is mainly used to eliminate the 17th and 19th harmonic orders, therefore, the currents due to these harmonic orders, , $I_{17} + I_{19}$, were added together at both converter station terminals. The q-factor of this tuned filter is always between the ranges of 2-4, so 4 was selected for this filter design. The values of C_1, C_2, R, L_1, and L_2 were calculated for both station terminals using equations (2-15), (2-16), (2-14), (2-17), (2-18) respectively. Therefore, having known the above stated parameters, the filter resistor losses due to double-tuned filter was calculated using equation (2-8).

Lastly, with the high pass filter which is mainly used to mitigate all the harmonics from the 23rd to 49th harmonic orders, therefore, the currents due to these harmonic orders, $I_{23} + I_{25} + \cdots \ldots \ldots + I_{49}$, were added together at both converter station terminals. The q-factor of band pass filters is always between the ranges of 1-2, so 2 was selected for this filter design. The values of C, R, and L were calculated for both station terminals using equations (2-19), (2-21) and (2-20) respectively. Therefore, having known the above stated parameters, the filter resistor losses due to high pass filter was calculated using equation (2-8). From the above results, the filter resistor loss is higher at the rectifier terminal of the converter station than at the inverter terminal, which shows that the rectifier station terminal has larger power loss contributions on the transmitted power.

5.2.4.2 Filter Reactor Losses

The filter reactor losses can be obtain using the same methods adopted during LCC-based HVDC technology, using equation (2-22).

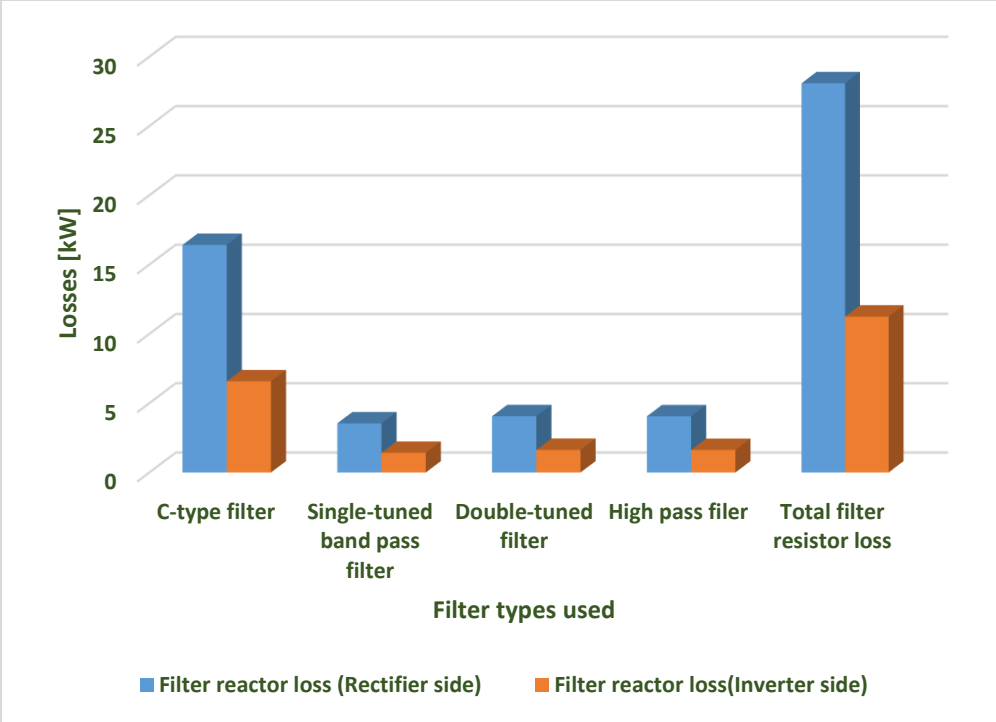

Figure 5-8: Filter reactor loss calculation at station terminals

Table 5-8 shows the chart representation of the results from the loss calculation of the filter reactor loss of various filter types used, using equation (2-22). The procedures used to calculate the filter resistor losses can also be similarly used to calculate the filter reactor losses. The only parameter needed to obtain is the harmonic inductive reactance, X_{Ln}, which is calculated using equation (2-23). Therefore, having known the above stated parameters, the filter reactor losses due to the various filter types were calculated using equation (2-22). From the above results, the filter reactor loss is higher at the rectifier terminal of the converter station than at the inverter terminal, which shows that the rectifier station terminal has larger power loss contributions on the transmitted power.

5.2.4.3 Capacitor Bank Losses (Filter Capacitor Losses)

The filter capacitor losses can be obtain using the same methods adopted during LCC-based HVDC technology, using equation (2-52).

The average loss/kVar designs of the capacitors are given below;

Low dielectric loss = 0.1 w/kVar.

Paper, oil impregnated* =2.0 – 2.5 w/kVar.

Paper, PCB impregnated* = 3.0 – 3.5 w/kVar.

Plastic file/paper, PCB impregnated* = 0.5 – 1.0 w/kVar.

Metallized film = under 0.5 w/kVar.

The asterik type are not manufactured anymore due to the non-biodegradability of the poly-chlorinated biphenyle (PCBs). Note that the Q_C used was 200MVar, then the power loss or shunt capacitor bank loss admits expression as equation (4.51), using low dielectric loss of 0.1 w/kVar then ;

Capacitor bank losses at both the converter station terminals admit expressions as:

Filter capacitor losses at the rectifier terminal = P = $\frac{0.1W}{kVar} \times kVar$

Filter capacitor losses at the inverter terminal = P = $\frac{0.1W}{kVar} \times kVar$

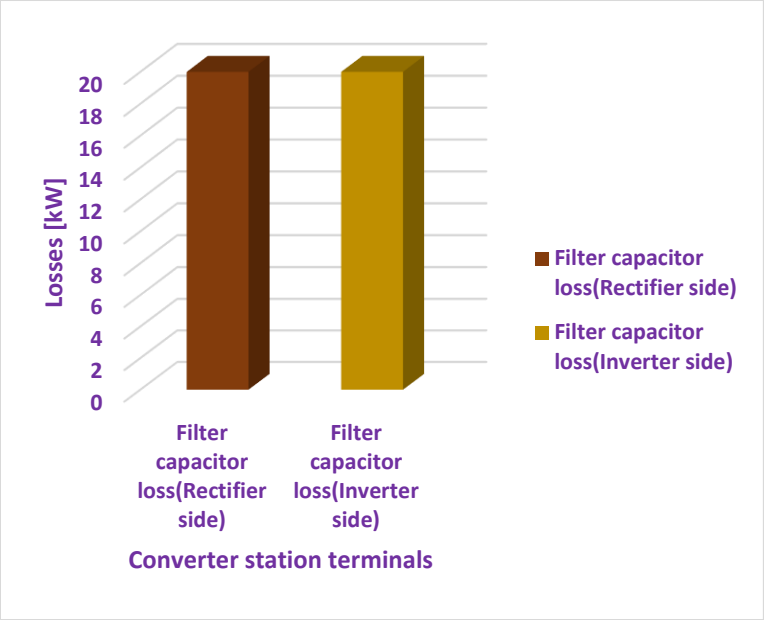

Figure 5-9: Filter capacitor loss calculations at station terminals

Figure 5-9 shows the chart representation of the results from the loss calculation of the filter capacitor loss using equation (2-24). From the above results, the filter capacitor loss at the rectifier terminal of the converter station is the same with that at the inverter terminal, which shows that both the station terminals have equal power loss contributions on the transmitted power.

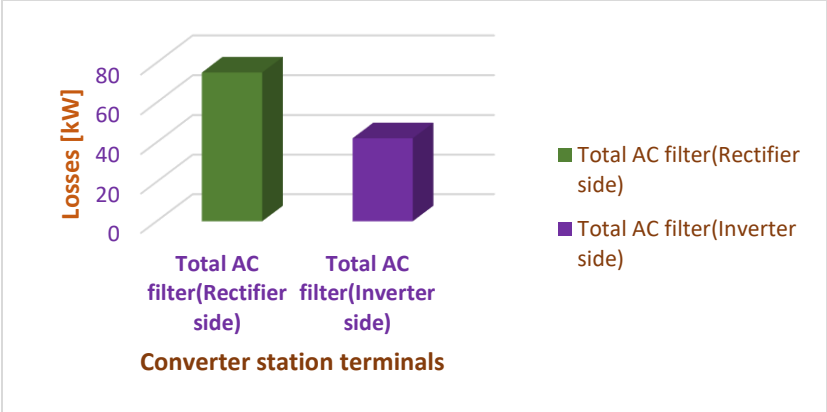

Figure 5-10: The total AC filter loss calculations at converter station terminals

Figure 5-10 shows the chart illustration of the loss calculations of total AC filter losses, which is obtained by summing up all the losses associated with the AC filters installed at each of the converter stations to give the total AC filter loss contribution to the overall system network. The total AC filter losses of the rectifier terminal is 75.105 kW and that of the inverter terminal is 42.066 kW. From the above results, the total AC filter loss is higher at the rectifier terminal of the converter station than at the inverter terminal, which shows that the rectifier station terminal has larger power loss contributions on the transmitted power.

5.2.5 DC Smoothing Reactor Losses

The DC Smoothing losses can be obtain using the same methods adopted during LCC-based HVDC technology, using equations (2-25) to (2-28).

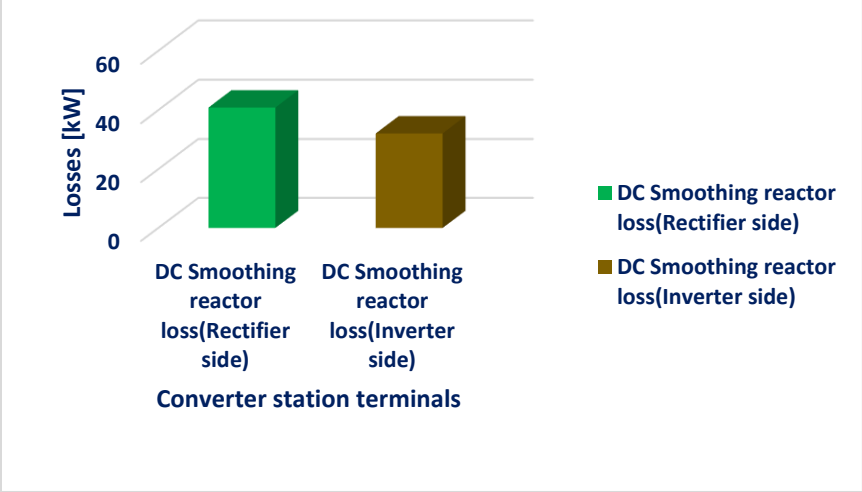

Figure 5-11: DC-Smoothing reactor loss calculations at converter station terminals

Table 5-11 shows the chart representation of the results from the loss calculations of the DC-Smoothing reactor loss of both the rectifier and inverter terminals using equations (2-25) to (2-28). Firstly, the hysteresis loss component, P_{hn}, was calculated for all the harmonic orders using equation (2-26). Afterwards, the eddy-current loss component, P_{en}, was evaluated for harmonic orders greater than 10, using equation (2-27). More so, the eddy-current loss component, P_{e2}, was as well evaluated for harmonic orders less and equal to 2 using equation (2-28). Finally, the sum of the results was put in equation (2-25) to obtain the magnetization loss, P_m. Similarly, the value of the direct current losses was also estimated using some conventional equations written on the table. From the above results, the DC-Smoothing reactor loss is higher at the rectifier terminal of the converter station than at the inverter terminal, which shows that the rectifier station terminal has larger power loss contributions on the transmitted power.

5.2.6 DC-Filter Capacitor Losses

The DC-Filter capacitor losses can be obtain using the same methods adopted during LCC-based HVDC technology, using equation (4-1), equation (4-2) and equation (2-57).

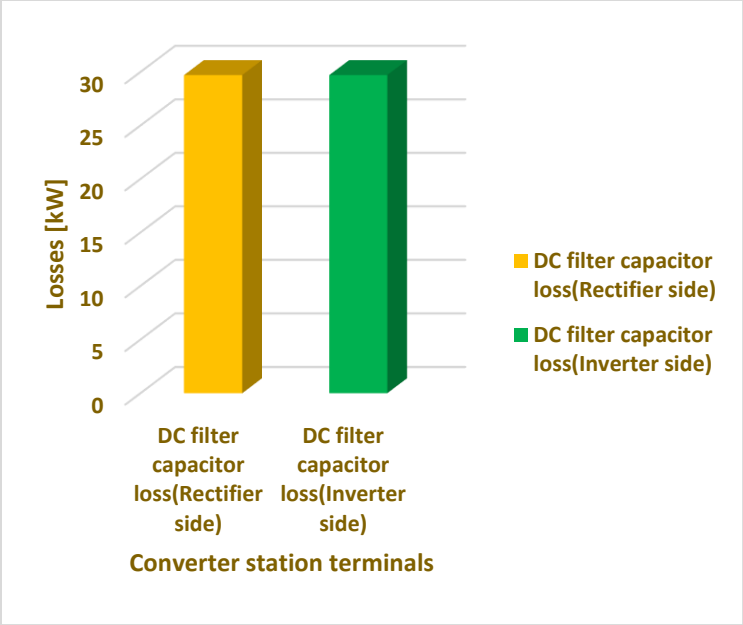

Figure 5-12: DC-filter capacitor loss calculations at converter station terminals

Figure 5-12 shows the chart illustration of the results from the loss calculations of the DC-filter capacitor losses using equation (4-1), equation (4-2) and equation (2-29). The first step was to calculate the rectifier dc voltage using equation (4-1), afterwards, the above result was used in equation (4-2) to compute the inverter dc voltage, finally, the value obtained above was used in equation (2-29) to evaluate the dc filter capacitor losses. From the above results, it can be deduced that the filter capacitor loss at the rectifier terminal of the converter station is the same with that at the inverter terminal, but not the same in all cases, it depends on the converter configurations and system operations.

5.2.7 Percentage Loss Calculations of each Converter Station Equipment

Table 5-24: The total losses of all the equipment of the VSC-based converter stations

Converter stations Equipment	Two-Level topology		Three-Level topology	
	Rectifier terminal	Inverter terminal	Rectifier terminal	Inverter terminal
IGBT+Diode valves losses	17.221 MW	17.711 MW	9.317 MW	9.872 MW
Converter transformer losses	333.07 kW	210.75 kW	333.07 kW	210.75 kW
AC Filter losses	75.105 kW	42.066 kW	75.105 kW	42.066 kW
DC Smoothing reactor losses	40.86 kW	32.132 kW	40.86 kW	32.132 kW
DC Capacitor losses	29.715 kW	29.715 kW	29.715 kW	29.715 kW
Total losses contributions by each terminal	17.700 MW	18.026 MW	9.796 MW	10.187 MW

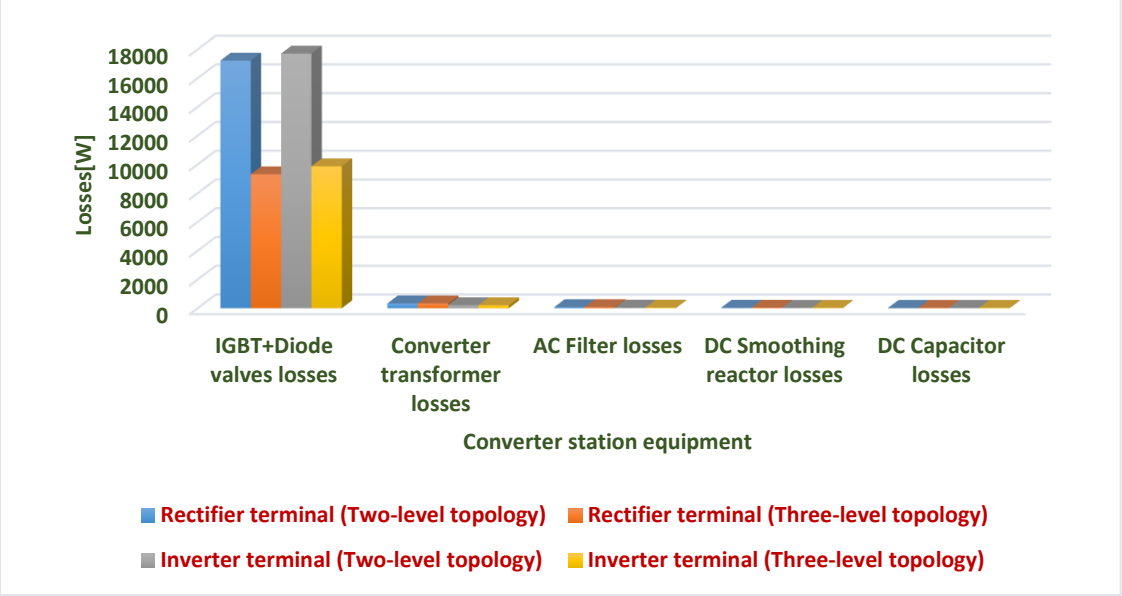

Figure 5-13: The total loss calculations of all the equipment of the converter stations

Table 5-24 and figure 5-13 show the analysis of the total loss proportion of each converter stations' equipment both at the rectifier and inverter terminals. From these illustrations, it can be deduced that the loss proportion of each equipment at the inverter terminal is higher than that of the rectifier terminal. Likewise, the loss of the IGBT valve module has the highest losses contributions at both converter station terminals. Finally, it can be deduced from the chart that the loss contribution of the two-level topology is higher than that of the three-level topology.

Table 5-25: Loss proportion of converter station equipment

Converter stations Equipment percentage loss	Loss percent for two-level topology.		Loss percent for three-level topology.	
	Rectifier terminal	Inverter terminal	Rectifier terminal	Inverter terminal
IGBT+Diode valves losses	97.29 %	98.25 %	95.11 %	96.91 %
Converter transformer	1.88 %	1.18 %	3.40 %	2.07 %
AC Filter	0.43 %	0.23 %	0.77%	0.41 %
DC Smoothing reactor	0.23 %	0.18 %	0.42 %	0.32 %
DC capacitor	0.17 %	0.16 %	0.30 %	0.29 %
% loss calculation of the total losses contribution of converter stations on HVDC network, assumimg the Power transmitted = 20MW	88.5 %	90.13 %	48.98 %	50.94 %

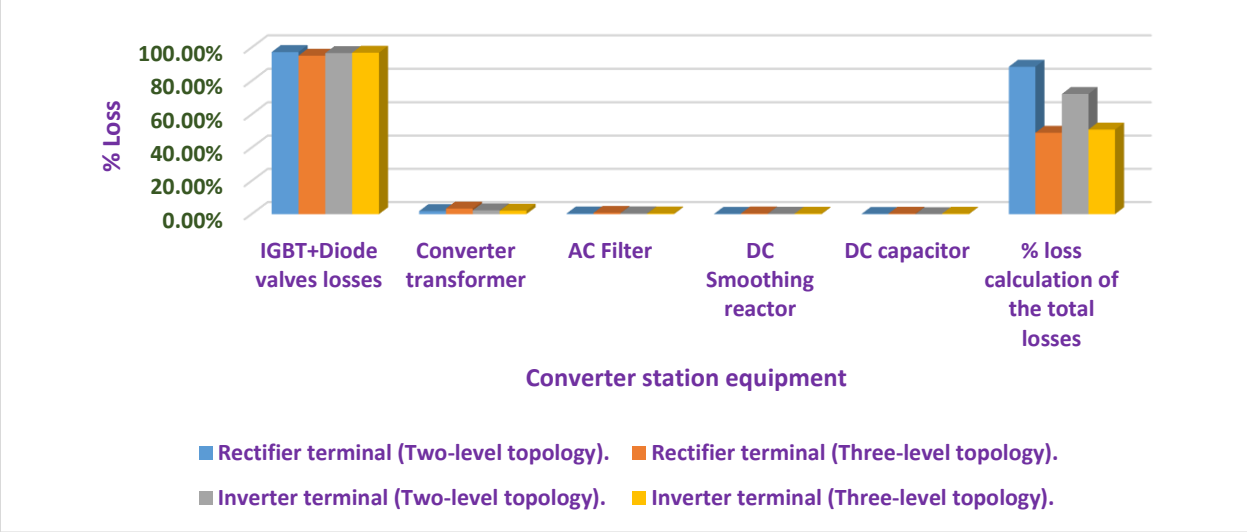

Figure 5-14: Percentage loss calculations of each converter station equipment

Table 5-25 and figure 5-14 show percentage loss analysis of each converter station equipment both at the rectifier and inverter terminals. From these illustrations, it can be deduced that the loss-percent proportion of the equipment at the inverter terminal is higher than that of the rectifier terminal. Likewise, the percentage loss of the IGBT valve module has the highest loss-percent contribution at both converter station terminals.

The losses of each equipment in converter station fall with the decrease of the transmission power under bipolar operational conditions. The losses of each equipment in the converter station increase with the decrease of the DC voltage under different single operartional conditions. The losses of each equipment in rectifier station are lower than those in inverter station. The loss proportion of each equipment in converter station considering both two-level and three-level topologies under the operartional mode condition of bipolar rated transmission power is seen on table 5-25.

It can be seen from table 5-24 and 5-25, that the losses of converter station are mainly composed of the losses of the IGBT valve modules. To decrease the total losses of HVDC system, the losses of the IGBT valve modules should be consider first.

Table 5-26: Comparison of different HVDC technologies based on their loss figures at the converter station terminals

HVDC Technologies	Rectifier terminal		Inverter terminal	
	Loss proportions	Loss percent	Loss proportions	Loss percent
Two-Level VSC HVDC	17.700 MW	62.55%	18.026 MW	62.64%
Three-Level VSC HVDC	9.796 MW	34.62%	10.187 MW	35.40%

LCC HVDC	801.154 kW	2.83%	565.65 kW	1.97%

Table 5-26 shows the comparison of different HVDC technologies based on their Loss Figure at the converter terminals. These values were obtained by summing all the loss profiles of each equipment of the converter stations at each terminals of the HVDC technologies used as case study in this Research work. Subsequently, the percentage losses were eveluated from the above results.

Table 5-27: Different HVDC technologies with their respective converter losses ratios

HVDC Technologies	Switching Frequency (Hz)	Converter loss ratio.
Two-level VSC	1000	4
Three-level VSC	1000	2.214
LCC HVDC	50	0.18

Finally, table 5-27 shows the various HVDC technologies with their respective converter loss ratios, from the table, it can be deduced that the two-level VSC-based HVDC technology has the highest percentage converter losses follow by the three-level VSC-based HVDC technology.

5.2.8 Power Losses Calculations of MMC-based HVDC Converter Stations

5.2.8.1 IGBT Submodule Conduction Losses Calculations for the Upper (positive) Arm

Table 5-28: Table showing the calculated values of the positive and the negative arms inserted and bypassed cells and also arm currents of MMC-based HVDC link

Results	Number of positive and negative arm inserted and bypassed cells	
Positive arm	Inserted cells $n_p^{in}(i)$	Bypassed cells $n_p^{by}(i)$
	4	36
Negative arm	Inserted cells $n_n^{in}(i)$	Bypassed cells $n_n^{by}(i)$
	36	4
Arm currents	$I_p(i)$	$I_n(i)$
	1561.35 A	669.07 A (Negative)

Table 5-28 shows the calculated values of the positive and the negative arms inserted and bypassed cells using equations (2-88) to (2-91). More so, the arm currents are obtained by using equations (2-82) and (2-83).

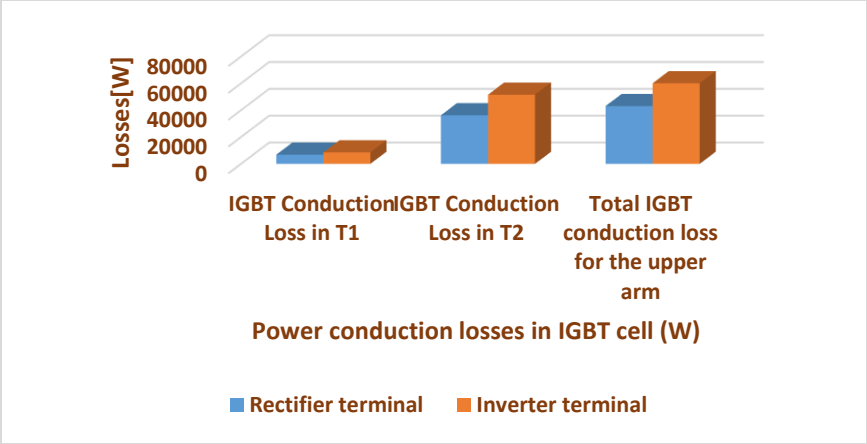

Figure 5-15: The IGBT power conduction Losses for the upper arm

Figure 5-15 shows the results of the calculations of IGBT power conduction losses at the upper arm using equations (3-23) and (3-24). The modulation index, m, the power factor and the peak value of sinusoidal output current are shown on table 5-28, similarly, the forward voltage at no-load, V_{ceo}, and the forward resistance, R_o, of the IGBT are readily available on the datasheet. The IGBT conduction loss of the inserted cell and the bypassed cell are estimated using equations (3-23) and (3-24). Subsequently, the results from this analysis are summed together to obtain the total IGBT conduction loss for the upper arm. From the above results, the IGBT conduction losses at the inverter terminal of the converter station is larger than that of the rectifier terminal, which shows that the inverter station terminal has larger power loss contributions on the transmitted power.

5.2.8.2 Diode Submodule Conduction Losses Calculations for the Upper (positive) Arm

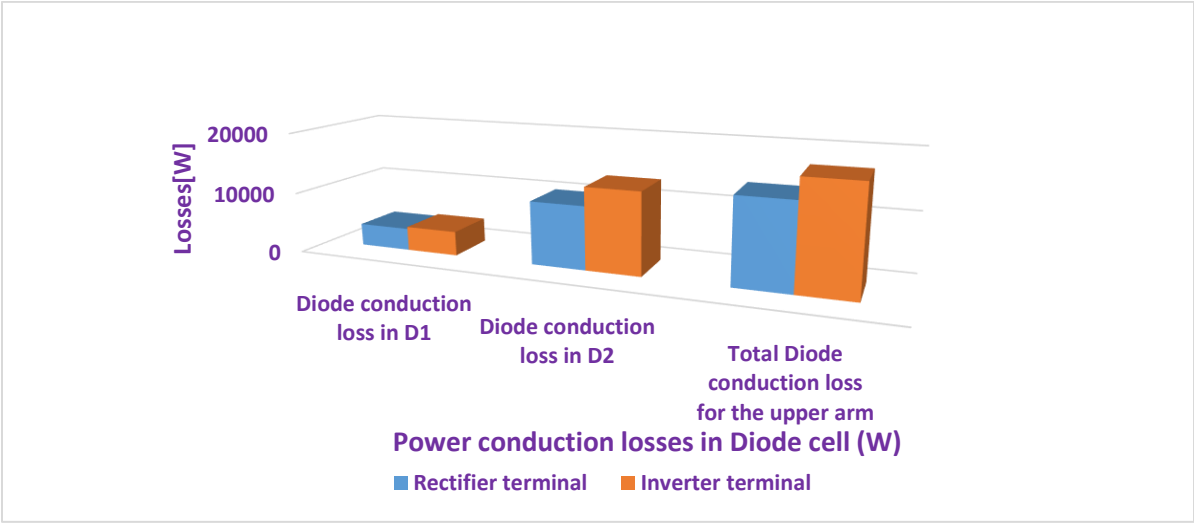

Figure 5-16: The diode submodule conduction losses for the upper (positive) arm

Figure 5-16 shows the results of the calculations of Diode power conduction losses at the upper arm using equations (3-25) and (3-26). The modulation index, m, the power factor and the peak value of sinusoidal output current are

shown on table 5-28, similarly, the diode threshold voltage, V_{Do}, and the diode forward resistance, R_D, of the diode are readily available on the datasheet. The diode conduction loss of the inserted cell and the bypassed cell are estimated using equations (3-25) and (3-26). Subsequently, the results from this analysis are summed together to obtain the total diode conduction loss for the upper arm From the above results, the diode conduction losses at the inverter terminal of the converter station is larger than that of the rectifier terminal, which shows that the inverter station terminal has larger power loss contributions on the transmitted power.

5.2.8.3 Total submodule Conduction Losses at the Upper Arm

Table 5-29: Table showing the total submodule conduction loss at the upper arm

Results	Submodule Conduction Loss	
	Rectifier terminal	Inverter terminal
Total conduction Loss (W) ($P_{t-cond} = P_{t-IGBT} + P_{t-Diode}$)	57071.7 W	77456.9 W
Arm 1+Arm 3+Arm 5 (Upper arms)	171215.1 W	232370.7 W

Table 5-29 shows the results of the calculations of total power losses, which is obtained by summing the IGBT and Diode conduction losses. Since there are three arms in the upper section, then the results are multiplied by three to obtain the total conduction loss at each of the station terminals. From the above results, the total power losses at the inverter terminal of the converter station is larger than that of the rectifier terminal, which shows that the inverter station terminal has larger power loss contributions on the transmitted power.

5.2.8.4 IGBT Submodule Conduction Losses Calculations for the Lower (Negative) Arm

Table 5-30: Calculations of IGBT power conduction losses for the lower arm

Results	IGBT cell	
Power conduction losses in IGBT cell (W)	Rectifier terminal	Inverter terminal
IGBT conduction loss in T_1 $P_{l1cond}^{in}(t)$	32949.73 W	48243.61 W
IGBT conduction loss in T_2 $P_{l2cond}^{by}(t)$	3566.53 W	5265.85 W
Total IGBT conduction loss for the Lower arm	36516.26 W	53509.46 W

Table 5-30 shows the results of the calculations of IGBT power conduction losses at the lower arm using equations (3-23) and (3-24). The modulation index, m, the power factor and the peak value of sinusoidal output current are shown on table 5-28, similarly, the forward voltage at no-load, V_{ceo}, and the forward resistance, R_o, of the IGBT are readily available on the datasheet. The IGBT conduction loss of the inserted cell and the bypassed cell are estimated using equations (3-23) and (3-24). Subsequently, the results from this analysis are summed together to obtain the total IGBT conduction loss for the lower arm. From the above results, the IGBT conduction losses at the inverter terminal

of the converter station is larger than that of the rectifier terminal, which shows that the inverter station terminal has larger power loss contributions on the transmitted power.

5.2.8.5 Diode Submodule Conduction Losses Calculations for the Lower (Negative) Arm

Table 5-31: Calculations of diode power conduction losses for the lower arm

Results	Diode cell	
Power conduction losses in Diode cell (W)	Rectifier terminal	Inverter terminal
Diode conduction loss in D_1 $P_{D1cond}^{in}(t)$	7192.149 W	10244.95 W
Diode conduction loss in D_2 $P_{D2cond}^{by}(t)$	499.03 W	838.23 W
Total Diode conduction loss for the Lower arm	7691.18 W	11083.18 W

Table 5-31 shows the results of the calculations of Diode power conduction losses at the lower arm using equations (3-25) and (3-26). The modulation index, m, the power factor and the peak value of sinusoidal output current are shown on table 5-28, similarly, the diode threshold voltage, V_{Do}, and the diode forward resistance, R_D, of the diode are readily available on the datasheet. The diode conduction loss of the inserted cell and the bypassed cell are estimated using equations (3-25) and (3-26). Subsequently, the results from this analysis are summed together to obtain the total diode conduction loss for the lower arm From the above results, the diode conduction losses at the inverter terminal of the converter station is larger than that of the rectifier terminal, which shows that the inverter station terminal has larger power loss contributions on the transmitted power.

5.2.8.6 Total Submodule Conduction Losses at the Lower Arm

Table 5-32: Table showing the total submodule conduction loss at the lower arm

Results	Submodule Conduction Loss	
	Rectifier terminal	Inverter terminal
Total conduction Loss (W) ($P_{t-cond} = P_{t-IGBT} + P_{t-Diode}$)	44207.44	64592.64 W
Arm 2+Arm 4+Arm 6 (Lower arms)	132622.32 W	193777.92 W

Table 5-32 shows the results of the calculations of total power losses, which is obtained by summing the IGBT and Diode conduction losses. Since there are three arms in the lower section, then the results are multiplied by three to obtain the total conduction loss at each of the station terminals. From the above results, the total power losses at the inverter terminal of the converter station is larger than that of the rectifier terminal, which shows that the inverter station terminal has larger power loss contributions on the transmitted power.

5.2.8.7 Overall Conduction Power Loss

Table 5-33: Table showing the overall conduction power loss of MMC-based converters

Results	Submodules Conduction Loss	
Overall conduction Loss (W) $P_{overall-loss} = P_{upp-arm-loss} + P_{low-arm-loss}$	Rectifier terminal	Inverter terminal
	303837.42 W	426148.62 W

Table 5-33 shows the results of the calculations of the overall conduction power loss of M2C-based converters. This is obtained by adding the conduction power loss contribution of the upper arm and the lower arm together. From the above results, the total power losses at the inverter terminal of the converter station is larger than that of the rectifier terminal, which shows that the inverter station terminal has larger power loss contributions on the transmitted power.

5.2.8.8 IGBT Submodule Switching Losses Calculations for the Upper (positive) Arm

Table 5-34: Calculations of IGBT power Switching losses for the upper arm

Results	IGBT cell	
Power switching losses in IGBT cell (W)	Rectifier terminal	Inverter terminal
IGBT switching loss in T_1 $P_{I1sw}^{in}(t)$	5581.74 W	5525.974 W
IGBT switching loss in T_2 $P_{I2sw}^{by}(t)$	8547.613 W	8045.72 W
Total IGBT switching loss for the upper arm	14129.35 W	13571.694 W

Table 5-34 shows the results of the calculations of IGBT power switching losses at the upper arm using equations (3-27) and (3-28). The peak value of sinusoidal output current, I_p, the switching frequency, f_{sw}, and the dc IGBT saturation voltage, V_{dc-sat}, are given on table 5-2. Similarly, the IGBT turn on switching energy, E_{on}, the IGBT turn off energy loss, E_{off}, and the nominal values of current, I_{nom}, and voltage, V_{nom}, to normalize the switching power loss are readily available on the IGBT datasheet. Subsequently, the results from this analysis are summed together to obtain the total IGBT switching loss for the upper arm. From the above results, the IGBT switching losses at the inverter terminal of the converter station is larger than that of the rectifier terminal, which shows that the inverter station terminal has larger power loss contributions on the transmitted power.

5.2.8.9 Diode Submodule Switching Losses Calculations for the Upper (positive) Arm

Table 5-35: Calculations of diode power switching losses for the upper arm

Results	Diode cell	
Power switching losses in Diode cell (W)	Rectifier terminal	Inverter terminal
Diode switching loss in D_1 $P_{D1sw}^{in}(t)$	3112.13 W	3093.29 W
Diode switching loss in D_2 $P_{D2sw}^{by}(t)$	4588.93 W	4419.37 W
Total Diode switching loss for the upper arm	7701.06 W	7512.66 W

Table 5-35 shows the results of the calculations of Diode power conduction losses at the upper arm using equations (3-29) and (3-30). The modulation index, m, the power factor and the peak value of sinusoidal output current are shown on table 5-28, similarly, the diode threshold voltage, V_{Do}, and the diode forward resistance, R_D, of the diode are readily available on the datasheet. The diode conduction loss of the inserted cell and the bypassed cell are estimated using equations (3-29) and (3-30). Subsequently, the results from this analysis are summed together to obtain the total diode switching loss for the upper arm From the above results, the diode switching losses at the inverter terminal of the converter station is larger than that of the rectifier terminal, which shows that the inverter station terminal has larger power loss contributions on the transmitted power.

5.2.8.10 Total Submodule Switching Losses at the Upper Arm

Table 5-36: The total submodule switching loss at the upper arm

Results	Submodule switching Loss	
	Rectifier terminal	Inverter terminal
Total switching Loss (W) ($P_{t-sw} = P_{t-IGBT} + P_{t-Diode}$)	21830.41 W	21084.354 W
Arm 1+Arm 3+Arm 5 (Upper arms)	65491.23 W	63253.062 W

Table 5-36 shows the results of the calculations of total power losses, which is obtained by summing the IGBT and Diode switching losses. Since there are three arms in the upper section, then the results are multiplied by three to obtain the total switching loss at each of the station terminals. From the above results, the total power losses at the rectifier terminal of the converter station is larger than that of the inverter terminal, which shows that the rectifier station terminal has larger power loss contributions on the transmitted power.

5.2.8.11 IGBT Submodule Switching Losses Calculations for the Lower (Negative) Arm

Table 5-37: Calculations of IGBT power switching losses for the lower arm

Results	IGBT cell	
Power switching losses in IGBT cell (W)	Rectifier terminal	Inverter terminal
IGBT switching loss in T_1 $P_{I1sw}^{in}(t)$	2759.723 W	2257.83 W
IGBT switching loss in T_2 $P_{I2sw}^{by}(t)$	1009.20 W (negative)	1064.97 W (negative)
Total IGBT switching loss for the Lower arm	1750.523 W	1192.86 W

Table 5-37 shows the results of the calculations of IGBT power switching losses at the lower arm using equations (3-27) and (3-28). The modulation index, m, the power factor and the peak value of sinusoidal output current are shown on table 5-28, similarly, the forward voltage at no-load, V_{ceo}, and the forward resistance, R_o, of the IGBT are readily available on the datasheet. The IGBT conduction loss of the inserted cell and the bypassed cell are estimated using equations (3-27) and (3-28). Subsequently, the results from this analysis are summed together to obtain the total IGBT switching loss for the lower arm. From the above results, the IGBT switching losses at the rectifier terminal of the converter station is larger than that of the inverter terminal, which shows that the rectifier station terminal has larger power loss contributions on the transmitted power.

5.2.8.12 Diode Submodule Switching Losses Calculations for the Lower (Negative) Arm

Table 5-38: Calculations of diode power switching losses for the lower arm

Results	Diode cell	
Power switching losses in Diode cell (W)	Rectifier terminal	Inverter terminal
Diode switching loss in D_1 $P_{D1sw}^{in}(t)$	406.894 W	237.33 W
Diode switching loss in D_2 $P_{D2sw}^{by}(t)$	1069.91 W (negative)	1088.75 W (negative)
Total Diode switching loss for the upper arm	663.02 W (negative)	851.42 W (negative)

Table 5-38 shows the results of the calculations of Diode power switching losses at the lower arm using equations (3-29) and (3-30). The modulation index, m, the power factor and the peak value of sinusoidal output current are shown on table 5-28, similarly, the diode threshold voltage, V_{Do}, and the diode forward resistance, R_D, of the diode are readily available on the datasheet. The diode switching loss of the inserted cell and the bypassed cell are estimated using equations (3-29) and (3-30). Subsequently, the results from this analysis are summed together to obtain the total diode switching loss for the lower arm From the above results, the diode switching losses at the rectifier terminal of the

converter station is larger than that of the inverter terminal, which shows that the rectifier station terminal has larger power loss contributions on the transmitted power.

5.2.8.13 Total Submodule Switching Losses at the Lower Arm

Table 5-39: Table showing the total submodule switching loss at the lower arm

Results	Submodule switching Loss	
	Rectifier terminal	Inverter terminal
Total switching Loss (W) ($P_{t-sw} = P_{t-IGBT} + P_{t-Diode}$)	1087.503 W	341.44 W
Arm 2+Arm 4+Arm 6 (Lower arms)	3262.51 W	1024.32 W

Table 5-39 shows the results of the calculations of total power losses, which is obtained by summing the IGBT and Diode switching losses. Since there are three arms in the lower section, then the results are multiplied by three to obtain the total switching loss at each of the station terminals. From the above results, the total power losses at the rectifier terminal of the converter station is larger than that of the inverter terminal, which shows that the rectifier station terminal has larger power loss contributions on the transmitted power.

5.2.8.14 Overall Switching Power Loss

Table 5-40: Table showing the overall switching power loss of MMC-based converters

Results	Submodules Switching Loss	
Overall switching Loss (W) $P_{overall-loss} = P_{upp-arm-loss} + P_{low-arm-loss}$	Rectifier terminal	Inverter terminal
	68753.74 W	64277.382 W

Table 5-40 shows the results of the calculations of the overall switching power loss of M2C-based converters. This is obtained by adding the switching power loss contribution of the upper arm and the lower arm together. From the above results, the total power losses at the rectifier terminal of the converter station is larger than that of the inverter terminal, which shows that the rectifier station terminal has larger power loss contributions on the transmitted power.

5.2.8.15 Overall Total Losses of MMC at each Converter Stations

Table 5-41: Table showing the overall switching power loss of MMC-based converters

Results	Submodules Overall total Losses	
Overall total Losses of M2C (W) $P_{overall-loss} = P_{tcond-loss} + P_{tsw-loss}$	Rectifier terminal	Inverter terminal
	372591.16 W	490426.002 W
3-Ø MMC total Losses	1.118 MW	1.4713 MW

Table 5-41 shows the results of the calculations of the overall total power loss of M2C-based converters. This is obtained by adding the total switching power loss contribution and the total conduction power loss contribution together. From the above results, the overall total power losses at the inverter terminal of the converter station is larger than that of the rectifier terminal, which shows that the inverter station terminal has larger power loss contributions on the transmitted power.

Table 5-42: Comparison of different HVDC technologies based on their converter loss figures at the converter station terminals

HVDC Technologies	Rectifier terminal		Inverter terminal	
	Loss proportions	Loss percent	Loss proportions	Loss percent
Two-Level VSC HVDC	17.221 MW	61.55%	17.711 MW	60.44%
Three-Level VSC HVDC	9.317 MW	33.30%	9.872 MW	33.69%
LCC HVDC	322.404 kW	1.15%	250.982 kW	0.86%
MMC HVDC	1.118 MW	4.0%	1.4713 MW	5.01%

Table 5-42 shows the comparison of different HVDC technologies based on their converter loss figure at the converter station terminals. Therefore, from the table, it can be deduced that the two-level VSC-based HVDC technology has the highest percentage converter losses, followed by the three-level VSC-based HVDC technology. It can be seen that the loss contribution of modular multilevel converters is lower than the two level and three level VSC HVDC technologies, which conforms with the theoretical background of this HVDC technologies.

5.3 Summary

This chapter describes the evaluation of power losses in VSC-based HVDC technologies. The loss mechanisms of various VSC topologies were considered, the topologies considered in this chapter are 2-level, 3-level and modular multilevel converter. The loss calculation method utilized in this chapter is based on analytical mathematical representations stipulated in standards IEC 62751-1-2 and the component datasheet. The difficulty of HVDC transmission system loss calculation falls in the loss calculation of the converter station. To understand the loss proportion of equipment in HVDC converter station and to decrease the losses of the HVDC system, analysis based on the formulas stipulated in the standard of IEC 62751-1-2 Determination of power losses in VSC-based high-voltage direct current (HVDC) converter stations and the formulas for power loss calculation for both the two-level and three-level converter topologies were used to calculate the losses of each equipment in the converter stations. The results obtained from the losses analyses of these various VSC topologies show that the loss contributions of MMC topology is very much lower than the loss profile of 2-level and 3-level topologies. The MMC-based configuration has core features of low switching frequency and flexible controlled so that its loss figures are smaller than that of the three-level and two-level VSC-based configuration.

CHAPTER 6
POWER LOSSES CALCULATION OF HVDC TECHNOLOGIES MODEL SIMULATION AND RESULTS

6.1 Introduction

The previous chapters have expressly shown the power losses calculation methodologies to evaluate the converter stations losses of various high voltage direct current technologies using Standards IEC 61803, IEEE std 1158, IEC 62751-1-2 and datasheet parameters. Due to the various loss generation mechanisms, each kind of equipment has a particular loss calculation model, which involves equipment inherent parameters and operational parameters changed with operation conditions. Therefore, it is expedient to acknowledge that the increased product variety in the area of power semiconductors demands comparisons beyond the information contained in datasheets. In respect of this, the various HVDC technologies (circuit simulations) models are implemented in Matlab-Simulink and permits the simulation of various power devices, modulation techniques and operating condition with ease. Subsequent to these circuit implementations, some results are obtained and consequently validated with other commercial power loss simulation tools or electronic software, such as Semisel and Melcosim [4, 92].

6.2 Circuit Simulations of Various HVDC Technologies

The evaluation of transmission power losses are essential to be investigated in power transmission systems and it is imperative to design a transmission system with minimal power loss. Power loss evaluation in transmission system can contribute to the overall system performance optimization by assessing both the economic and technical system benefits and comprehending the components that contribute to maximum power loss [7, 83]. Hence, to evaluate the losses of converter station equipment, the system operation of a point-to-point HVDC system was modelled and simulated using Matlab-Simulink program. The rectifier control operation was modelled as a constant dc source and the control operation of the inverter as constant extinction angle, majorly for efficient, reliable and stable system operation. It is worthy of note that, the proposed method of valve losses determination is based on analytical formulae for both the operating and standby conditions. However, it is expedient to apply numerical solutions using real-time or non-real-time simulations to obtain such input parameters, for example switching energies, valve current, dc voltage etc. This approach is much faster and accurate (less prone to error) than applying purely analytical means which requires complex analysis to obtain some of these necessary input parameters. Moreover, to obtain accurate input parameters, it is expected that such simulations should be an accurate modelling of the system under investigation. At this junction, it is very essential to investigate the circuit simulations of various HVDC technologies such as LCC-based and VSC based HVDC systems. Afterward, both approaches (analytical and simulations) are compared based on the results obtained [58, 95].

6.2.1 LCC-Based HVDC Technology

Chapter 4 of this dissertation explicitly explained the analytical approach to calculating the power loss contributions of key equipment of the LCC-based HVDC converter stations during operating and standby conditions. The losses

were calculated from component characteristics, using suitable mathematical models of the converters as indicated in standards IEC 61803 and IEEE 1158. In this section, the analytical formulae used to estimate the various station equipment losses were modelled into blocks on Matlab-Simulink environment as illustrated in figure 6-1. These blocks were connected together to form LCC-based HVDC network. The description of the network is discussed below. The system was simulated and the losses of this HVDC technology were obtained from the scopes and the results were tabulated [3, 96].

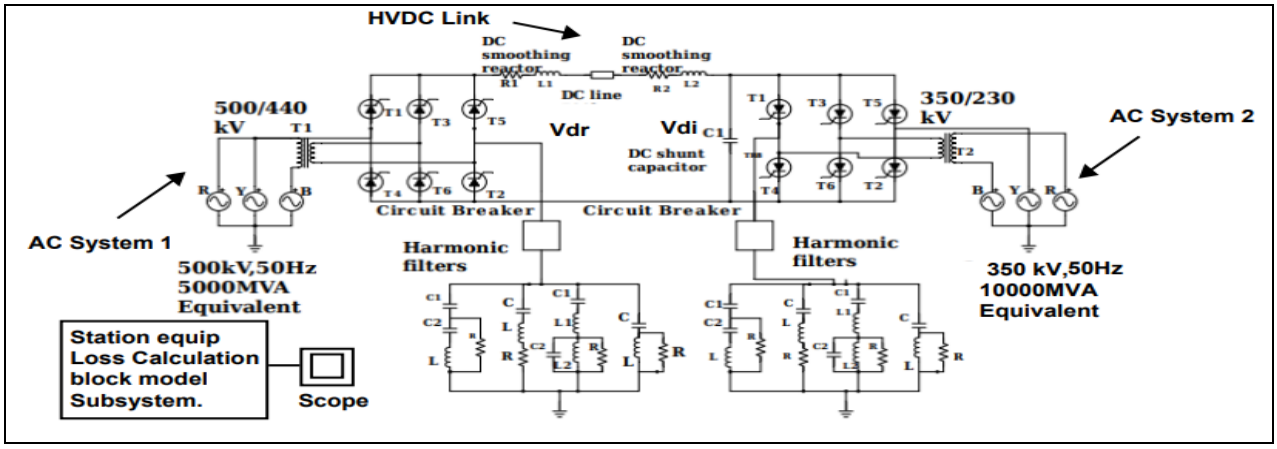

Figure 6-1: Circuit simulation of 6-pulse LCC-Based HVDC technology

Figure 6-1 describes A 1000 MW (500 kV, 2 kA) DC interconnection, which is utilized to transport power from a 500 kV, 5000 MVA, 50 Hz network to a 350 kV, 10,000 MVA, 50 Hz network. Both the network has a power rating of 5000 MVA and frequency of 50 Hz [92, 97]. Therefore, the system and the converters are connected through a 5000 MVA three-phase transformer (three windings).). It is worthy of note that, HVDC system majorly converts from ac to dc through the rectifier station and also converts dc to ac through the inverter station. Therefore, the voltage reduces through these conversions as a result of the HVDC components between the rectifier and inverter stations. At first, the 500 kV was stepped down to 440 kV by the stepdown transformer, as a result of the subsequent conversions, the voltage was further reduced to 350 kV which could be calculated using some equation available in literature [56] analytically to justify the value. Finally, the voltage was stepped down by the step down transformer to 230 kVThe thyristors are fired at an angle of 19° and also the overlap angle between the commutating thyristors was taken to be 10° in order for accurate and effective operation of the system and likewise to obtain optimum voltage value at the inverter side. More so, the rectifier and the inverter consist of 6-pulse Thyristor Bridge, which are connected, in series via a DC line of 500 km distributed parameter line and a 0.5 H smoothing reactor at both side of the line. Subsequently, the harmonic compensation has been taken care of, mainly by installing AC filters, which comprises of one capacitor banks of 600 Mvar reactive power for harmonic reduction. In the circuit simulation modelled in this research, two-gamma measurement blocks are modelled for both the rectifier and inverter, whose subsystem components are illustrated in figures 6-2 and 6-3. The essence of these controllers is mainly to control the firing angle and the extinction angle for efficient operation of the system. The trigger set mainly convert the firing angle in suitable firing pulses for each individual valve and the synchronization of these pulses to the AC system. In rectifier control system, the dc link current is kept constant by subjecting the rectifier with constant current control (pole control).The firing angle is

mainly adjusted with current error, to maintain the dc current constant. Also in inverter control system, the inverter adopts the constant extinction angle control. However, in steady state normal operating conditions, it operates with CEA control [98, 99].

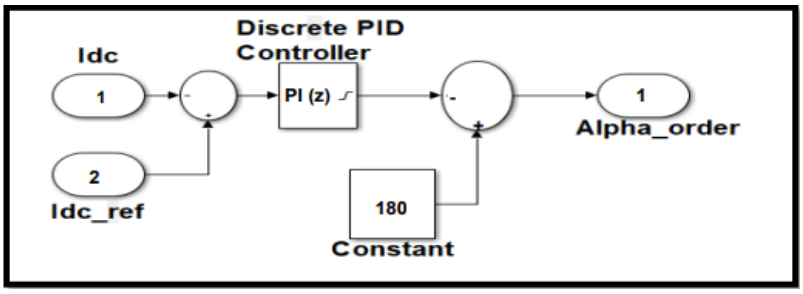

Figure 6-2: Subsystem components of Alpha Order

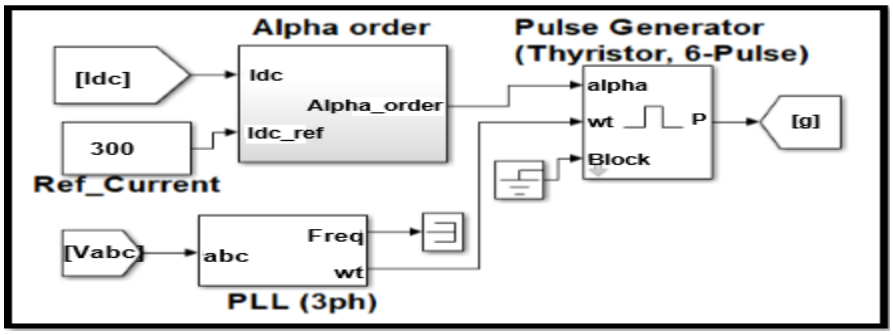

Figure 6-3: Subsystem components of Rectifier current control (Firing angle measurement)

Figure 6-2 and 6-3 describes the rectifier control system whose major aim is to generate pulse signal to trigger the gate of the thyristor. The PID controller determines the conduction angle, which is used to generate the firing pulse for the thyristor. The PLL block generates the firing angle in radian (wt) and frequency from the three-phase voltage, which is utilized by the pulse generator to energize the gate of the six-thyristor valves. A PI current regulator controls the converter output current. A step signal is applied to the reference input to test the dynamic response of the current regulator.

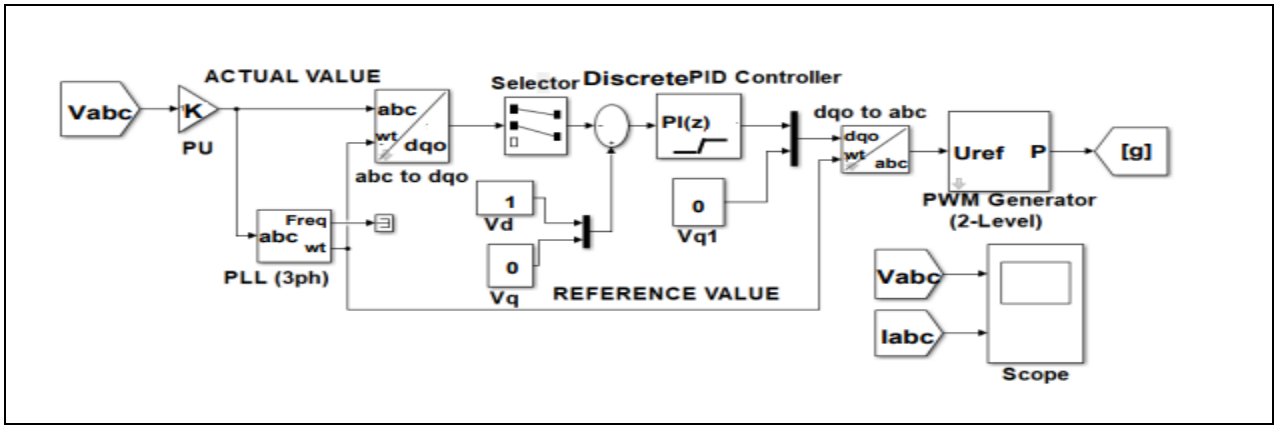

Figure 6-4: Subsystem components of Inverter gamma control

Figure 6-4 describes the implementation of inverter control system. The selector is used to select d and q from the abc-to-dqo transformation block. A PLL block is used to generate the frequency and the angle in radian (wt). The voltage from dqo is transformed to abc by Clarke transformation. Finally, the PWM generator generates the pulses of the thyristor based on the input from the transformation block [23].

6.2.1.1 Power Losses Calculation of LCC-based HVDC System

An intuitive way to obtain the converter-station valve power losses is to simply compare the AC side measured power and the DC side power. The studies in the previous chapters pointed out the inherent inaccuracy in the measurement data, in the attempt to determine the station losses by simply subtracting the output power measured, from the input power. More so, such method is not able to observe the distribution of valve power loss and the factors that influence valve power losses. It was further suggested that the total losses of HVDC converter station should be obtained mainly by the addition of various equipment losses on the converter station. In view of this, the total losses calculation algorithm of LCC-based HVDC converter station are integrated in a block in Matlab Simulink [2, 7].

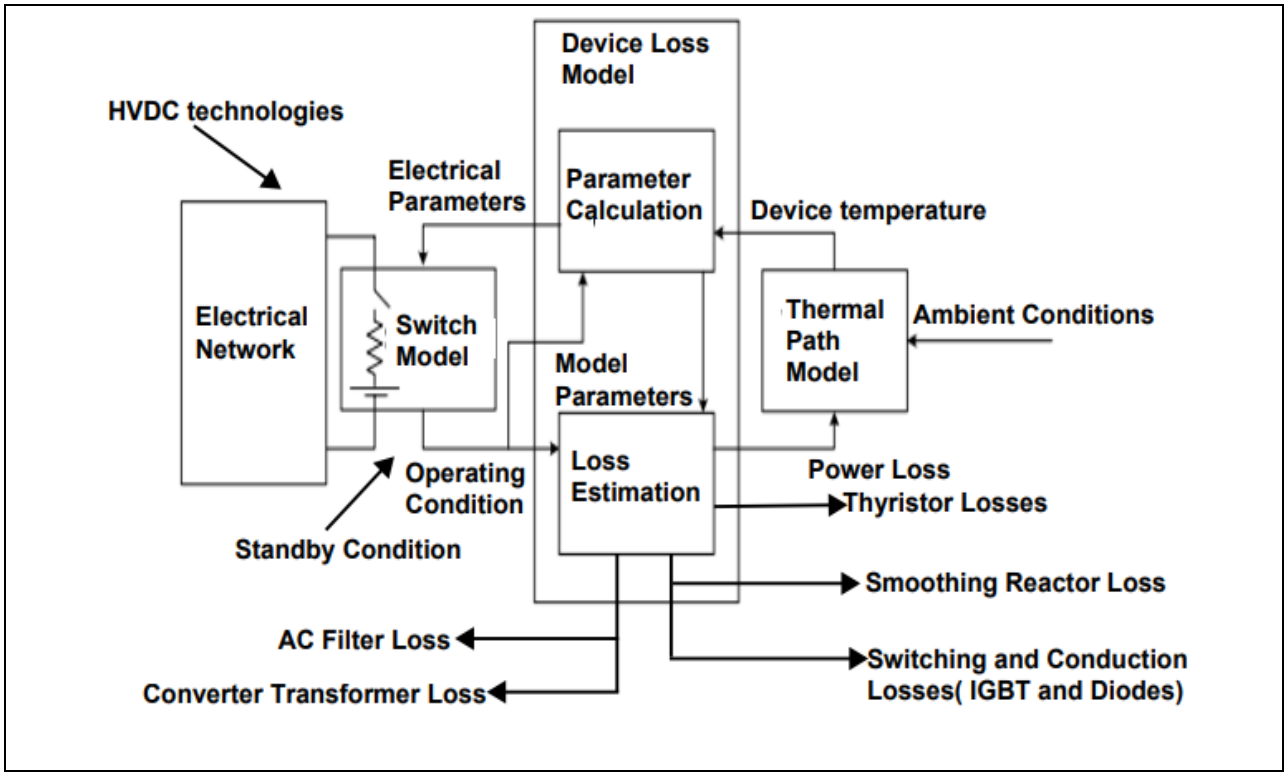

Figure 6-5: Matlab-Simulink Losses Block Model (HVDC technologies) [66]

Figure 6-5 describes the loss model of HVDC converter station equipment of various HVDC technologies. The parameter calculation is carried out based on the formulae in the standards and the device datasheet. The loss estimation of these station equipment is evaluated during operating and standby conditions.

6.2.1.2 Simulation Results using Various Simulation Schemes for Losses Estimation

Table 6-1: Simulation parameters

Required parameters	V_{abc}	f	$A_{temp}°C$	R	L_s	T_j	R_t	V_{TO}
Values	500 kV	50 Hz	40 ℃	0.002 Ω	98.03e-3 H	125℃	0.198mΩ	0.98 V

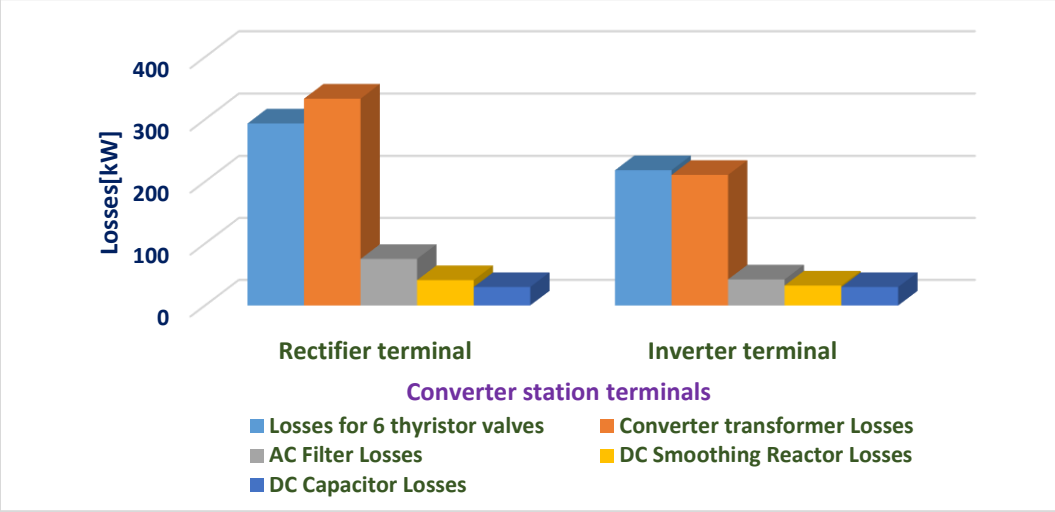

Figure 6-6: LCC-based converter stations equipment losses using Matlab-Simulink algorithm

Table 6-1 shows the simulation input parameters used in the Matlab-Simulink algorithm to compute the power losses of various equipment on the converter stations. The I^2R losses of the converter station equipment were modelled in the block called loss calculation, and the outcome of the power losses of the converter station equipment such as thyristor valves, converter transformer, AC filters, and DC Capacitor are illustrated in figure 6-6.

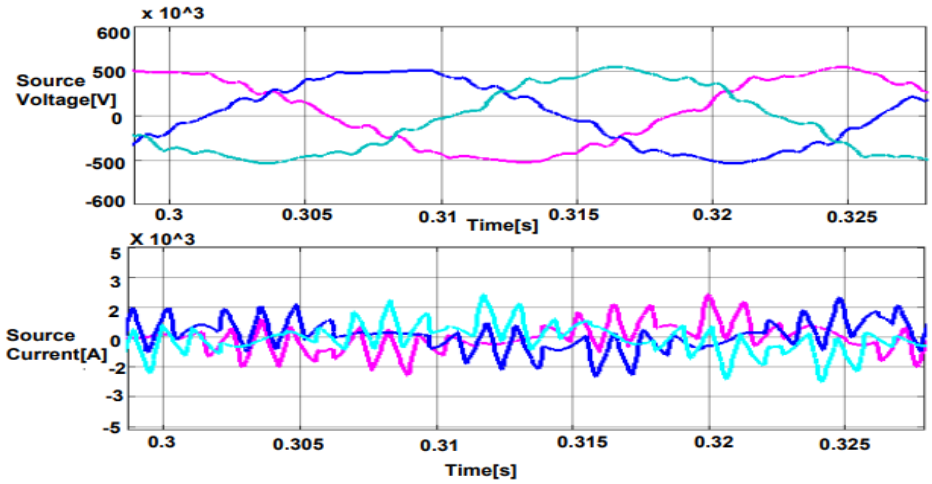

Figure 6-7: Source Voltage and current waveforms before applying harmonic filters

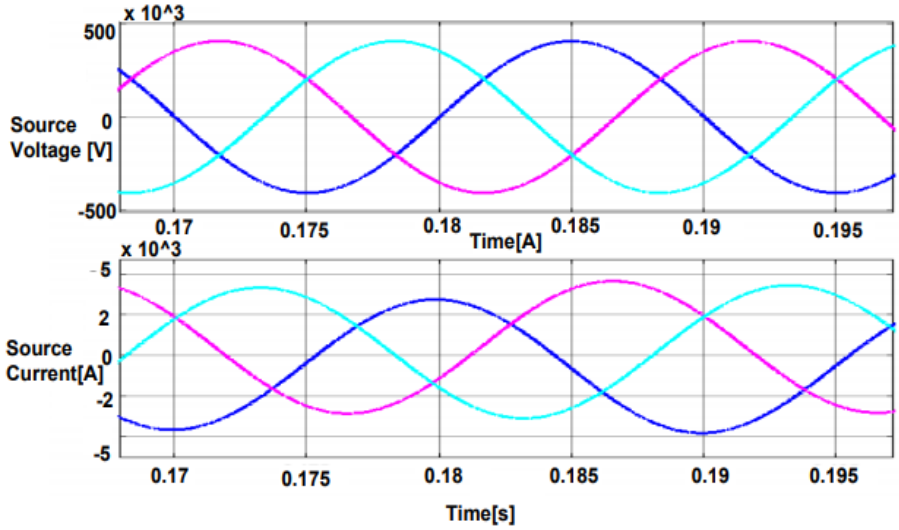

Figure 6-8: Source Voltage and Current waveforms after applying harmonic filters

Figure 6-7 and 6-8 show the waveforms of the source voltage and current before and after the installation of harmonic filters respectively. The converters and converter transformer introduced the harmonic contents, which cause the ripples as shown in Figure 6-7. From the total harmonic distortion analysis carried out, the following characteristics harmonics were noticed, 3rd, 5th, 7th, 11th, 12th, 17th, and 19th harmonics. Subsequent to the installation of the harmonic filters such as the C-type, single-tuned, double-tuned, and high pass filters at the converter terminals, the harmonic contents were mitigated which results in Figure 6-8 that shows the waveform of filtered source voltage and current.

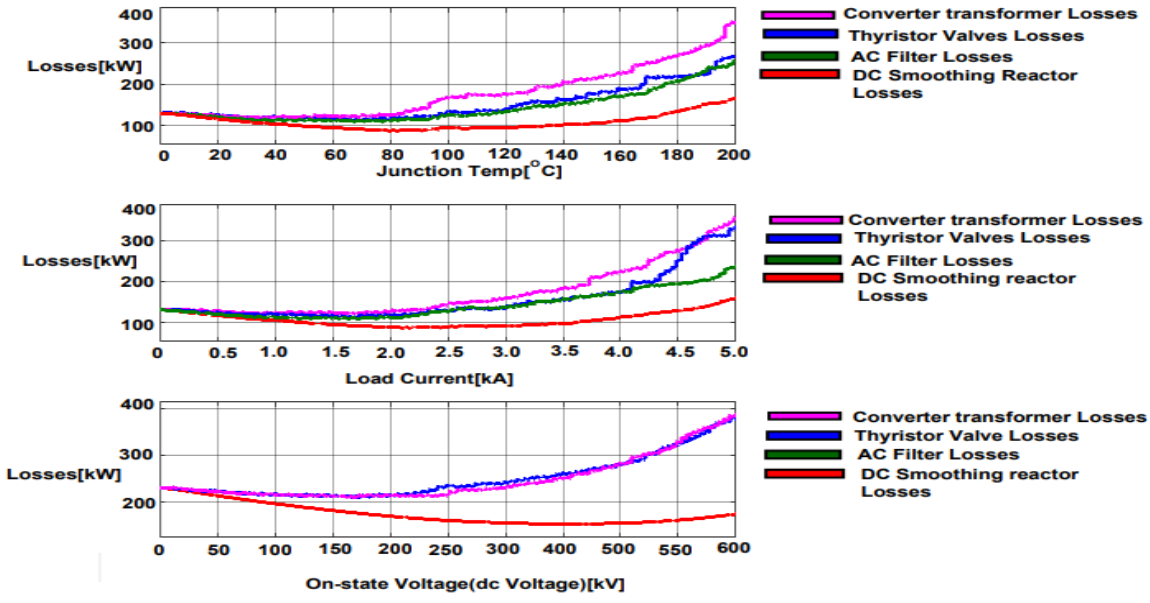

Figure 6-9: Variation of converter station's equipment losses with converter station operating parameters (Rectifier terminal)

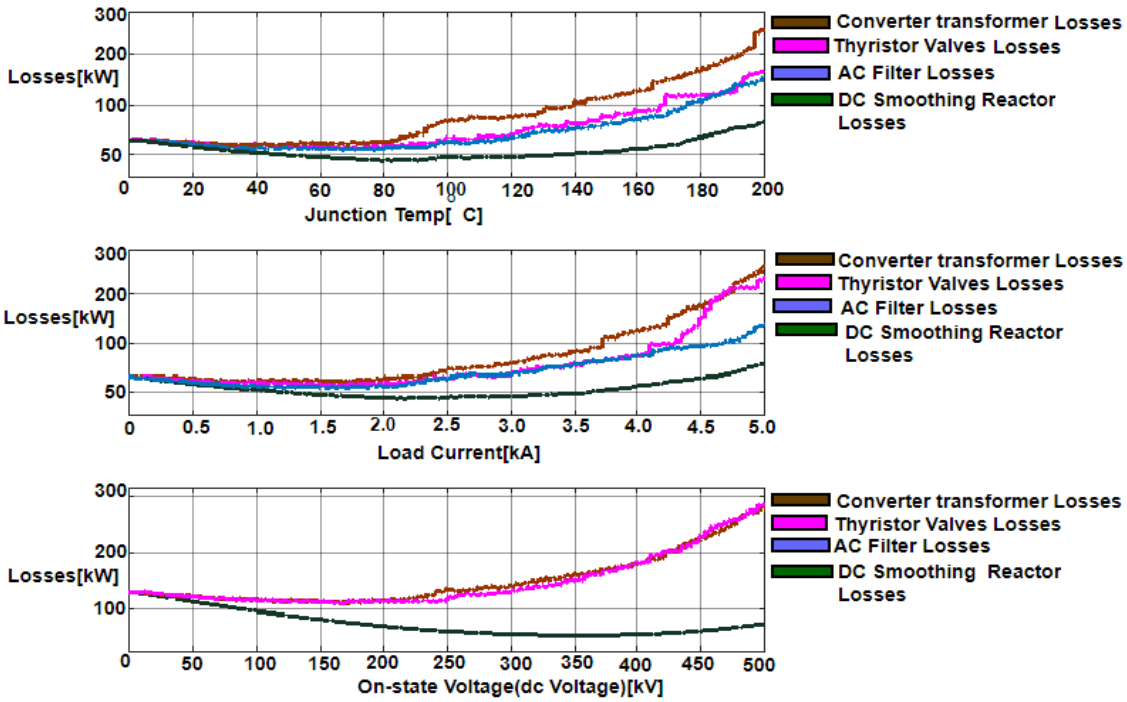

Figure 6-10: Variation of converter station equipment losses with converter station operating parameters (Inverter terminal)

Figure 6-9 and 6-10 show the results of the various key equipment losses on HVDC converter station as they vary with the operating parameters. These results were obtained from the scope of the block, model of Matlab-Simulink Algorithm. Theoretically, it is imperative to note that the actual losses in each piece of equipment depend on the ambient temperature, which is a function of the junction temperature. Losses also depend on the operating conditions to which it is applied, therefore, invariably depend on it operating parameters such as ambient temperature, load current, dc voltage, firing angle etc. Therefore, in order for the summation of the individual losses to be a sufficiently accurate representation of the actual total HVDC converter station losses, the ambient and operating conditions for each piece of equipment must be defined, based on the ambient and operating conditions of the entire HVDC converter station. The losses of the key converter station equipment such as thyristor valves, converter transformer, AC filters, and DC smoothing reactor were estimated and varied with some operating parameters such as, the junction temperature, load current and dc voltage. The essence is to indicate loss dependence and its linear relationship on these parameters. The suggested and accepted method of estimating the power losses of converter station applies, i.e. the summation of various converter stations equipment losses. The Matlab-Simulink algorithm was also modelled in a block to compute the junction temperature T_j, since the junction to case thermal resistance Rth_{j-c}, case to heatsink thermal resistance Rth_{c-h} and heatsink to ambient thermal resistance Rth_{h-a} values are readily available on component datasheet. The results obtained were also compared with other results from commercial losses calculation simulation tool such as Semisel program. Simisel program is an online losses calculation simulation tool powered by Semikron. The result obtained from the semisel program are shown below.

Table 6-2: Given simulation parameters

Required parameters	Values
Threshold voltage, V_{TO} at 25°C Threshold voltage, V_{TO} at 125°C	0.82 V 0.98 V
Slope resistance, r_T at 25°C Slope resistance, r_T at 125°C	0.17 mΩ 0.198 mΩ
Junction to sink thermal resistance, Rth_{j-s}	0.043 K/W

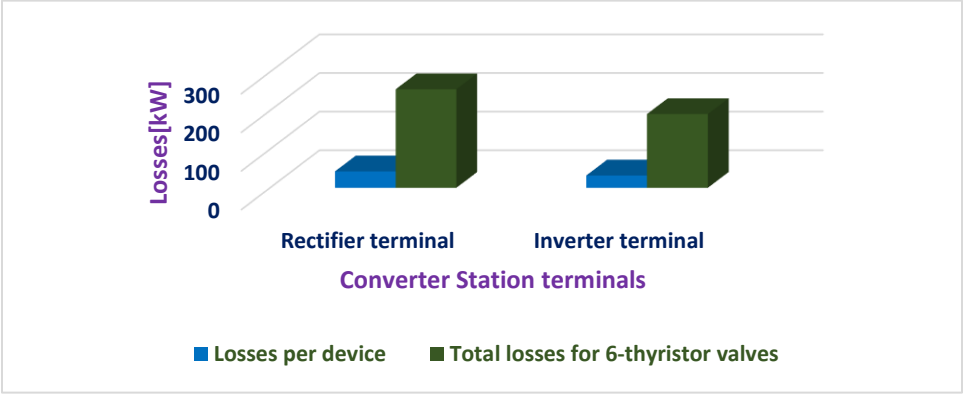

Figure 6-11: Thyristor valves losses on semisel simulator platform

Figure 6-11 describes the losses calculation on online commercial platform known as Semisel program powered by Semikron. Table 6-2 and Figure 6-11 show the required parameters for the simulation and the results obtained after the simulation respectively.

6.2.2 VSC-based HVDC Technologies

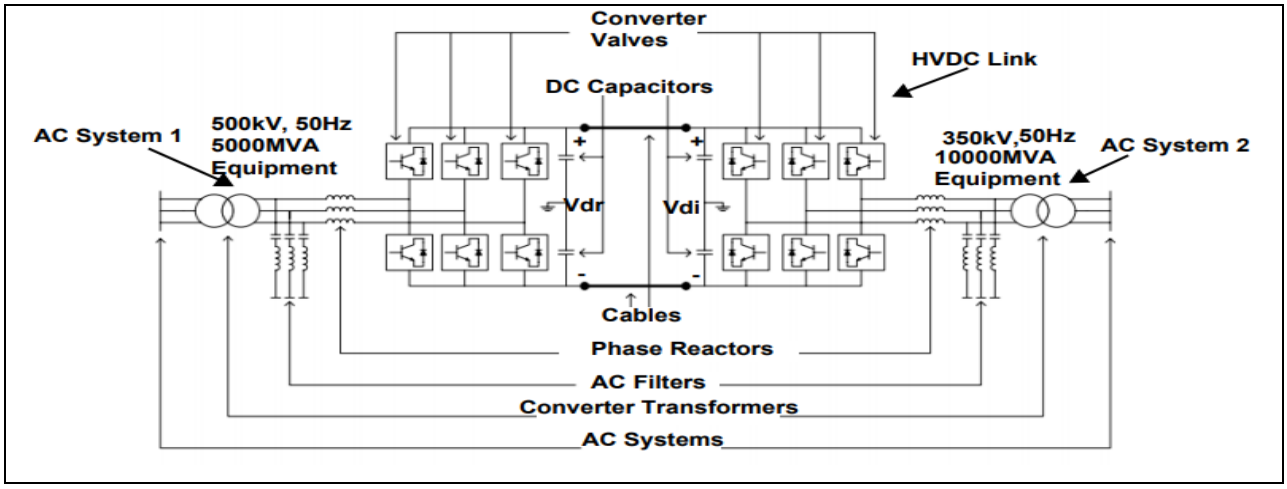

Figure 6-12: Block diagram of two-level VSC HVDC technology

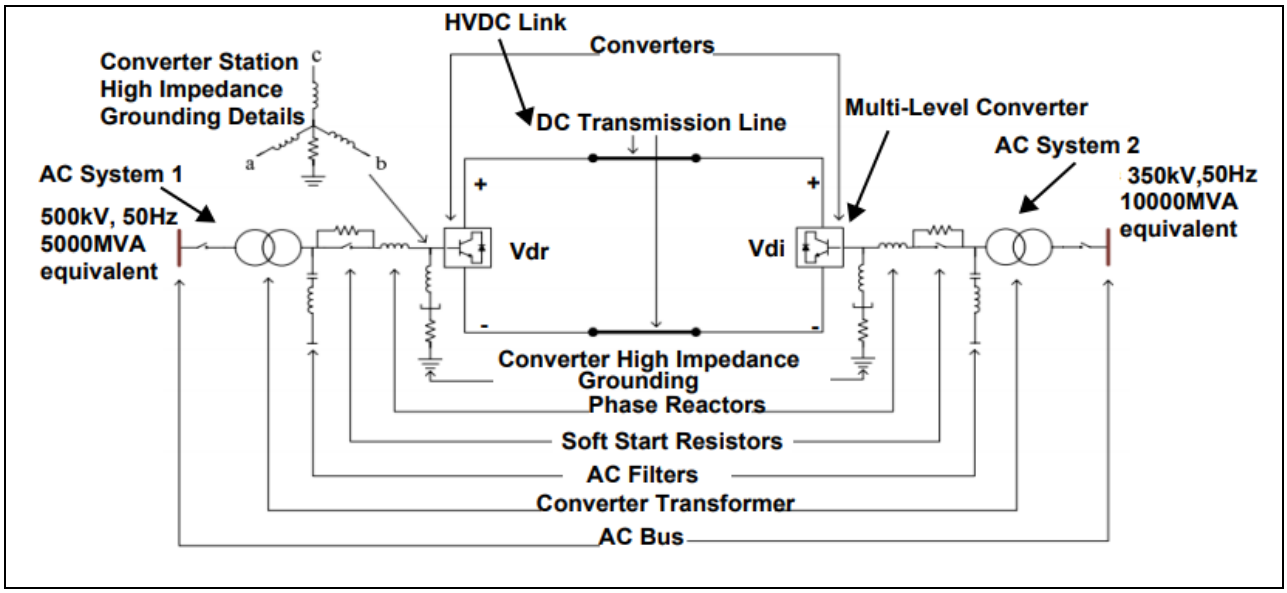

Figure 6-13: Block diagram of multi-level VSC HVDC technology

Figure 6-12 depicts the two-level VSC HVDC technologies with a 200 MVA, 100 kV DC forced –commutated voltage-source converter interconnection, which is used to transport power from a 500 kV, 5000 MVA, 50Hz system to another identical AC system. More so, the rectifier and the inverter are two and three level VSC converters using IGBTs and freewheeling diodes. The Sinusoidal Pulse Width Modulation (SPWM) switching utilizes a single-phase triangular carrier wave with a frequency of 20 times the fundamental frequency (1 kHz). The AC side of the system consists of the converters, the step down $Y_g - D$ transformer, the converter reactor and the AC filters. The DC side consists of the DC filters, the shunt capacitors etc. The 600 Mvar shunt AC filters are mainly 27^{th} and 54^{th} high-pass tuned around the two dominating harmonics. The DC capacitors are connected to the VSC terminals. Therefore, these connections have an influence on the system dynamics and voltage ripples on the DC sides. The rectifier and the inverter are interconnected through a pie cable configuration of 500 km distance apart and 8mH smoothing reactors.

Figure 6-13 shows a multi-level VSC HVDC technology, a 500 kV, 5000 MVA, 50Hz system were utilized to transmit power from the rectifier terminal to the inverter terminal. At the inverter terminal, a 2800 volts DC source, 1000 MW, three-phase multi-level delivers variable power to the distribution power system. More so, the inverter output is connected to the 230 kV, 5000 MVA, 50Hz system through a 350/230 kV transformer. The control system mainly contains two PI controllers (one current regulator and one PQ regulator) to generate the needed inverter pulses in order to achieve the reference output power. Note that, the leg of phase-A is implemented using three-Half IGBT with Loss Calculation blocks. More so, both the conduction and switching losses are computed and injected into a thermal network. The achievable output power versus switching frequency for the three-phase multi-level converter station are illustrated by the simulation. Furthermore, the half-bridge is modeled by two IGBT and freewheeling diode blocks, which are pulsed from an external pulse generator. It is worth noting that, the loss estimations are based on the specifications read from the manufacturer's datasheet.

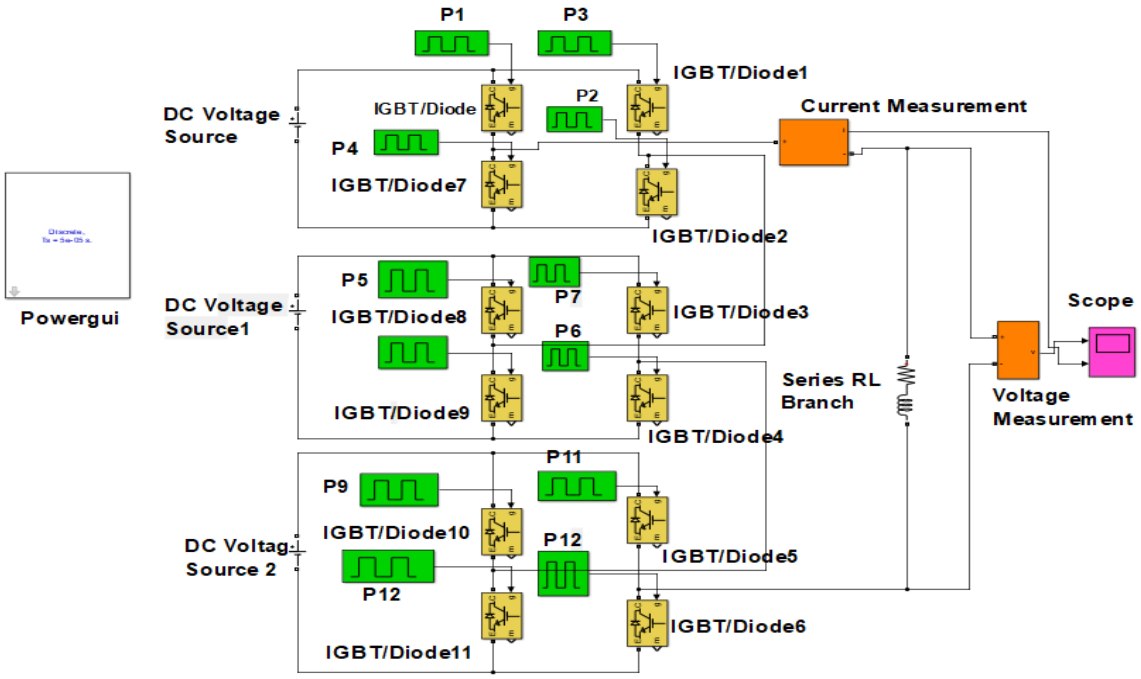

Figure 6-14: Arrangement of IGBT modules, which form the subsystems of various VSC configurations

Figure 6-14 shows the method of IGBT Modules arrangement in the subsystem blocks of various VSC configurations. The above arrangement is mainly for the inverter terminal, this is like a prototype for other VSC configurations both at the rectifier and inverter station terminals.

6.2.2.1 Power Losses Calculation of VSC-based HVDC System

The power losses estimation algorithm of various VSC technologies of HVDC system such as two, three and multi-level technologies are executed by two Matlab files, a Simulink program (.mdl file) and the main file (.m structure). The Simulink file is activated from the main file. The power losses are majorly estimated in four groups, which are, IGBT conduction losses, IGBT switching losses, diode conduction losses and diode switching losses.

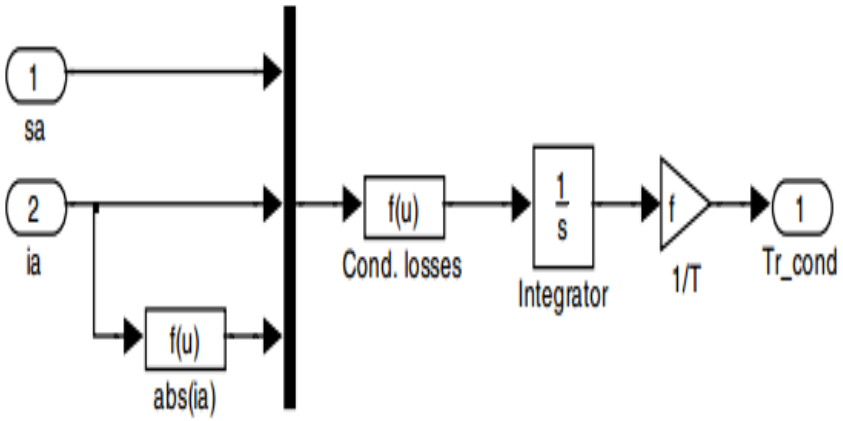

Figure 6-15: Matlab-Simulink: Conduction calculation block model

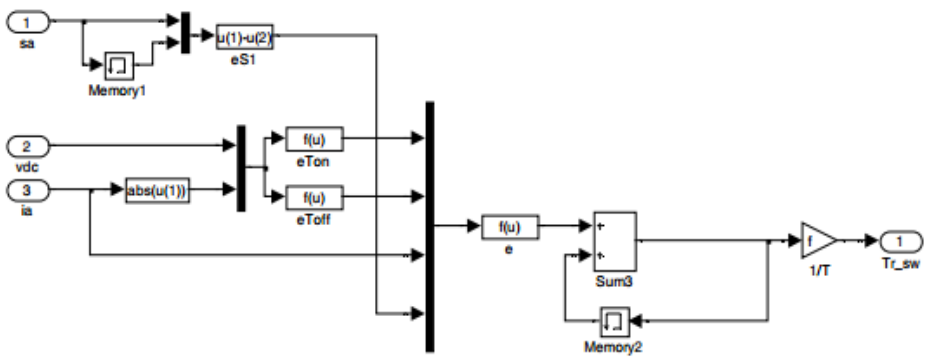

Figure 6-16: Matlab-Simulink: switching losses calculation block model

Figure 6-15 and 6-16 show the Matlab-Simulink Implementation of Conduction and switching losses calculation based on the formula stipulated in the previous chapters. The block model actually provides the losses of one leg of the IGBT Module. Therefore, due to the same dc-link voltage, switching patterns and ac current are applied to the other phase legs. Since the configuration is three-phase the total losses by multiplying the results by three.

6.2.2.2 Simulation Results for VSC Technologies using Matlab-Simulink Algorithm

Table 6-3: Simulation parameters

Required parameters	V_{ce-dc}	f_{sw}	$A_{temp}°C$	R	L_s	T_j	R_o	R_d
Values	2800V	1 kHz	60 ℃	0.002 Ω	98.03e-3 H	125℃	0.001677	0.001167

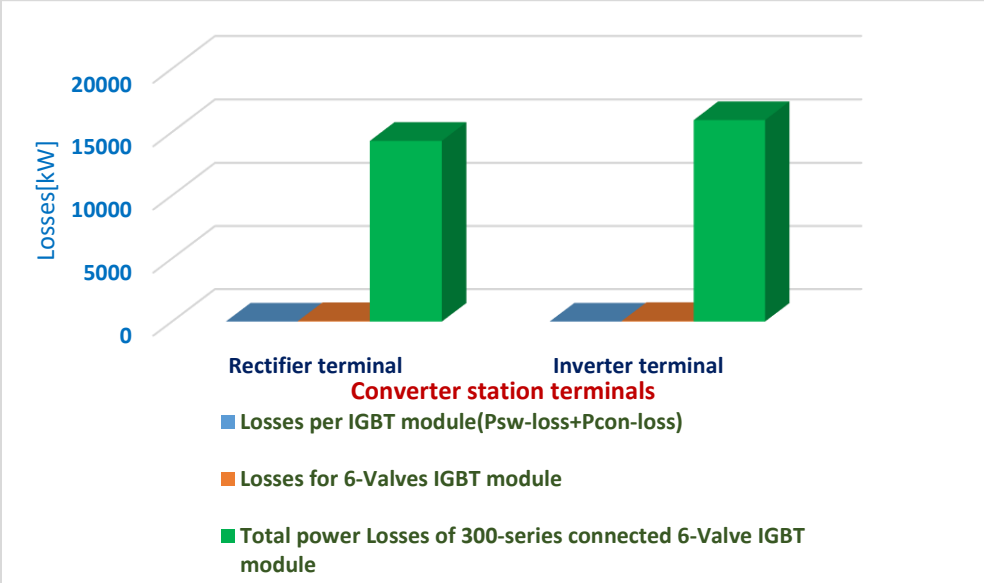

Figure 6-17: Two-level VSC technology power losses estimations using Matlab-Simulink algorithm

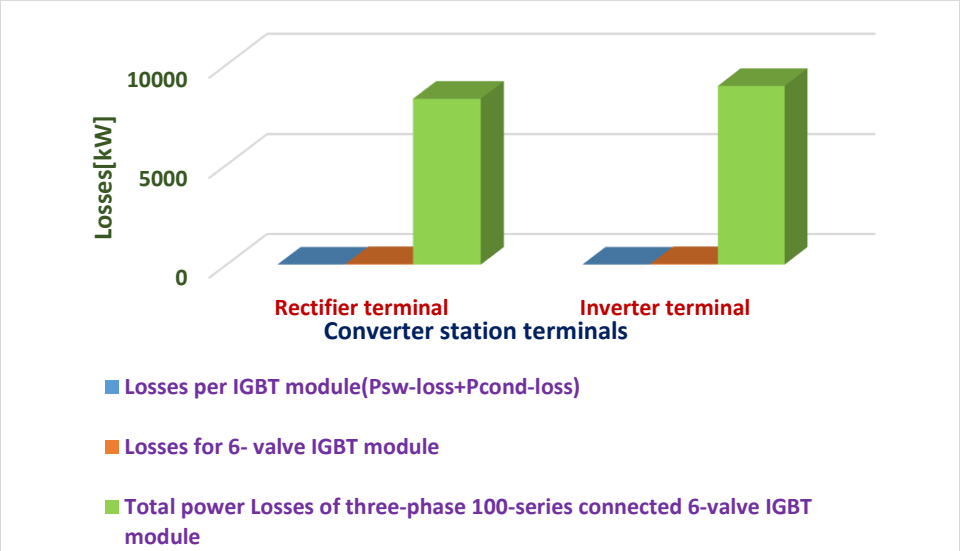

Figure 6-18: Three-level VSC technology power losses calculations using Matlab-Simulink algorithm

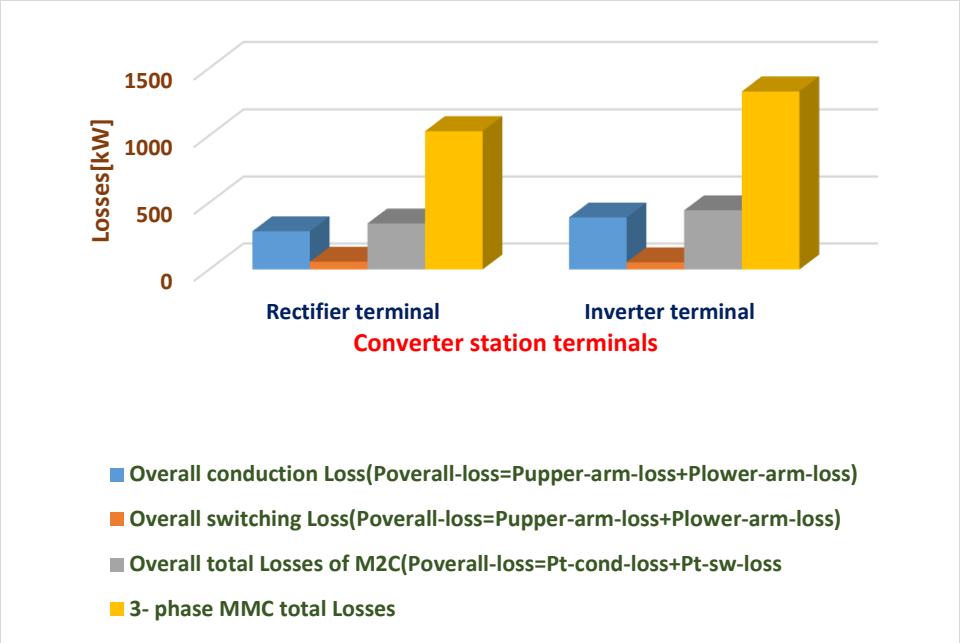

Figure 6-19: Multi-level VSC technology power losses calculations using Matlab-Simulink algorithm

Table 6-3 shows the simulation parameters used in the Matlab-Simulink algorithm to compute the power losses of IGBT modules at each converter station terminals. The I^2R losses i.e., the square of the rms current passing through the power device (IGBT modules) and its equivalent resistance at both converter station terminals (Conduction losses), also the product of the voltage and current of the main semiconductor using the oscilloscope were modelled in the block called loss calculation. Therefore, the outcome of the Simulation results of the IGBT modules power losses at both converter station for all the VSC technologies are illustrated in Figure 7-17, 7-18 and 7-19.

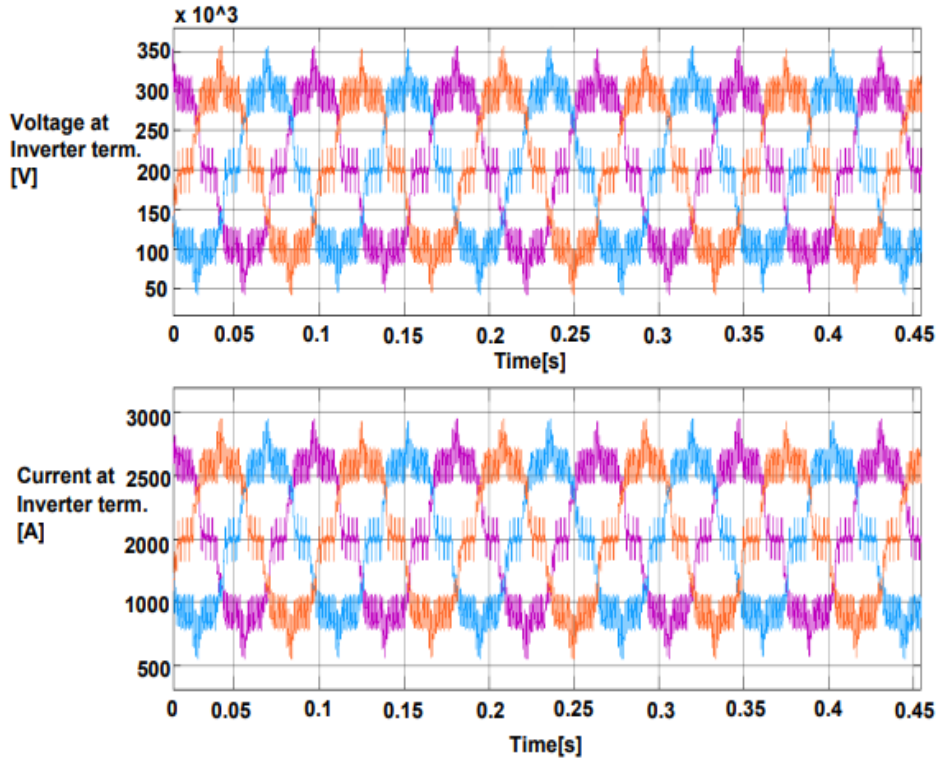

Figure 6-20: The Inverter terminal's Voltage and current waveforms during 2-Level VSC simulation

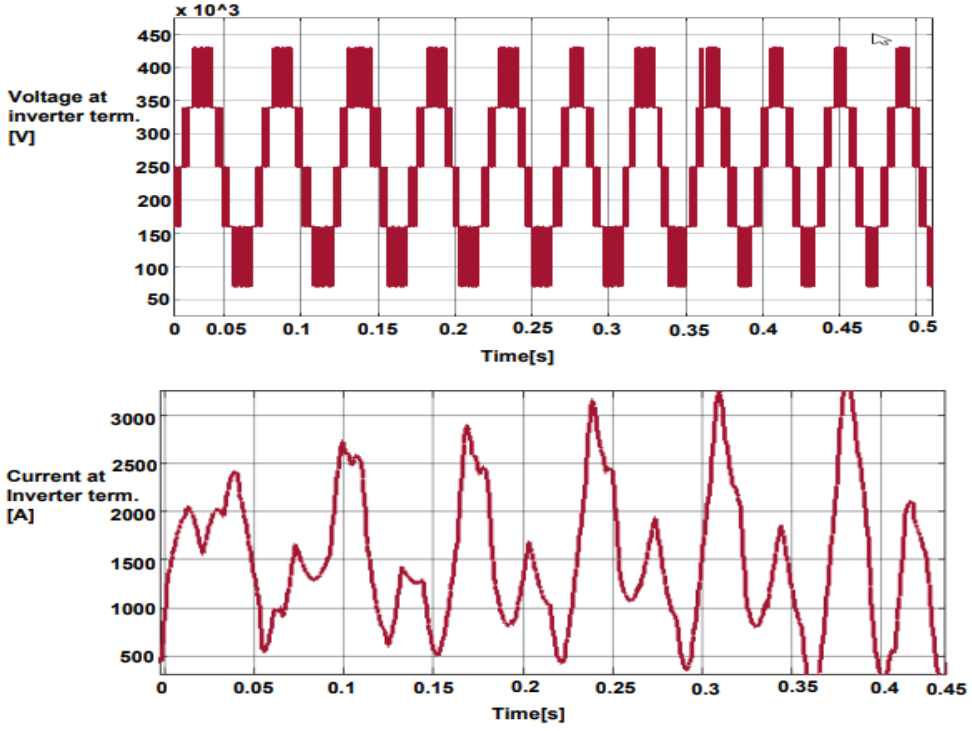

Figure 6-21: The Inverter terminal's Voltage and current waveforms during 3-Level VSC simulation

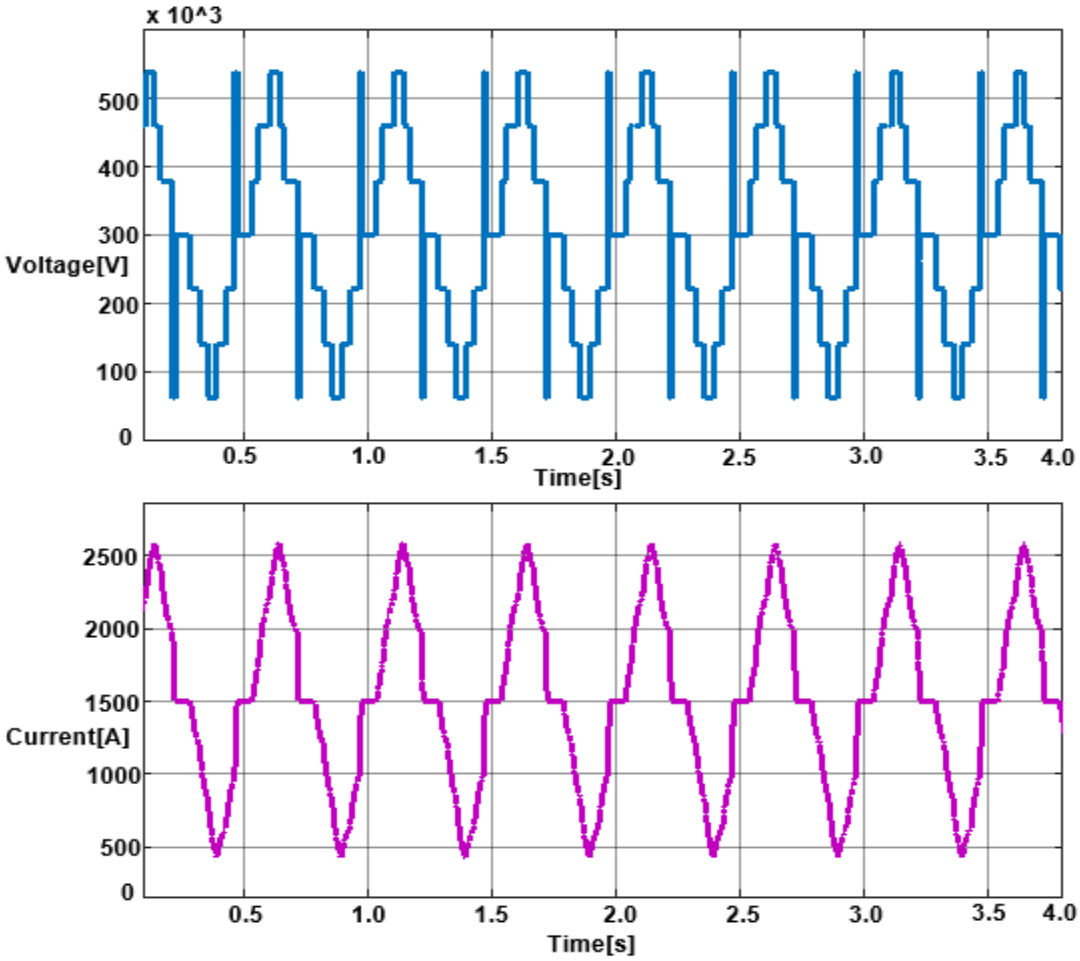

Figure 6-22: The Inverter terminal's Voltage and current waveforms during Multi-Level VSC simulation

Figure 6-20, 6-21 and 6-22 describe the output waveform at the inverter terminal for 2-level, 3-level and multi-level VSC configurations during the operating condition of the station i.e. the station energized and the valves are operating. The waveforms show the voltage and current at the inverter terminal for various VSC technologies. During standby mode i.e. when the stations are energized and the valves blocked, zero harmonic current flows in the system and results to no losses in the system.

Figure 6-23 illustrates the relationship and the effect of both IGBT and FWD losses on two operating parameters such as modulation index and power factor. Fig. 6-23 is obtained by setting the transmission capacity of the system to 1500kW, which results to the losses at both upper and lower submodule of the IGBT and FWD shown below.

Therefore, it can be seen that their losses decreases when the power factor and modulation index of the system increases. The losses of IGBT are larger than the losses of its corresponding FWD. Hence, with a fixed transmission power, the losses of the system can be drastically reduced by increasing the modulation index and power factor.

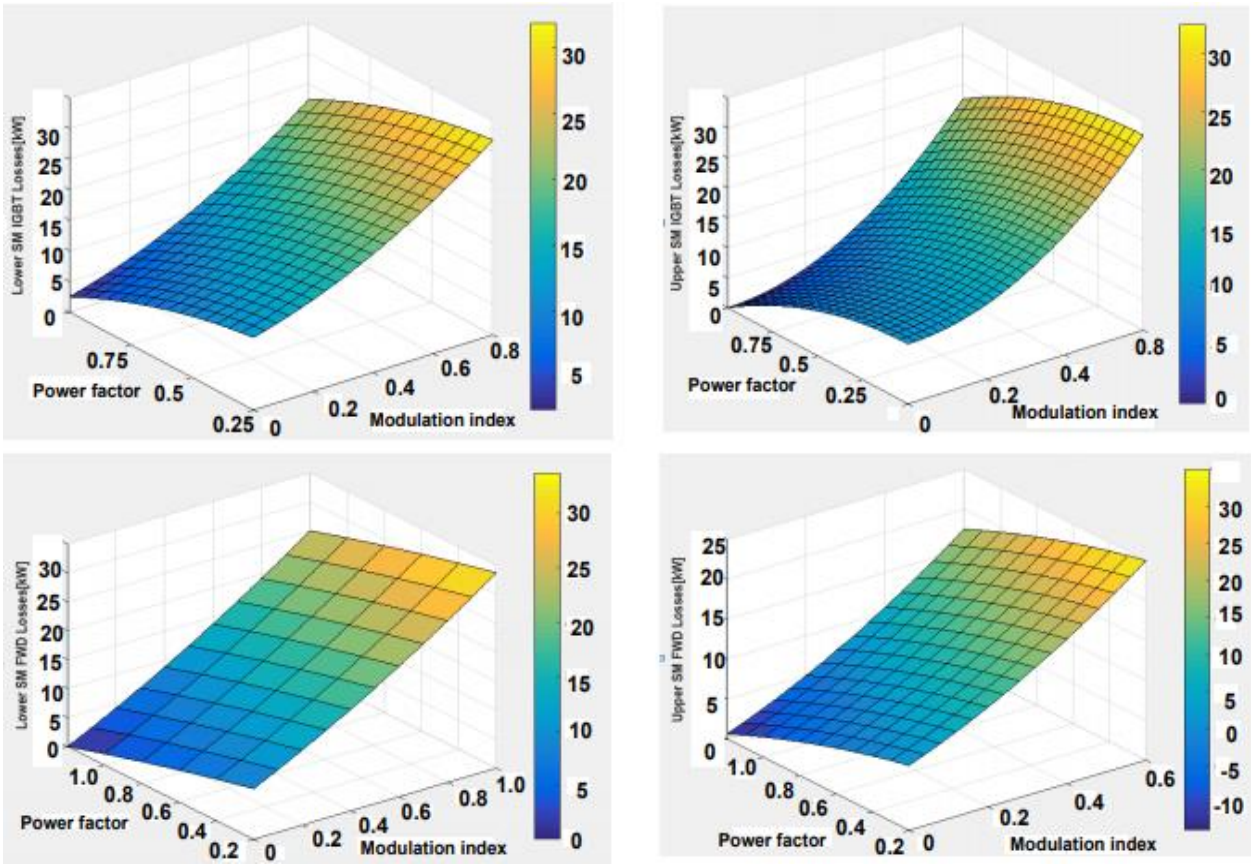

Figure 6-23: The 3-D map of IGBT's and FWD's Losses of MMC topology

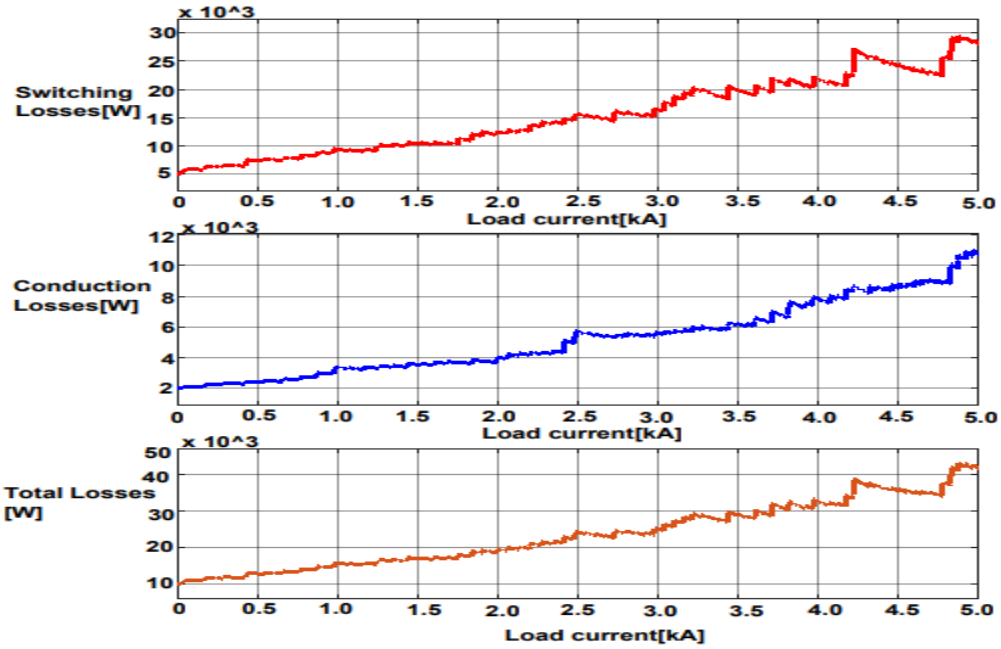

Figure 6-24: The variation of the switching, conduction and total losses of 6-valves IGBT Module for 2-Level VSC configuration with respect to the Load current

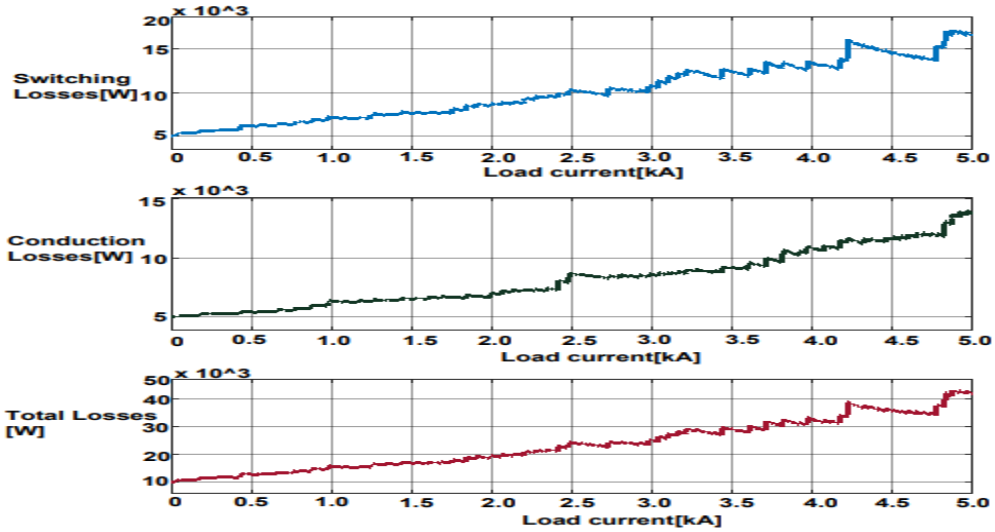

Figure 6-25: The variation of the switching, conduction and total losses of 6-valves IGBT Module for 3-Level VSC configuration with respect to the Load current

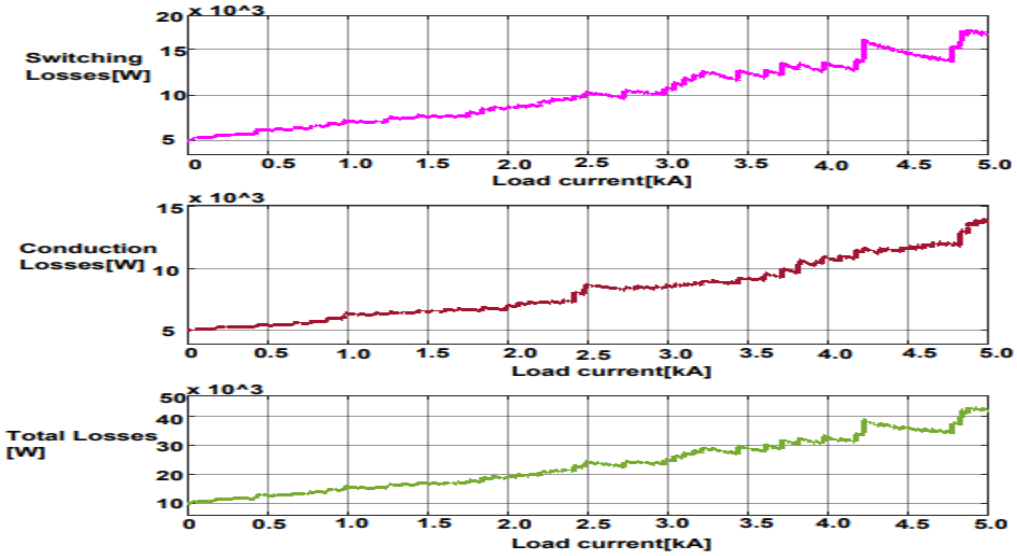

Figure 6-26: The variation of the switching, conduction and total losses for both upper and lower arm of Multi-Level VSC configuration with respect to the Load current

Figure 6-24, 6-25 and 6-26 show the results obtained from the scope of the block model of Matlab-Simulink Algorithm, which calculate both the switching losses and conduction losses of IGBT Modules for various VSC configurations as they vary with respect to the load currents. The Matlab-Simulink algorithm was also modelled in a block to compute the junction temperature T_j, since the junction to case thermal resistance Rth_{j-c}, case to heatsink thermal resistance Rth_{c-h} and heatsink to ambient thermal resistance Rth_{h-a} values are readily available on component datasheet. The results obtained using Matlab-Simulink block model were also compared with other results from commercial losses calculation simulation tool such as Semisel and Melcosim program to validate the accuracy

of the results obtained on Matlab-Simulink Algorithm. The result obtained from the Semisel and Melcosim program are shown below.

Table 6-4: Simulation parameters

IGBT	V_{ce}	I_c	PF	MR	f_{sw}	f_o	T_s	T_{jmax}	$R_{g(on)}$	$R_{g(off)}$
	2800 V	1000 A	0.856	0.85	1kHz	50Hz	$125°C$	$150°C$	2.4Ω	2.7Ω

Diode	C_f	V_{TO}	R_d	V_f	I_f	$R_{th(j-c)}$	A_{temp}	N_s	E_{on}	E_{off}
	1	1.2 V	0.0012	2.57V	450A	0.055K/W	$60°C$	6	6450 mJ	4650 mJ

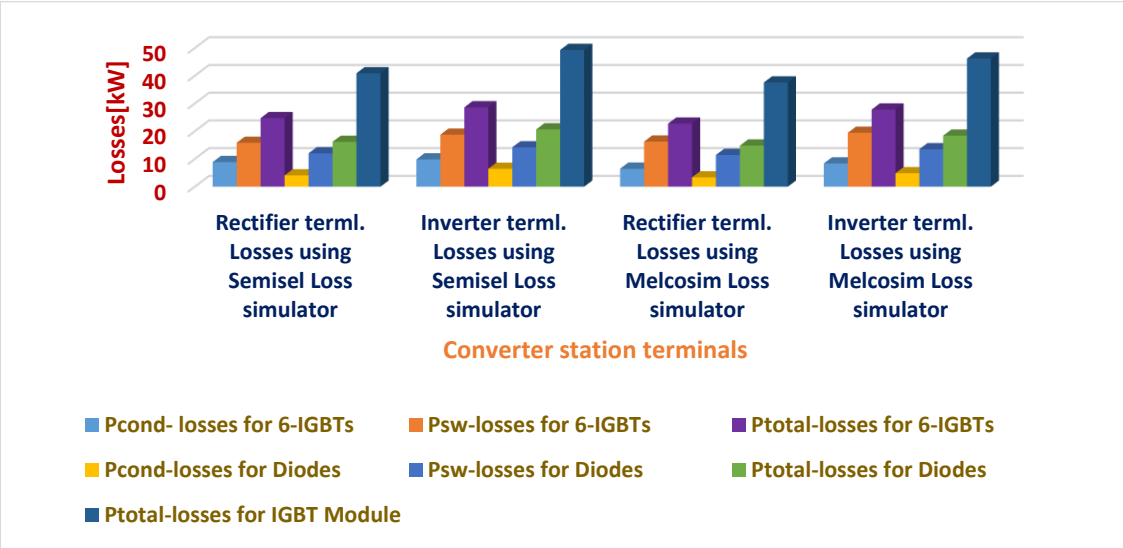

Figure 6-27: Power losses calculations of two-level VSC-based configuration using other loss simulators

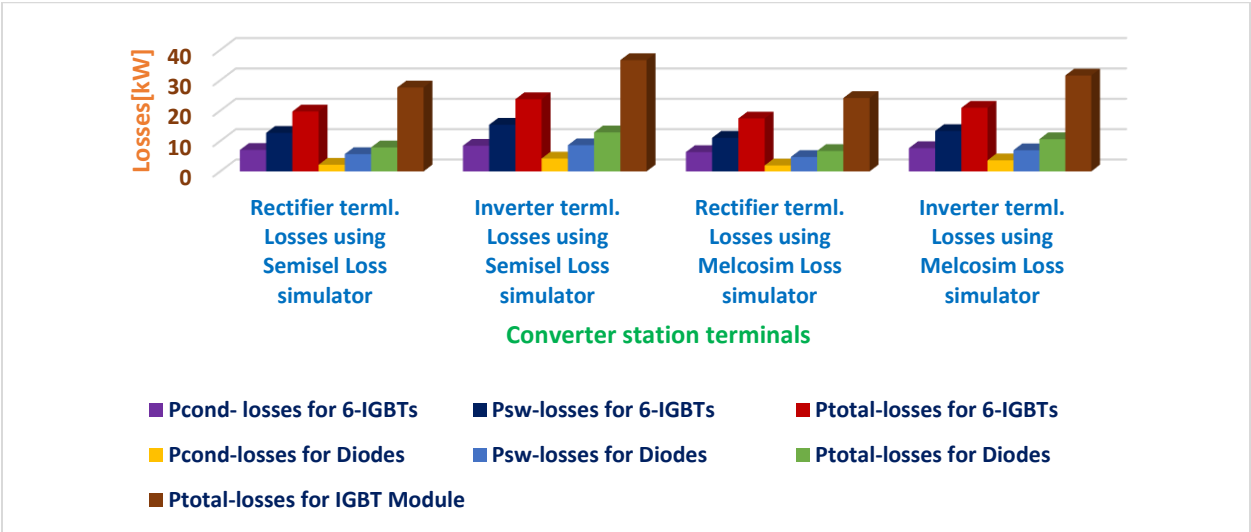

Figure 6-28: Power losses calculations of three-level VSC-based configuration using other loss simulators

Figure 6-27 and 6-28 describe the losses calculation on online commercial platform known as Semisel program powered by Semikron and Melcosim, which is a power loss simulator software developed by Mitsubishi corporation mainly for proper selection of IGBT module within its maximum junction temperature limit. The results obtained using Matlab-Simulink block model were also compared to validate the accuracy of the results obtained on Matlab-Simulink Algorithm. Table 6-4, Fig.6-27, and Fig. 6-28 show the required parameters for the simulation and the results obtained after the simulation respectively.

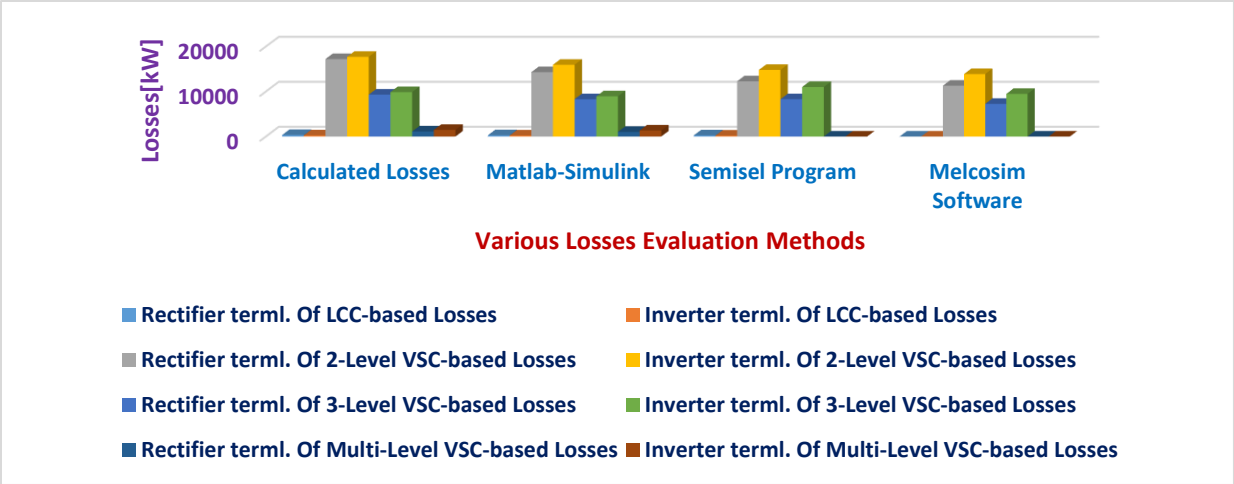

Figure 6-29: Losses Comparisons of HVDC technologies using various Losses calculations simulation platforms

Figure 6-29 shows the losses comparisons of the calculated, Matlab-Simulink, Semisel and Melcosim values obtained during their analyses and simulation respectively. From Fig. 6-28, it is obvious that the results obtained as a result of using standard IEC 61803, IEC 62751-1-2 and datasheet are quite reasonably higher than the other platforms. It can be seen that the difference between various methods applied was small. The power losses results depict that the calculated losses values differ on a maximum of 9.04% in comparison with the Matlab-Simulink platform, 20.9% in comparison with the Semisel application and 34.5% in comparison with the Melcosim program. Matlab-Simulink Algorithm has an important feature, which is its flexibility. Reason being that the power device parameters, operating condition, modulation strategy and configurations are very easy to be modified.

6.3 Conclusion

In conclusion, various mathematical schemes have been investigated in this research, majorly for loss estimation of various HVDC technologies utilizing both commercial online losses simulation tools such as Semisel, also the losses simulation software were simultaneously used to validate the accuracy of the other programs, software like Matlab-Simulink and Melcosim. These schemes are simple to implement and subsequently does not slow down numerical simulation time. The discrepancies between the various schemes adopted in this research works during the estimation of the losses of different HVDC technologies are not too large as described above using the percentage difference between the calculated loss values and the other schemes respectively. Finally, from the results obtained, it is obvious that the accuracy of the resulting total losses is principally not influenced by the various loss calculation scheme. It mainly depends upon the datasheets or experimental measurements.

CHAPTER 7
CONCLUSIONS AND RECOMMENDATIONS

7.1 Conclusions

The aim of this research is to investigate the analytical and simulation calculation methods of power losses of HVDC converter stations in accordance with the stipulated Standards IEC 61803, IEEE Std 1158 and IEC 62751-1-2, Determination of power losses in high –voltage direct current (HVDC) converter stations alongside with the datasheet parameters of the electronic devices. In this research-work, the following transmission technologies were investigated, VSC-based (2-level, 3-level and modular multilevel converter) and LCC-based HVDC converter technologies. This research makes it possible to predict the loss figure or profile of various HVDC technologies most exactly, likewise to clearly show the dependency of the losses on circuit parameters and operating point and besides to have a good basis for the comparison of both converter systems. The main objective was to investigate, determine, identify and evaluate the loss contributions of each components of various HVDC converter stations such as LCC-based HVDC and VSC-based (Two-level, three-level and Multi-level configurations) HVDC technologies using analytical approach and subsequently validate the results obtained by simulation approach in order to prove the viability of the HVDC loss study .

Therefore, the loss figures of individual equipment of LCC-based HVDC converter stations that contribute large amount of losses were investigated and analyzed based on the mathematical expressions stipulated in the Standards IEC 61803 coupled with the datasheet parameters. Afterwards, the results obtained due to the aforementioned approaches were illustrated in tables and charts (figures). The calculation procedures for calculating the eight loss mechanisms of thyristor valves, the load and no-load losses of converter transformer, the losses of smoothing reactor, and the losses due to the AC filters installed at the converter terminal were presented. The essence of installing the AC filters was to reduce the ill-effect harmonic contents or better still to compensate for the reactive power being consumed by the converters. The loss proportions of each equipment in converter stations under the operartional mode condition of bipolar rated transmission power were also analyzed. From the results of the loss evaluations of LCC-based HVDC technology, the converter transformers have the highest loss contribution, followed by thyristor valves, DC smoothing reactors, then finally, AC filters. The results were in conformity with the typical breakdown of the percentage total losses of LCC-based HVDC Converter Station illustrated in standards IEEE 1158 and IEC 61803.

More so, the determination and analyses of power losses of VSC-based converter stations were investigated. Three different topologies were considered which are two-level, three-level and modular multilevel converter configurations, under each topologies, the conduction and switching losses of both the IGBTs and the freewheeling diodes were analytically assessed. The total power losses contributions of each VSC-based technologies were obtained by summing the loss profiles due to conduction and switching action of the IGBTs modules. The results obtained due to the loss estimations were illustrated in form of tables and charts to show the loss contributions of each equipment on

VSC-based HVDC converter stations pictorially. The total losses and the percentage loss proportions of converter station equipment were also analyzed for further illustrations. The comparisons of different HVDC technologies based on their loss figures at the converter station terminals were illustrated. The loss mechanisms of various VSC-based topologies such as the two, three level and modular multilevel converter configurations were calculated using the mathematical expressions obtained in various literatures that were reviewed, IEC 62751-1-2 and coupled with the datasheet parameters. From the results obtained it could be deduced that the two-level VSC-based HVDC technology has the highest percentage converter losses, followed by the three-level VSC-based HVDC technology. It can be seen that the loss contribution of modular multilevel converters is lower than the two level and three level VSC HVDC technologies and this is due to its characteristics of low switching frequency.

Furthermore, the Matlab-Simulink modeling of HVDC technologies using the mathematical expressions used during the analytical approach were also investigated to provide an independent crosscheck on the results obtained using idealized mathematical representations (analytical technique). These loss expressions were modeled in a blocks and afterwards were implemented on Matlab-Simulink environment. The circuit simulations of various HVDC technologies in line with the loss evaluation of these technologies i.e. LCC-based, two-level, three-level and Multi-level configurations, were comprehensively illustrated. Subsequent to the simulation of the modeled HVDC technologies, the simulation results obtained due to various simulation scheme or platform were illustrated using tables and chart (figures). Hence, in order to validate the loss results obtained from Matlab-Simulink environment, some other loss simulation software were used such as Melcosim and a commercial power loss simulation tools known as Semisel, all these efforts are to validate and compare the results.

In general, it is worth noting that, these loss percentages should be taken as approximate, reason being that, these numbers were obtained for components in different systems. Invariably, the actual circuit losses obviously depend on its operating point and the transmission system. Note that, the converter transformer used in HVDC systems experiences the normal operating loss due to the sinusoidal current flow and also has additional losses due to the flow of harmonic current through the device. The transformer losses were found to be about 41.6% at the rectifier and 37.26% at the inverter terminals. Furthermore, the losses contributions by the thyristor valves were found to be 40.2% at the rectifier and 44.4% at the inverter terminal, alternatively, the losses in the snubber circuits and the thyristor valves are preferably measured by simply determining the amount of heat that is dissipated or removed by the cooling system. The losses due to the snubber circuits are infinitesimally small compared to other converter stations equipment, therefore these losses were neglected throughout the converter station's loss evaluations.

7.2 Recommendations for Future Research

Measurement of HVDC converters losses is one of the most important figures of merit for a converter valve. The present situation of loss evaluation is that such losses are often calculated and not measured. For investors, that decides on transmission system alternatives, accurate knowledge of the expected losses form an essential part of project evaluation. In respect of this, proper measurement of losses in HVDC system is important. The power losses of various

HVDC technologies can be directly evaluated in economic terms (minimizing losses will also reduce emission of greenhouse gases). Therefore, it is expedient to introduce alternative methods for establishing loss evaluation factors of HVDC technologies, which is evaluating the economic costs of losses in HVDC converter stations. Therefore, the author recommends the application of HVDC converter and its impact on the different types of losses, the technical and economic analyses of HVDC technologies to be studied and to investigate the economic feasibility and viability of HVDC system on loss minimization and also investigate its benefits from financial point of view for further research.

Furthermore, the next step of this study would be the expansion of the model used in this research work to compute the HVDC converter station losses. It would be very interesting to model a more realistic HVDC system and analyze the losses of each equipment on the converter stations. More so, all the simulations in this study were done for rated voltage and power of the converters, but it is of importance that the operation at different power and voltage level to be investigated due to its effect on converter's efficiency. Generally, the cost in terms of investment and operation is an interesting factor, which is to be considered in future study, and it is the most important from the companies' point of view. Finally, the application

REFERENCES

[1] H. Pang, G. Tang, and Z. He, "Evaluation of losses in VSC-HVDC transmission system," in Power and Energy Society General Meeting-Conversion and Delivery of Electrical Energy in the 21st Century, 2008 IEEE, pp. 1-6, 2008.

[2] H. Lips, "Loss determination of HVDC thyristor valves," IEEE transactions on power delivery, vol. 3, pp. 358-362, 1988.

[3] M. Cepek, J. Douville, G. Fecteau, and R. Malewski, "Loss measurement in high voltage thyristor valves," IEEE transactions on power delivery, vol. 9, pp. 1222-1236, 1994.

[4] S. C. o. t. I. P. E. Society, "IEEE Recommendation Practice for Determination of Power Losses in High-Voltage Direct-Current (HVDC) Converter Stations.," IEEE Xplore, pp. 1- 53, 26-Sept-1991 1991.

[5] M. Ebeed, "Power Losses in voltage sourced converter (VSC) valves for high-voltage direct current (HVDC) systems- Modular Multilevel Converters," International Electrotechnical Commission, Geneva, Switzerland, pp. 1-19, 08-2014 2014-08, IEEE.

[6] Z.-y. LI, Z. REN, and Y.-j. CHEN, "Loss study of HVDC system [J]," Electric Power Automation Equipment, vol. 1, p. 002, 2007, IEEE.

[7] N. B. Negra, J. Todorovic, and T. Ackermann, "Loss evaluation of HVAC and HVDC transmission solutions for large offshore wind farms," Electric power systems research, vol. 76, pp. 916-927, 2006.

[8] M.-K. Kim, D.-G. Woo, B.-K. Lee, N.-J. Kim, and J.-S. Kim, "Loss analysis of power conversion equipment for efficiency improvement," The Transactions of the Korean Institute of Power Electronics, vol. 19, pp. 80-90, 2014, IEEE.

[9] "A General Scheme for Calculating Switching- and Conduction-Losses of Power Semiconductors in Numerical Circuit Simulations of Power Electronic Systems.pdf" pp 1-25,2015, IEEE.

[10] IEEE, "IEEE RECOMMENDED PRACTICE FOR DETERMINATION OF POWER LOSSES IN HIGH-VOLTAGE DIRECT-CURRENT(HVDC) CONVERTER STATIONS.," IEE Proceedings-Electric Power Applications, p. 53, 1991.

[11] N. Flourentzou, V. G. Agelidis, and G. D. Demetriades, "VSC-based HVDC power transmission systems: An overview," IEEE Transactions on power electronics, vol. 24, pp. 592-602, 2009.

[12] M. Ikonen, O. Laakkonen, and M. Kettunen, "Two-level and three-level converter comparison in wind power application," ed, 2005, IEEE.

[13] G. Kalcon, G. P. Adam, O. Anaya-Lara, G. Burt, and K. Lo, "Analytical efficiency evaluation of two and three level VSC-HVDC transmission links," International Journal of Electrical Power & Energy Systems, vol. 44, pp. 1-6, 2013.

[14] P. S. Jones and C. C. Davidson, "Calculation of power losses for MMC-based VSC HVDC stations," in Power Electronics and Applications (EPE), 2013 15th European Conference, pp. 1-10, 2013.

[15] L. Yang, C. Zhao, and X. Yang, "Loss calculation method of modular multilevel HVDC converters," in Electrical Power and Energy Conference (EPEC), 2011 IEEE, pp. 97-101, 2011.

[16] D. D. A.-T. datasheet, "[Online]. Available: http://www.dynexsemi.com," Datasheet, p. 8, December, 2014.

[17] B. Andersen, L. Xu, P. Horton, and P. Cartwright, "Topologies for VSC transmission," Power Engineering Journal, vol. 16, pp. 142-150, 2002.

[18] F. Casanellas, "Losses in PWM inverters using IGBTs," IEE Proceedings-Electric Power Applications, vol. 141, pp. 235-239, 1994.

[19] M. H. Bierhoff and F. W. Fuchs, "Semiconductor losses in voltage source and current source IGBT converters based on analytical derivation," in Power Electronics Specialists Conference, 2004. PESC 04. 2004 IEEE 35th Annual, pp. 2836-2842, 2004.

[20] M. P. Bahrman and B. K. Johnson, "The ABCs of HVDC transmission technologies," IEEE power and energy magazine, vol. 5, pp. 32-44, 2007.

[21] D. H. C. Mr. Ankit Patel, Mr. Vinod Patel, Mr. Kaushal Patel, "Prediction of IGBT Power Losses and Junction Temperature in I60kW VVVF Inverter Drive " Journal of Electrical Engineering, pp. 1-7, 2015.

[22] K. Padiyar, HVDC power transmission systems: technology and system interactions: New Age International, 1990.

[23] M. Jodeyri, J. Cao, C. Zhou, and G. Tang, "Thyristor valve for the 12-pulse converter for the 3 Gorges-Shanghai II HVDC transmission scheme," in Power System Technology (POWERCON), 2010 International Conference, pp. 1-7,2010.

[24] A. M. Trzynadlowski and S. Legowski, "Minimum-loss vector PWM strategy for three-phase inverters," IEEE Transactions on Power Electronics, vol. 9, pp. 26-34, 1994.

[25] J. Bergauer, L. Schindele, and M. Braun, "Optimised space vector control reducing switching losses in current source inverters," in Proc. on Int. Conf. and Exhibit. on Power Electr. and Motion Contr., EPE-PEMC, Kosice, 2000.

[26] K. Zhou and D. Wang, "Relationship between space-vector modulation and three-phase carrier-based PWM: a comprehensive analysis [three-phase inverters]," IEEE transactions on industrial electronics, vol. 49, pp. 186-196, 2002.

[27] T. Halkosaari and H. Tuusa, "Optimal vector modulation of a PWM current source converter according to minimal switching losses," in Power Electronics Specialists Conference, 2000. PESC 00. 2000 IEEE 31st Annual, pp. 127-132, 2000.

[28] L. Mestha and P. Evans, "Analysis of on-state losses in PWM inverters," in IEE Proceedings B (Electric Power Applications), pp. 189-195, 1989.

[29] D.-W. Chung and S.-K. Sul, "Minimum-loss PWM strategy for 3-phase PWM rectifier," in Power Electronics Specialists Conference, 1997. PESC'97 Record., 28th Annual IEEE, pp. 1020-1026, 1997.

[30] F. Edwards, A. Husbands, and F. Perry, "The development and design of high-voltage impulse generators," Proceedings of the IEE-Part I: General, vol. 98, pp. 155-168, 1951.

[31] M. H. Okba, M. H. Saied, M. Mostafa, and T. Abdel-Moneim, "High voltage direct current transmission-A review, part I," in Energytech, 2012 IEEE, pp. 1-7, 2012.

[32] J. Kuffel and P. Kuffel, High voltage engineering fundamentals: Newnes, 2000, IEEE.

[33] N. Parus, "An investigation into the effects of floating objects on the electrical breakdown of air insulation under steady state high voltage direct current conditions," 2015, IEEE.

[34] X. Chen and P. Wang, "RESEARCH ON THE ASSESSMENT METHOD OF RESIDENTIAL DISTRICT LINE LOSS RATE BASED ON STATISTICAL REGULATION OF MARKETING DATA," in Energy and Mechanical Engineering: Proceedings of 2015 International Conference on Energy and Mechanical Engineering, pp. 122-130, 2016.

[35] G. Daelemans, K. Srivastava, M. Reza, S. Cole, and R. Belmans, "Minimization of steady-state losses in meshed networks using VSC HVDC," in Power & Energy Society General Meeting, 2009. PES'09. IEE, pp. 1-5, 2009.

[36] M. Arunachalam, R. Babu, B. Bose, and D. Dutta, "Evaluation of losses in thyristor valve for SVC application," in Power Electronics, Drives and Energy Systems for Industrial Growth, 1996., Proceedings of the 1996 International Conference, pp. 399-402, 1996.

[37] H. P. Lips, "Loss determination of HVDC thyristor valves," IEEE transactions on power delivery, vol. 3, pp. 358-362, 1988.

[38] T. Machida, H. Kaminosono, T. Umezu, M. Sugimoto, and K. Yokoyama, "Control and Protective System of HVDC Transmission by HVDC Simulator (Thyristor Converter)," IEEE Transactions on Power Apparatus and Systems, pp. 2778-2785, 1971.

[39] Y. Beausejour and G. Karady, "Valve damping circuit design for HVDC systems," IEEE Transactions on Power Apparatus and Systems, pp. 1615-1621, 1973.

[40] A. G. Peter and K. A. Saha, "Comparative study of harmonics reduction and power factor enhancement of six and 12-pulses HVDC system using passive and shunt APFs harmonic filters," in 2018 International Conference on the Domestic Use of Energy (DUE, pp. 1-10, 2018.

[41] P. Manohar, V. Kelamane, D. Kaushik, and W. Ahmed, "Improved controls for LCC-VSC hybrid HVDC system," in Circuits, Controls and Communications (CCUBE), 2013 International conference, pp. 1-5, 2013.

[42] Sanjib Kumar Nandi, Ridown Rashid Riadh, Siddikur Rahman. "Investigation of THD on a 12-pulse HVDC transmission network and mitigation of harmonic currents using passive filters", 2015 2nd International Conference on Electrical Information and Communication Technologies (EICT), 2015.

[43] A. G. Peter and K. A. Saha, "Power losses assessments of LCC-based HVDC converter stations using datasheet parameters and IEC 61803 STD," in 2018 International Conference on the Domestic Use of Energy (DUE), pp. 1-10, 2018.

[44] B. S. Ram, Forest, J.A.C "Study of HVDC converter transformer temperature and hot spots due to effects of harmonic currents.," Canadian Electrical Association, CEA Report 211 T 423,, p. September 1985, 1985.

[45] U. Drofenik and J. W. Kolar, "A general scheme for calculating switching-and conduction-losses of power semiconductors in numerical circuit simulations of power electronic systems," in Proceedings of the 2005 International Power Electronics Conference (IPEC'05), pp.4-8, Niigata, Japan, April, 2005.

[46] M. Hwang, W. Grady, and H. Sanders, "Assessment of winding losses in transformers due to harmonic currents," in International Conference on Harmonics in Power Systems, pp. 81-88, 1984.

[47] T. C. I. J. Alan C. Forest, "Harmonic Load Losses in HVDC Converter Transformers.," IEEE Transactions on Power Delivery, vol. 6, p. 5, 1991.

[48] J. A. C. Forrest, "Harmonic load losses in HVDC converter transformers," IEEE Transactions on Power Delivery, vol. 6, pp. 153-157, 1991.

[49] A. B. Nassif and W. Xu, "Passive harmonic filters for medium-voltage industrial systems: Practical considerations and topology analysis," in Power Symposium, 2007. NAPS'07. 39th North American, pp. 301-307, 2007.

[50] A. P. S. HVDC, "Reactive Power Compensation and Harmonic Filters for HVDC Classic," Books, January 2015.

[51] X.-P. Zhang, "Multiterminal voltage-sourced converter-based HVDC models for power flow analysis," IEEE Transactions on Power Systems, vol. 19, pp. 1877-1884, 2004.

[52] S. Shah, R. Hassan, and J. Sun, "HVDC transmission system architectures and control-A review," in Control and Modeling for Power Electronics (COMPEL), 2013 IEEE 14th Workshop, pp. 1-8, 2013.

[53] R. Marquardt, "Modular Multilevel Converter: An universal concept for HVDC-Networks and extended DC-Bus-applications," in Power Electronics Conference (IPEC), 2010 International, pp. 502-507, 2010.

[54] M. A. AboElHassan, S. Kamel, and M. Ebeed, "Simple modeling of HVDC systems into Newton-Raphson load flow algorithm," in Power Systems Conference (MEPCON), 2016 Eighteenth International Middle East, pp. 832-836, 2016.

[55] Y. Jiang-Hafner, H. Duchen, M. Karlsson, L. Ronstrom, and B. Abrahamsson, "HVDC with voltage source converters-a powerful standby black start facility," in Transmission and Distribution Conference and Exposition, 2008. T&D. IEEE/PES, pp. 1-9, 2008.

[56] A. Ekstrom and L. Eklund, "HVDC thyristor valve development," IEEE transactions on power electronics, pp. 177-185, 1987.

[57] L. Ängquist, A. Antonopoulos, D. Siemaszko, K. Ilves, M. Vasiladiotis, and H.-P. Nee, "Inner control of modular multilevel converters-an approach using open-loop estimation of stored energy," in Power Electronics Conference (IPEC), 2010 International, pp. 1579-1585, 2010.

[58] G. Asplund, K. Eriksson, and K. Svensson, "DC transmission based on voltage source converters," in CIGRE SC14 Colloquium, South Africa, pp. 1-7, 1997.

[59] K. Hosseini and J. Mahler, "Semiconductor device comprising a semiconductor chip stack and method for producing the same," ed: Google Patents, 2011.

[60] S. Meier, S. Norrga, and H.-P. Nee, "New voltage source converter topology for HVDC grid connection of offshore wind farms," 2004.

[61] Z. Mingyuan, S. Jianqing, L. Weichao, G. Shiguang, and T. Zhengjun, "Calculation Method of a Fast Power Loss for IGBT Modules [J]," Marine Electric & Electronic Engineering, vol. 1, p. 012, 2009.

[62] F. Blaabjerg, U. Jaeger, and S. Munk-Nielsen, "Power losses in PWM-VSI inverter using NPT or PT IGBT devices," IEEE Transactions on power electronics, vol. 10, pp. 358-367, 1995.

[63] T.-J. Kim, D.-W. Kang, Y.-H. Lee, and D.-S. Hyun, "The analysis of conduction and switching losses in multi-level inverter system," in Power Electronics Specialists Conference, 2001. PESC. 2001 IEEE 32nd Annual, pp. 1363-1368, 2001.

[64] A. Yazdani and R. Iravani, Voltage-sourced converters in power systems: modeling, control, and applications: John Wiley & Sons, 2010.

[65] Y. Zhang, G. P. Adam, T. Lim, S. J. Finney, and B. Williams, "Voltage source converter in high voltage applications: Multilevel versus two-level converters," 2010.

[66] K. A. Tehrani, I. Rasoanarivo, and F.-M. Sargos, "Power loss calculation in two different multilevel inverter models (2DM 2)," Electric Power Systems Research, vol. 81, pp. 297-307, 2011.

[67] D. C. Noman Rao, "Calculating Power Losses in an IGBT Module using Dynex power control datasheet," Application Note, pp. 1-16, 2014.

[68] A. Hassanpoor, S. Norrga, and A. Nami, "Loss evaluation for modular multilevel converters with different switching strategies," in Power Electronics and ECCE Asia (ICPE-ECCE Asia), 2015 9th International Conference, pp. 1558-1563, 2015.

[69] S. Rohner, S. Bernet, M. Hiller, and R. Sommer, "Modulation, losses, and semiconductor requirements of modular multilevel converters," IEEE transactions on Industrial Electronics, vol. 57, pp. 2633-2642, 2010.

[70] D. Peftitsis, G. Tolstoy, A. Antonopoulos, J. Rabkowski, J.-K. Lim, M. Bakowski, et al., "High-power modular multilevel converters with SiC JFETs," IEEE Transactions on Power Electronics, vol. 27, pp. 28-36, 2012.

[71] M. Saeedifard and R. Iravani, "Dynamic performance of a modular multilevel back-to-back HVDC system," IEEE Transactions on power delivery, vol. 25, pp. 2903-2912, 2010.

[72] Q. Li, Z. He, and G. Tang, "Investigation of the harmonic optimization approaches in the new modular multilevel converters," in Power and Energy Engineering Conference (APPEEC), 2010 Asia-Pacific, pp. 1-6, 2010.

[73] C. Oates and C. Davidson, "A comparison of two methods of estimating losses in the modular multi-level converter," in Power Electronics and Applications (EPE 2011), Proceedings of the 2011-14th European Conference, pp. 1-10, 2011.

[74] L. Angquist, A. Antonopoulos, D. Siemaszko, K. Ilves, M. Vasiladiotis, and H.-P. Nee, "Open-loop control of modular multilevel converters using estimation of stored energy," IEEE transactions on industry applications, vol. 47, pp. 2516-2524, 2011.

[75] A. Hassanpoor, S. Norrga, H.-P. Nee, and L. Ängquist, "Evaluation of different carrier-based PWM methods for modular multilevel converters for HVDC application," in IECON 2012-38th Annual Conference on IEEE Industrial Electronics Society, pp. 388-393, 2012.

[76] A. Nami, J. Liang, F. Dijkhuizen, and G. D. Demetriades, "Modular multilevel converters for HVDC applications: Review on converter cells and functionalities," IEEE Transactions on Power Electronics, vol. 30, pp. 18-36, 2015.

[77] K. Ilves, A. Antonopoulos, S. Norrga, and H.-P. Nee, "A new modulation method for the modular multilevel converter allowing fundamental switching frequency," IEEE Transactions on power electronics, vol. 27, pp. 3482-3494, 2012.

[78] J. L. Afonso, M. Aredes, E. Watanabe, and J. S. Martins, "Shunt active filter for power quality improvement," 2001.

[79] J. L. Afonso, C. Couto, and J. S. Martins, "Active filters with control based on the pq theory," 2000.

[80] A. Lesnicar and R. Marquardt, "An innovative modular multilevel converter topology suitable for a wide power range," in Power Tech Conference Proceedings, 2003 IEEE Bologna, p. 6 pp. Vol. 3, 2003.

[81] A. Hassanpoor, L. Ängquist, S. Norrga, K. Ilves, and H.-P. Nee, "Tolerance band modulation methods for modular multilevel converters," IEEE Transactions on Power Electronics, vol. 30, pp. 311-326, 2015.

[82] M. Hagiwara and H. Akagi, "Control and experiment of pulsewidth-modulated modular multilevel converters," IEEE Transactions on Power Electronics, vol. 24, pp. 1737-1746, 2009.

[83] T. W. May, Y. M. Yeap, and A. Ukil, "Comparative evaluation of power loss in HVAC and HVDC transmission systems," in Region 10 Conference (TENCON), 2016 IEEE, pp. 637-641, 2016.

[84] C.-K. Kim, V. K. Sood, G.-S. Jang, S.-J. Lim, and S.-J. Lee, HVDC transmission: power conversion applications in power systems: John Wiley & Sons, 2009.

[85] G. Li, C. Li, and D. Van Hertem, "HVDC technology overview," HVDC Grids: For Offshore and Supergrid of the Future, vol. 45, 2016.

[86] C. Du, "The control of VSC-HVDC and its use for large industrial power systems," 2003.

[87] S.-G. Lee, D.-W. Kang, Y.-H. Lee, and D.-S. Hyun, "The carrier-based PWM method for voltage balance of flying capacitor multilevel inverter," in Power Electronics Specialists Conference, 2001. PESC. 2001 IEEE 32nd Annual, pp. 126-131, 2001.

[88] M. P. Dr. Dusan Graovac, "IGBT Power Losses Calculation Using the Data-Sheet Parameters " Application Note, vol. 1.1, pp. 1-7, 1-January-2009 2009.

[89] M. Rahimo, U. Schlapbach, A. Kopta, R. Schnell, and S. Linder, "SPT+, the next generation of low-loss HV-IGBTs," in Proceedings PCIM, 2005.

[90] R. Chokhawala, B. Danielsson, and L. Angquist, "Power semiconductors in transmission and distribution applications," in Power Semiconductor Devices and ICs, 2001. ISPSD'01. Proceedings of the 13th International Symposium, pp. 3-10, 2001.

[91] K. Bergman, "Silicon carbide-the power semiconductor material of the future," in Fuel and Energy Abstracts, pp. 274, 1996.

[92] S. Singaravelu and S. Seenivasan, "Modelling and Simulation of Monopolar HVDC Transmission System Feeding a Strong AC Network with Firefly Algorithm based Optimal PI controller," International Journal of Computer Applications, vol. 102, 2014.

[93] K. Singh, H. S. Saini, H. S. Sandhu, and A. Faridkot, "METHODOLOGY OF HVDC TRANSMISSION SYSTEM."pp.1-12, vol.3, 2015, IEEE.

[94] R. Rudervall, J. Charpentier, and R. Sharma, "High voltage direct current (HVDC) transmission systems technology review paper," Energy week, vol. 2000, p. 2, 2000, IEEE.

[95] J. Bernardes and S. Swindler, "Modeling and analysis of thyristor and diode reverse recovery in railgun pulsed power circuits," in Pulsed Power Conference, 2005 IEEE, pp. 79-82, 2005.

[96] M. Daryabak, S. Filizadeh, J. Jatskevich, A. Davoudi, M. Saeedifard, V. Sood, et al., "Modeling of LCC-HVDC systems using dynamic phasors," IEEE Transactions on Power Delivery, vol. 29, pp. 1989-1998, 2014.

[97] L. D. Lidong Zhang, "A Novel Method to Mitigate Commutation Failures in HVDC Systems," Proceedings PowerCon 2002. International Conference, vol. 1, pp. 51-56, 13-17 Oct. 2002, IEEE.

[98] J. Arrillaga, High voltage direct current transmission: Iet, 1998.

[99] H. Huang and V. Ramaswami, "Design of UHVDC converter station," in Transmission and Distribution Conference and Exhibition: Asia and Pacific, 2005 IEEE/PES, 2005, pp. 1-6.

[100] D. p. control, "Dynex DIM1200ASM45-TS000 data-sheet Manual," Data-sheet Manual, pp. 1-8, 4-December-2014

.

APPENDICES

Appendix A

Datasheet Manual for Thyristor DCR3030V42

AN 5950

Understanding i^2 Phase Control Thyristor Datasheets

Application Note

AN5950-1 Sept 2009 LN26885

Authors: Dinesh Chamund, Colin Rout

PART NUMBER

DCR3030V42

The part numbering scheme for the Dynex i^2 Phase Control Thyristor is as follows:

DCR = Dynex Control Rectifier

3030 = Headline average current rating (A)

V = Package code

42 = Maximum repetitive voltage rating (V)/100

CURRENT RATINGS

T_{case} = 60°C unless stated otherwise

Symbol	Parameter	Test Conditions	Max.	Units
Double Side Cooled				
$I_{T(AV)}$	Mean on-state current	Half wave resistive load	3030	A
$I_{T(RMS)}$	RMS value	-	4760	A
I_T	Continuous (direct) on-state current	-	4550	A

SURGE RATINGS

Symbol	Parameter	Test Conditions	Max.	Units
I_{TSM}	Surge (non-repetitive) on-state current	10ms half sine, T_{case} = 125°C	40.6	kA
I^2t	I^2t for fusing	V_R = 0	8.24	MA^2s

THERMAL AND MECHANICAL RATINGS

Symbol	Parameter	Test Conditions		Min.	Max.	Units
$R_{th(j-c)}$	Thermal resistance – junction to case	Double side cooled	DC	-	0.00746	°C/W
		Single side cooled	Anode DC	-	0.0130	°C/W
			Cathode DC	-	0.0178	°C/W
$R_{th(c-h)}$	Thermal resistance – case to heatsink	Clamping force 54kN	Double side	-	0.002	°C/W
		(with mounting compound)	Single side	-	0.004	°C/W
T_{vj}	Virtual junction temperature	(blocking)		-	125	°C
T_{stg}	Storage temperature range			-55	125	°C
F_m	Clamping force			48.0	59.0	kN

DYNAMIC CHARACTERISTICS

Symbol	Parameter	Test Conditions		Min.	Max.	Units
I_{RRM}/I_{DRM}	Peak reverse and off-state current	At V_{RRM}/V_{DRM}, T_{case} = 125°C		-	200	mA
dV/dt	Max. linear rate of rise of off-state voltage	To 67% V_{DRM}, T_j = 125°C, gate open		-	1500	V/µs
dI/dt	Rate of rise of on-state current	From 67% V_{DRM} to 2x $I_{T(AV)}$	Repetitive 50Hz	-	200	A/µs
		Gate source 30V, 10Ω, t_r < 0.5µs, T_j = 125°C	Non-repetitive	-	400	A/µs
$V_{T(TO)}$	Threshold voltage – Low level	200A to 1700A at T_{case} = 125°C		-	0.82	V
	Threshold voltage – High level	1700A to 7000A at T_{case} = 125°C		-	0.98	V
r_T	On-state slope resistance – Low level	200A to 1700A at T_{case} = 125°C		-	0.292	mΩ
	On-state slope resistance – High level	1700A to 7000A at T_{case} = 125°C		-	0.198	mΩ
t_{gd}	Delay time	V_D = 67% V_{DRM}, gate source 30V, 10Ω t_r = 0.5µs, T_j = 25°C		TBD	TBD	µs
t_q	Turn-off time	T_j = 125°C, V_R = 200V, dI/dt = 1A/µs, dV_{DR}/dt = 20V/µs linear		250	500	µs
Q_S	Stored charge	T_j = 125°C, dI/dt – 1A/µs, $V_{R\,pk}$ =3000V, V_{RM}= 1700V		1600	3500	µC
I_L	Latching current	T_j = 25°C, V_D = 5V		-	3	A
I_H	Holding current	T_j = 25°C, R_{G-K} = ∞, I_{TM} = 500A, I_T = 5A		-	300	mA

Datasheet Manual for IGBT Module DIM1200ASM45-TS000

DYNEX

DYNEX DMOS+

DIM1200ASM45-TS000

Single Switch IGBT Module

Replaces DS6102-3

DS6102-4 December 2014 (LN32160)

ABSOLUTE MAXIMUM RATINGS

Stresses above those listed under 'Absolute Maximum Ratings' may cause permanent damage to the device. In extreme conditions, as with all semiconductors, this may include potentially hazardous rupture of the package. Appropriate safety precautions should always be followed. Exposure to Absolute Maximum Ratings may affect device reliability.

T_{case} = 25°C unless stated otherwise

Symbol	Parameter	Test Conditions	Max.	Units
V_{CES}	Collector-emitter voltage	V_{GE} = 0V	4500	V
V_{GES}	Gate-emitter voltage		±20	V
I_C	Continuous collector current	T_{case} = 90°C	1200	A
$I_{C(PK)}$	Peak collector current	1ms, T_{case} = 120°C	2400	A
P_{max}	Max. transistor power dissipation	T_{case} = 25°C, T_j = 125°C	12.5	kW
I^2t	Diode I^2t value	V_R = 0, t_p = 10ms, T_j = 125ºC	460	kA^2s
V_{isol}	Isolation voltage – per module	Commoned terminals to base plate. AC RMS, 1 min, 50Hz	7.4	KV
Q_{PD}	Partial discharge – per module	IEC1287, V_1 = 4800V, V_2 = 3500V, 50Hz RMS	10	pC

ELECTRICAL CHARACTERISTICS

T_{case} = 25°C unless stated otherwise.

Symbol	Parameter	Test Conditions	Min	Typ	Max	Units
I_{CES}	Collector cut-off current	V_{GE} = 0V, V_{CE} = V_{CES}			4	mA
		V_{GE} = 0V, V_{CE} = V_{CES}, T_{case} = 125°C			90	mA
I_{GES}	Gate leakage current	V_{GE} = ± 20V, V_{CE} = 0V			1	µA
$V_{GE(TH)}$	Gate threshold voltage	I_C = 120mA, V_{GE} = V_{CE}		5.8		V
$V_{CE(sat)}$	Collector-emitter saturation voltage	V_{GE} = 15V, I_C = 1200A		2.7		V
		V_{GE} = 15V, I_C = 1200A, T_j = 125°C		3.5		V
I_F	Diode forward current	DC		1200		A
I_{FM}	Diode maximum forward current	t_p = 1ms		2400		A
V_F	Diode forward voltage	I_F = 1200A		2.8		V
		I_F = 1200A, T_j = 125°C		3.2		V
C_{ies}	Input capacitance	V_{CE} = 25V, V_{GE} = 0V, f = 1MHz		150		nF
Q_g	Gate charge	±15V Including external C_{ge}		17		µC
C_{res}	Reverse transfer capacitance	V_{CE} = 25V, V_{GE} = 0V, f = 1MHz		12		nF
L_M	Module inductance			10		nH
R_{INT}	Internal transistor resistance			90		µΩ
SC_{Data}	Short circuit current, I_{SC}	T_j = 125°C, V_{CC} = 3400V $t_p \leq$ 10µs, $V_{GE} \leq$ 15V $V_{CE\ (max)} = V_{CES} - L^{*} \times dI/dt$ IEC 60747-9		4800		A

Note:
* L is the circuit inductance + L_M

ELECTRICAL CHARACTERISTICS

T_{case} = 25°C unless stated otherwise

Symbol	Parameter	Test Conditions	Min	Typ.	Max	Units
$t_{d(off)}$	Turn-off delay time	I_C = 1200A V_{GE} = ±15V V_{CE} = 2800V $R_{G(ON)}$ = 2.4Ω $R_{G(OFF)}$ = 2.7Ω C_{ge} = 220nF L_S ~ 165nH		3000		ns
t_f	Fall time			600		ns
E_{OFF}	Turn-off energy loss			4500		mJ
$t_{d(on)}$	Turn-on delay time			900		ns
t_r	Rise time			350		ns
E_{ON}	Turn-on energy loss			4800		mJ
Q_{rr}	Diode reverse recovery charge	I_F = 1200A V_{CE} = 2800V dI_F/dt = 3000A/µs		1340		µC
I_{rr}	Diode reverse recovery current			1030		A
E_{rec}	Diode reverse recovery energy			2220		mJ

T_{case} = 125°C unless stated otherwise

Symbol	Parameter	Test Conditions	Min	Typ.	Max	Units
$t_{d(off)}$	Turn-off delay time	I_C = 1200A V_{GE} = ±15V V_{CE} = 2800V $R_{G(ON)}$ = 2.4Ω $R_{G(OFF)}$ = 2.7Ω C_{ge} = 220nF L_S ~ 165nH		3100		ns
t_f	Fall time			560		ns
E_{OFF}	Turn-off energy loss			4650		mJ
$t_{d(on)}$	Turn-on delay time			900		ns
t_r	Rise time			360		ns
E_{ON}	Turn-on energy loss			6450		mJ
Q_{rr}	Diode reverse recovery charge	I_F = 1200A V_{CE} = 2800V dI_F/dt = 3000A/µs		2200		µC
I_{rr}	Diode reverse recovery current			1100		A
E_{rec}	Diode reverse recovery energy			3750		mJ

Table A-1: System Parameters of the HVDC Systems

Components	Actual value	
	Rectifier side	Inverter side
Transformer rating	500/440 kV, 1000 MVA	350/230 kV
Transformer resistance	2 Ω	2 Ω
Transformer reactance	55.5 mH	55.5 mH
Coupling reactor	41.8 mH	41.8 mH
VSC converter rating	1000 MVA	1000 MVA
DC cable resistance	0.05 Ω/km(500km long) =25 Ω	0.05 Ω/km (500km long) =25 Ω
V_{ce-dc}	2800 V	2000 V
DC link voltage	561.64 kV	561.51 kV
$N_{IGBT\ valve}$(number of IGBTs connected in series)	300	300
Number of valves at each station.	6	6

Table A-2: Datasheet parameters for Dynex IGBT module DIM1200ASM45-TS000 [67, 100]

Input				
V_{ce-dc}			2800 V	
I_{rms}	S	1000 MVA	Rectifier side = 1312.16 A	
	V_s	440 kV		
	$\frac{S}{\sqrt{3} \times V_s}$		Inverter side = 1649.57 A	
I_p	$\sqrt{2} \times I_{rms}$		Rectifier side=1855.7 A	Inverter side=2332.84 A
Switching frequency f_{sw}			1 KHz	
Converter Power factor $\cos\theta$			0.85	
Modulation index (m)			0.856	
Ambient Temp $°C$			60	
DATASHEET				
DIM1200ASM45-TS000				
Case temperature=T_{case} = 125$°C$ unless stated otherwise.				
IGBT			DIODE	
$E_{on}(J)$	6.45		$E_{rec}(J)$	3.75
$E_{off}(J)$	4.65		-	-
$I_{nom}(A)$	1200		$I_{nom}(A)$	1200
$V_{nom}(V)$	2800		$V_{nom}(V)$	2800
$V_{ceo}(V)$	1.44		$V_{do}(V)$	1.79
$R_o(\Omega)$	0.001677		$R_d(\Omega)$	0.001167
$R_{th(j-c)}(°C/W)$	0.008		$R_{th(j-c)}(°C/W)$	0.016
$R_{th(c-h)}(°C/W)$	0.006		$R_{th(c-h)}(°C/W)$	0.006
$R_{th(j-h)}(°C/W)$	0.014		$R_{th(j-h)}(°C/W)$	0.022
$R_{th(hs-a)}(°C/W)$	0.007		$R_{th(hs-a)}(°C/W)$	0.007

Appendix B

The Results of the Loss Calculations of some Converter Station Equipment

Table B-1: Damping loss per valve calculations (Losses of damping Resistor)

Parameters needed for calculations.		m	μ	α	f	V_L
		0	10°	19°	50 Hz	311.13kV
W_5 Damping Loss per valve (Rectifier side)	First branch	R_1	C_1		$W_{5f-branch}$=3.185 kW	
		5 kΩ	10nF		$W_{5s-branch}$=2.854 kW	
	Second branch	R_2	C_2		W_{5total}=6.038 kW	
		7 kΩ	8nF			
W_5 Damping Loss per valve (Inverter side)	First branch	R_1	C_1		$W_{5f-branch}$=2.0152kW	
		5 kΩ	10nF		$W_{5s-branch}$=1.8056kW	
	Second branch	R_2	C_2		W_{5total} =3.8207 kW	
		7 kΩ	8nF			
$W_{5standby}$ Damping Loss per valve (Rectifier)	First branch	R_1	C_1	Z_1	W_{51stby}=1.592 kW	
		5 kΩ	10nF	318.35 kΩ	W_{52stby}=1.426 kW	
	Second branch	R_2	C_2	Z_2	W_{5stby}=3.018 kW	
		7 kΩ	8nF	397.95 kΩ		
$W_{5standby}$ Damping Loss per valve (Inverter)	First branch	R_1	C_1	Z_1	W_{51stby}=1.0073kW	
		5 kΩ	10nF	318.35kΩ	W_{52stby}= 902.46W	
	Second branch	R_2	C_2	Z_2	W_{5stby}= 1.909kW	
		7 kΩ	8nF	397.95kΩ		

Table B-2: Rectifier Converter Station Transformer Losses Calculations using Method 1

Required Parameters			α	R_1	μ	f	$E_{ph} = \frac{V_L}{\sqrt{3}}$	X_t
			19	2 Ω	10	50	254.03 kV	60Ω
n	K_1	K_2	F	$I_n\ (A)$	(kn)	$R_n = R_1 * (kn)$	$I_n^2(kA)$	$I_n^2 R_n(kW)$
1	0	0.0868	0.0868	351.04	1.00	2.00	123.23	246.45
5	0.0855	0.0833	0.0687	55.55	4.34	8.68	3.09	26.17
7	0.0833	0.0803	0.0667	38.49	5.65	11.30	1.48	16.74
11	0.0766	0.0722	0.0606	22.29	13.00	26.00	0.50	12.92
13	0.0722	0.0671	0.0568	17.68	16.50	33.00	0.31	10.31
17	0.0616	0.0556	0.0479	11.403	26.60	53.20	0.13	6.92
19	0.0556	0.0492	0.0431	9.153	33.80	67.60	0.084	5.66
23	0.0427	0.0361	0.0326	5.734	46.40	92.8	0.033	3.05
25	0.0361	0.0295	0.0273	4.421	52.90	105.8	0.02	2.07
29	0.0230	0.0167	0.0171	2.385	69.00	138.00	0.01	0.79
31	0.0167	0.0107	0.0124	1.617	77.10	154.20	0.003	0.40
35	0.0051	0	0.0051	0.5900	92.40	184.80	0.0004	0.065
37	0	-0.0046	0.0046	0.4993	101.00	202.00	0.0002	0.05
41	-0.0086	-0.0119	0.0089	0.8743	121.00	242.00	0.0001	0.18
43	-0.0119	-0.0146	0.0111	1.0402	133.00	266.00	0.00005	0.29
47	-0.0167	-0.0180	0.0142	1.2188	159.00	318.00	0.00003	0.47
49	-0.0180	-0.0188	0.0150	1.2375	174.00	348.00	0.00001	0.53
$I_{n-total} = 525.223\ A$				$(I_n^2 R_n)_{total} = 333.07\ kW$				

Table B-3: Rectifier Converter Station Transformer Losses Calculations using per unit Method

Required Parameters			α	R_1	μ	f	$E_{ph} = \frac{V_L}{\sqrt{3}}$	X_t
			19	2 Ω	10	50	254.03 kV	60Ω

n	K_1	K_2	F	$I_n\ (A)$	(kn)	$R_n = R_1 * (kn)$	$I_n/2kA$ Per unit	$I_n^2 k_n$ $(per\ unit)$
1	0	0.0868	0.0868	351.04	1.00	2.00	0.1755	0.0308
5	0.0855	0.0833	0.0687	55.55	4.34	8.68	0.0278	0.0033
7	0.0833	0.0803	0.0667	38.49	5.65	11.30	0.0192	0.0021
11	0.0766	0.0722	0.0606	22.29	13.00	26.00	0.0111	0.0016
13	0.0722	0.0671	0.0568	17.68	16.50	33.00	0.0088	0.0013
17	0.0616	0.0556	0.0479	11.403	26.60	53.20	0.0057	0.0009
19	0.0556	0.0492	0.0431	9.153	33.80	67.60	0.0046	0.0007
23	0.0427	0.0361	0.0326	5.734	46.40	92.8	0.0029	0.0004
25	0.0361	0.0295	0.0273	4.421	52.90	105.8	0.0022	0.0003
29	0.0230	0.0167	0.0171	2.385	69.00	138.00	0.0012	0.0001
31	0.0167	0.0107	0.0124	1.617	77.10	154.20	0.0008	0.0001
35	0.0051	0	0.0051	0.5900	92.40	184.80	0.0003	0.00006
37	0	-0.0046	0.0046	0.4993	101.00	202.00	0.0002	0.00007
41	-0.0086	-0.0119	0.0089	0.8743	121.00	242.00	0.0004	0.00008
43	-0.0119	-0.0146	0.0111	1.0402	133.00	266.00	0.0005	0.00009
47	-0.0167	-0.0180	0.0142	1.2188	159.00	318.00	0.0006	0.0001
49	-0.0180	-0.0188	0.0150	1.2375	174.00	348.00	0.0006	0.0001
$I_{n-total} = 525.223\ A$					$(I_n^2 R_n)_{total} = 0.0416\ pu$			

Table B-4: Inverter Converter Station Transformer Losses Calculations using Method 1

Required Parameters			α	R_1	μ	f	$E_{ph} = \frac{V_L}{\sqrt{3}}$	X_t
			19	2 Ω	10	50	202.07 kV	60Ω
n	K_1	K_2	F	$I_n\ (A)$	(kn)	$R_n = R_1 * (kn)$	$I_n^2(kA)$	$I_n^2 R_n(kW)$
1	0	0.0868	0.0868	279.234	1.00	2.00	77.972	155.944
5	0.0855	0.0833	0.0687	44.190	4.34	8.68	1.953	16.56
7	0.0833	0.0803	0.0667	30.613	5.65	11.30	0.937	10.59
11	0.0766	0.0722	0.0606	17.732	13.00	26.00	0.314	8.17
13	0.0722	0.0671	0.0568	14.0621	16.50	33.00	0.198	6.534
17	0.0616	0.0556	0.0479	9.0703	26.60	53.20	0.0823	4.38
19	0.0556	0.0492	0.0431	7.2807	33.80	67.60	0.0530	3.583
23	0.0427	0.0361	0.0326	4.5608	46.40	92.8	0.0208	1.93
25	0.0361	0.0295	0.0273	3.5169	52.90	105.8	0.0124	1.312
29	0.0230	0.0167	0.0171	1.8975	69.00	138.00	0.0036	0.497
31	0.0167	0.0107	0.0124	1.2859	77.10	154.20	0.00165	0.254
35	0.0051	0	0.0051	0.4693	92.40	184.80	0.00022	0.0407
37	0	-0.0046	0.0046	0.3972	101.00	202.00	0.00016	0.0323
41	-0.0086	-0.0119	0.0089	0.6955	121.00	242.00	0.00048	0.116
43	-0.0119	-0.0146	0.0111	0.8275	133.00	266.00	0.00069	0.184
47	-0.0167	-0.0180	0.0142	0.9695	159.00	318.00	0.00094	0.299
49	-0.0180	-0.0188	0.0150	0.9844	174.00	348.00	0.00097	0.338
$I_{n-total} = 417.79\ A$					$(I_n^2 R_n)_{total} = 210.75\ kW$			

Table B-5: Filter Resistor Loss Calculations

Required parameters			Q	V	f
			200 MVar	311.13 kV	50 Hz
C-type filter (Rectifier side) P_r =16.421 kW	n	5th and 7th	5th and 7th		
	q		50		
	I	$I_5 + I_7$	Rectifier	Inverter	
			94.0381 A	74.8030 A	
(Inverter side) P_r = 6.5746 kW	C_1		6.8566 μF	10.836 µF	
	R		1.8569 Ω	1.1750 Ω	
	L		0.0591 H	0.0374 H	
Single-tuned band pass filter. (Rectifier side) P_r =3.544 kW	n	11th and 13th	11th and 13th		
	q		20		
	I	$I_{11} + I_{13}$	Rectifier	Inverter	
			39.9691 A	31.7936 A	
(Inverter side) P_r = 1.4188 kW	C		6.5223 µF	10.308 µF	
	R		2.2183 Ω	1.4036 Ω	
	L		0.0128 H	0.0081 H	
Double tuned filter (Rectifier side) P_r =2.9991 kW	n	17th and 19th	17th and 19th		
	q		4		
	I	$I_{17} + I_{19}$	Rectifier	Inverter	
			20.5556 A	16.3510 A	
(Inverter side) P_r =1.2007 kW	C_1		6.5950 µF	10.423 µF	
	C_2		6.5950 µF	10.423 µF	
	R		7.0979 Ω	4.4912 Ω	
	L_1		0.0053 H	0.0034 H	
	L_2		0.0043 H	0.0027 H	
High pass filter (Rectifier side) P_r =4.0567 kW	n	23rd - 49th	23rd - 49th		
	q		2		
	I	I_{23} to I_{49}	Rectifier	Inverter	
			19.6170 A	15.6044 A	
(Inverter side) P_r =1.6242 kW	C		6.5642 µF	10.374 µF	
	R		10.5417 Ω	6.6702 Ω	
	L		0.0029 H	0.0018 H	
The total filter resistor loss (Rectifier)	$P_{rtotal-rectifier}$		27.021 kW		
The total filter resistor loss (Inverter)	$P_{rtotal-inverter}$		10.818 kW		

Table B-6: Filter Reactor Loss Calculations

C-type filter (Rectifier side) P_R =16.421 kW	n	5th and 7th	5th and 7th	
	Q_n		50	
	I^2	$(I_5 + I_7)^2$	Rectifier	Inverter
			8.843kA	5.596kA
(Inverter side) P_R =6.5746 kW	L		0.0591H	0.0374H
	X_{Ln}		92.8473Ω	58.7490Ω
Single-tuned band pass filter. (Rectifier side) P_R =3.5438 kW	n	11th and 13th	11th and 13th	
	Q_n		20	
	I^2	$(I_{11} + I_{13})^2$	Rectifier	Inverter
			1.598kA	1.01kA
(Inverter side) P_R = 1.4188kW	L		0.0128H	0.0081H
	X_{Ln}		44.3667Ω	28.0729Ω
Double tuned filter (Rectifier side) P_R =4.0626 kW	n	17th and 19th	17th and 19th	
	Q_n		4	
	I^2	$(I_{17} + I_{19})^2$	Rectifier	Inverter
			422.55A	267.36 A
(Inverter side) P_R =1.6296kW	L_1		0.0053H	0.0034H
	L_2		0.00005H	0.0027H
	$L_1 + L_2$		0.0053H	0.0034H
	X_{Ln}		38.4596Ω	24.3804Ω
High pass filter (Rectifier side) P_R =4.0567 kW	n	23rd - 49th	23rd - 49th	
	Q_n		2	
	I^2	$(I_{23}\ to\ I_{49})^2$	Rectifier	Inverter
			384.83A	243.5A
(Inverter side) P_R =1.6242kW	L_1		0.0029H	0.0018H
	X_{Ln}		21.0833Ω	13.3404Ω
The total filter reactor loss (Rectifier)	$P_{Rtotal-rectifier}$		28.084 kW	
The total filter reactor loss (Inverter)	$P_{Rtotal-inverter}$		11.247kW	

Table B-7: Rectifier Terminal DC Smoothing Reactor Loss Calculations

n	P_{hn} (Hysteresis loss component in per unit)	P_{en} (The eddy-current loss component, in per unit) for n > 10	P_{e2} (The eddy-current loss component, in per unit) for n =2	I_n (Harmonic currents) A
1	0.1755	-	0.0308	351.04
5	0.1389	-	0.0193	55.55
7	0.1347	-	0.0181	38.49
11	0.1226	4.1200×10^{-4}	-	22.29
13	0.1149	2.8170×10^{-4}	-	17.68
17	0.0969	1.3402×10^{-4}	-	11.403
19	0.0870	9.1292×10^{-5}	-	9.153
23	0.0659	3.9415×10^{-5}	-	5.734
25	0.0553	2.4434×10^{-5}	-	4.421
29	0.0346	7.6607×10^{-6}	-	2.385
31	0.0251	3.6373×10^{-6}	-	1.617
35	0.0103	5.1481×10^{-7}	-	0.5900
37	0.0092	3.7917×10^{-7}	-	0.4993
41	0.0179	1.2237×10^{-6}	-	0.8743
43	0.0224	1.7739×10^{-6}	-	1.0402
47	0.0286	2.5461×10^{-6}	-	1.2188
49	0.0303	2.6801×10^{-6}	-	1.2375
$P_{hn-total} = 1.1701$		$P_{en-total} = 1.2462 \times 10^{-3}$	$P_{e2-total} = 0.06826$	
$P_e = P_{en-total} + P_{e2-total} = 0.0692$				

The direct current loss calculation (Rectifier side)	I_o (dc current)	R	L
	2 kA	0.02 Ω	0.2 mH
	X_L	$2\pi fL$	0.0628 Ω
	Z	$\sqrt{R^2 + X_L^2}$	0.0659 Ω
	P_0 (direct current losses)	$I_o^2 Z$	263.75 kW

$P_m = 0.125(\sum P_h + \sum P_e)P_0 = 40.861\ kW$

P_m= The magnetization loss.

Table B-8: Inverter Terminal DC Smoothing Reactor Loss Calculations

n	P_{hn} (Hysteresis loss component in per unit)	P_{en} (The eddy-current loss component, in per unit) for n > 10	P_{e2} (The eddy-current loss component, in per unit) for n =2	I_n (Harmonic currents) A
1	0.1396	-	0.0195	279.234
5	0.1105	-	0.0122	44.190
7	0.1071	-	0.0115	30.613
11	0.0975	2.6069×10^{-4}	-	17.732
13	0.0914	1.7824×10^{-4}	-	14.0621
17	0.0771	8.4803×10^{-5}	-	9.0703
19	0.0692	5.7765×10^{-5}	-	7.2807
23	0.0524	2.4940×10^{-5}	-	4.5608
25	0.0440	1.5461×10^{-5}	-	3.5169
29	0.0275	4.8473×10^{-6}	-	1.8975
31	0.0199	2.3015×10^{-6}	-	1.2859
35	0.0082	3.2574×10^{-7}	-	0.4693
37	0.0073	2.3992×10^{-7}	-	0.3972
41	0.0143	7.7428×10^{-7}	-	0.6955
43	0.0178	1.1224×10^{-6}	-	0.8275
47	0.0228	1.6111×10^{-6}	-	0.9695
49	0.0241	1.6958×10^{-6}	-	0.9844
$P_{hn-total} = 0.9808$		$P_{en-total} = 0.6000 \times 10^{-3}$	$P_{e2-total} = 0.0432$	
$P_e = P_{en-total} + P_{e2-total} = 0.0438$				

The direct current loss calculation (Rectifier side)	I_o (dc current)	R	L
	2 kA	0.02 Ω	0.2 mH
	X_L	$2\pi fL$	0.0628 Ω
	Z	$\sqrt{R^2 + X_L^2}$	0.0659 Ω
	P_0 (direct current losses)	$I_o^2 Z$	263.75 kW

Rectifier terminal - $P_m = 0.125(\sum P_h + \sum P_e)P_0 = 40.861\ kW$

Inverter terminal - $P_m = 0.125(\sum P_h + \sum P_e)P_0 = 32.132\ kW$

Appendix C

HVDC TECHNOLOGIES CIRCUIT SIMULATION MODELS

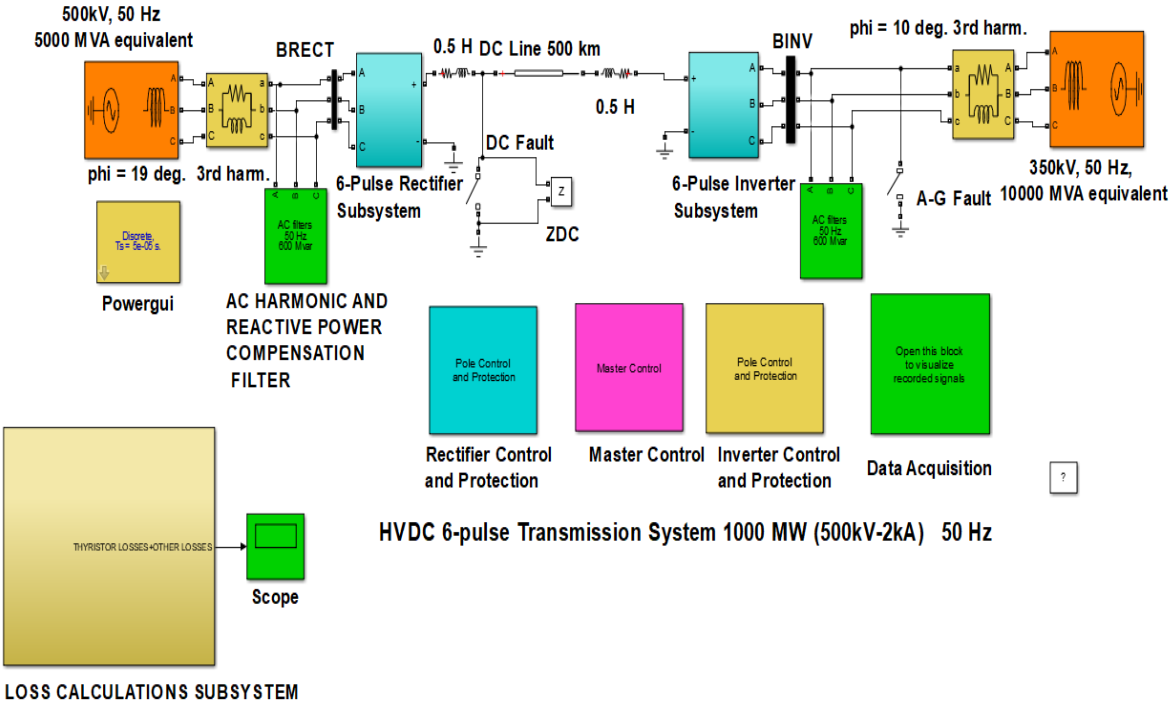

Figure C-1: Circuit Simulation of 6-pulse LCC-Based HVDC technology

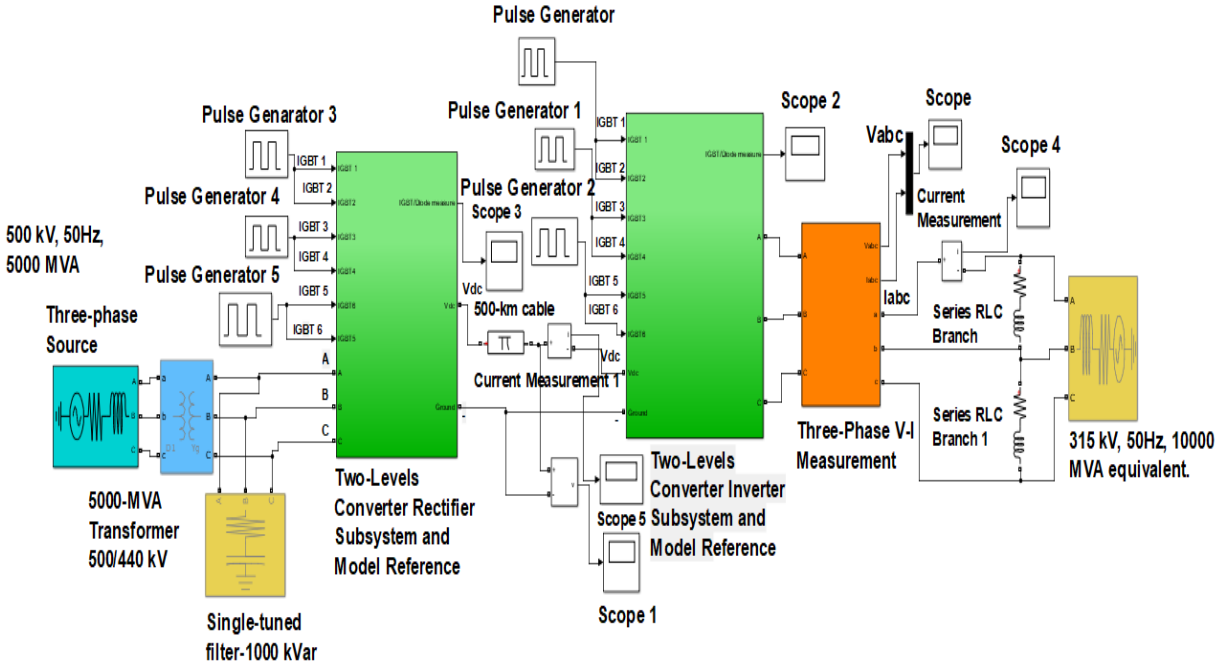

Figure C-2: Circuit Simulation of Two-Level VSC HVDC technology

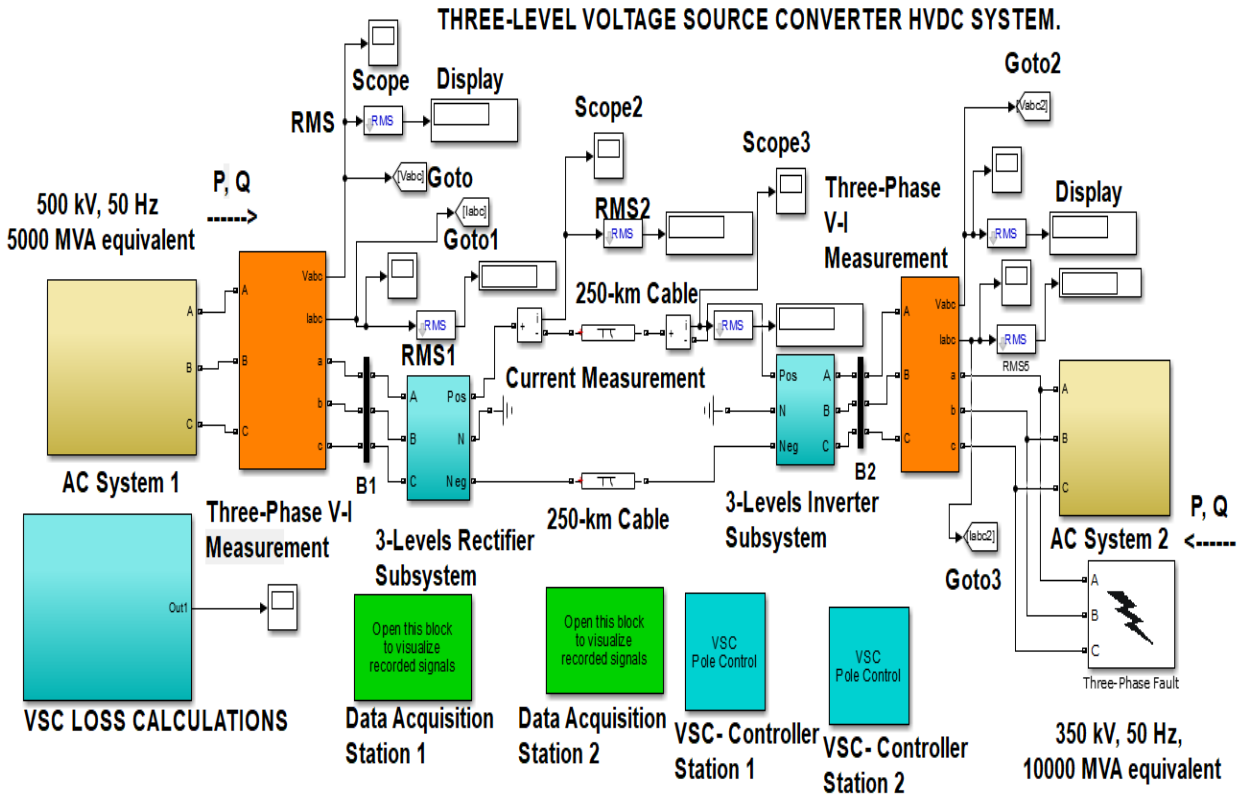

Figure C-3: Circuit Simulation of Three-Level VSC HVDC technology

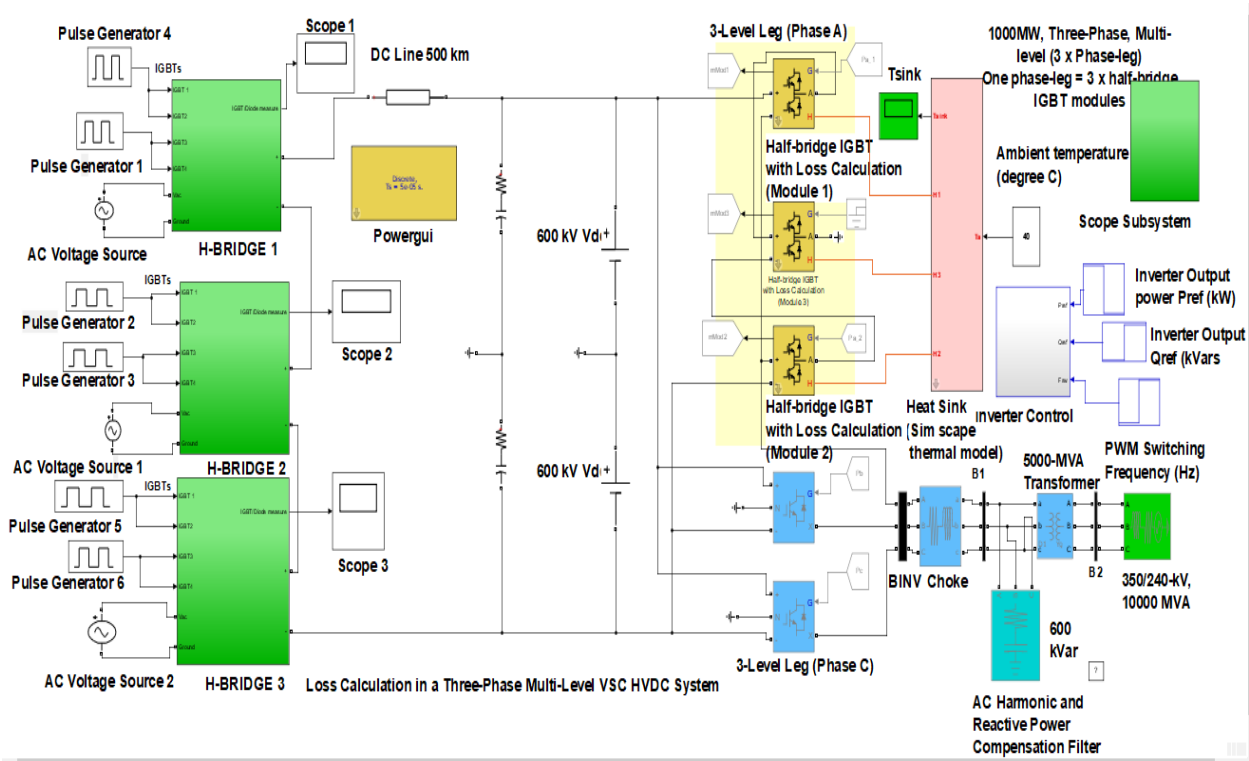

Figure C-4: Circuit Simulation of Multi-Level VSC HVDC technology